ELSEVIER

Coordination Chemistry Reviews
197 (2000) 397–481

COORDINATION CHEMISTRY REVIEWS

www.elsevier.com/locate/ccr

Recent advances in the understanding of the syntheses, structures, bonding and energetics of the homopolyatomic cations of Groups 16 and 17

S. Brownridge [a], I. Krossing [a,1], J. Passmore [a,*], H.D.B. Jenkins [b,2], H.K. Roobottom [b]

[a] *Department of Chemistry, University of New Brunswick, Fredericton, N.B., Canada E3B 6E2*
[b] *Department of Chemistry, University of Warwick, Coventry, CV4 7AL, UK*

Received 26 May 1999; accepted 13 December 1999

This review is dedicated to Dr Ron J. Gillespie who has played a major role in the discovery and development of the homopolyatomic cations of the elements, including those of Groups 16 and 17. One of us (J. Passmore) had the privilege of being introduced to this area as a Post Doctoral Fellow (1968/1969) with Ron Gillespie, and thanks to Ron for the example he has been, and the encouragement he has given over the years.

Contents

* Corresponding author. Tel.: +1-506-4534821; fax: +1-506-4534981.
[1] Co-corresponding author. Present address: University of Karlsruhe, 76128 Karlsruhe, Germany.
[2] Co-corresponding author. Tel.: +44-2476-523261; fax: +44-2476-524112.
E-mail addresses: krossing@achpc9.chemie.uni-karlsruhe.de (I. Krossing), passmore@unb.ca (J. Passmore), msrfn@snow.cvs.warwick.ac.uk (H.D.B. Jenkins)

PII: S0010-8545(00)00230-7

Abstract

In this review the preparation and structures of all known salts of the known homopolyatomic cations of the chalcogens and halogens are reviewed. We show that the structures of these cations, many of which are non-classical and cluster-like, arise from positive charge delocalisation, i.e. the reduction of Coulomb repulsion by diluting the unfavourable localised charges over all the atoms in the ion. The charge delocalisation leads to a combination of intra- (and inter-) cationic $\pi^*-\pi^*$, $np_\pi-np_\pi$, weak np^2-np^2 ($n \geq 3$) and $np^2 \rightarrow n\sigma^*$ interactions. The latter are important especially for the polymeric tellurium homopolyatomic cations and account for most of their intriguing geometries. This thesis is based on the results of quantitative theoretical studies on the simpler cations (I_4^{2+}, I_3^+, I_5^+, M_4^{2+}, M_8^{2+} and M_4^{2+} (M = S, Se, Te)), and we apply these simple bonding models to qualitatively explain the geometries of all the remaining cations. The geometries of the more cluster like cations can also be rationalised by the Wade–Mingos rules, consistent with the positively charged atoms approximately adopting positions on a sphere so minimising the electrostatic Coulomb repulsion. Thus the structures of these and related cations have been integrated into the main stream of inorganic chemistry. In the second part of this article we provide an understanding of the thermodynamics governing the syntheses of most of the known chalcogen and halogen cations. This is based on our new relationship between lattice enthalpies and thermochemical volumes/radii (for both real and hypothetical salts), on known experimental gas phase enthalpies of formation, as well as high level calculations (in contrast to earlier work, all of these calculations now reproduce the experimental geometries, vibrational spectra and energetics of the cations in question, e.g. M_8^{2+}, M_4^{2+}, I_4^{2+}). We now can quantitatively understand why $S_4^{2+}(AsF_6^-)_2$ is formed and not $2S_2^+(AsF_6^-)$; why S_4Cl_2 adopts a chain like molecular geometry and not a salt like structure containing the square planar 6π aromatic S_4^{2+} dication, and account for all the features in the structure of S_8^{2+}. We lay the foundation for establishing whether or not as yet unknown homopolyatomic cation salts can be prepared in the solid state. A short overview of methods to estimate thermodynamic properties is given as well as extensive tabular appendixes of thermodynamic data of relevant cations and anions (standard enthalpies of formation, fluoride ion affinities, lattice potential enthalpies etc.).

Keywords: Homopolyatomic cations; Wade–Mingos clusters; Fluoride ion affinities; Thermodynamics

1. Introduction

In the late 18th and early 19th century, it was shown that elemental sulphur, selenium and tellurium dissolve in oleum giving intensely coloured solutions, later iodine was shown to give blue solutions. The nature of these coloured solutions was the subject of many studies and considerable speculation [1,2]. Early work, that has stood the test of time includes that of Masson who deduced the existence of I_3^+ and I_5^+ from aromatic iodination reactions. However it was not until the 1960s that the nature of these species began to be elucidated convincingly [3]. The first well characterised homopolyatomic cation of the electronegative elements was the colourless $[O_2^+][PtF_6^-]$ prepared by Bartlett [4,5] and pure crystalline compounds including single crystals were obtained for the first time in the late 1960s and 1970s. The advent of routine single-crystal X-ray crystallography and structure solution by

direct methods led to the elucidation of the solid state structures of many of these coloured species. However the structures themselves presented problems, e.g. the nature of the very long transannular interactions in the S_8^{2+} and Se_8^{2+} dications. A variety of synthetic routes to obtain salts of pure homopolyatomic chalcogen and halogen cations were developed, and an increasing number of non-classically bonded cations were isolated as salts of weakly basic and nonoxidisable anions (e.g. MF_6^-, (M = As, Sb), SO_3F^-, $AlCl_4^-$, WCl_6^- etc.). Whilst a number of reviews on these topics have been published [6–14] most of them focus on the preparation, characterisation and structure of these homopolyatomic cations. Many of these structures are now included in inorganic chemistry textbooks, however the bonding governing the geometries of many of them is only partly accounted for. In 1989, Passmore et al. [11] embarked on developing the related thermochemistry and interpreting the nature of the bonding of some of the unusual non-classically bonded homopolyatomic cations and proposed that np_π–np_π ($n \geq 3$), π^*–π^* bonding, bond alternation and the cluster-like geometries of these cations resulted from positive charge delocalisation. This was further developed in his 1992 review on homopolyatomic selenium cations [14]. If indeed the charge delocalisation model proves to be correct, then these unusual structures should be relatively easily understood.

We are now in a much better position to understand the nature of the bonding and the energetics underlying the salts of the homopolyatomic cations of Groups 16 and 17. Advances have been made in obtaining estimates of the lattice potential energies of salts of all A_mB_y stoichiometries [15–17]; high level computational chemistry is now able to provide us with highly accurate gas phase geometries and energetics of chalcogen and halogen homo- (and hetero-) polyatomic cations [16,18–33]. Estimates can also be made of solvation energies employing polarised continuum models of solvation [34,35]. We have also obtained some experimental enthalpies of formation by fluorine bomb calorimetry [36,37]. This combination of many techniques then allows us to answer questions such as: why is it that one particular cation is found and yet not another? Specific examples might be: why is $[S_4^{2+}][AsF_6^-]_2$ found but not $[S_2^+][AsF_6^-]$ (cf. $[O_2^+][AsF_6^-]$) or why does $[Te_6^{4+}]$-$[AsF_6^-]_4$ exist but not $[S_6^{4+}][AsF_6^-]_4$? Why should S_4Cl_2 adopt a chain-like, molecular geometry and not the salt-like structure of the square planar 6π aromatic S_4^{2+} dication which is found in a variety of $[S_4^{2+}][A^-]_2$ salts (A^- = non-basic anion)? Will the qualitative model we proposed above account for the geometries of the homopolyatomic cations and related species and be substantiated by the quantitative high level quantum mechanical calculations? How much lower in energy are the observed non-classical geometries relative to their classical analogues? Will these models also serve to interpret the geometries of the numerous new homopolyatomic tellurium cations that have been recently prepared [13]? Is it possible to form inverted E^+X^- salts, where an electronegative chalcogen or halogen atom E takes the place of the electropositive metal atom in simple salt structures like NaCl? We note that similar counter-intuitive salts, e.g. of the type Na^+Na^-, are now known by completing the sodium cation by a crown ether or cryptand ligands [38]. Can a simple metathesis reaction be employed in the synthesis of homopolyatomic cations

of the chalcogens or halogens? Is it possible to rationalise some of the structures of the homopolyatomic Groups 16 and 17 cations based on Wade's and Mingos' well established rules [39–41] which have been applied successfully to account for the structures of the related Bi_5^{3+} and Bi_8^{2+} cations?

Using all the newly available information, we aim: (i) to review the recent literature since the previous 1989 review [11]; (ii) to estimate unknown thermodynamic quantities; (iii) to provide predictions regarding new synthetic targets; (iv) to describe and interpret the bonding principles that are observed for many of these unusual cationic species; and (v) answer a variety of questions of the kind posed above. We will leave a review article covering the extensive and fascinating chemistry [42] of the homopolyatomic cations of the halogens and the chalcogens for a later occasion. The focus of the review is the isolated salts of these homopolyatomic cations, and we only refer to theoretical and experimental studies of these cations in the gas phase in relation to those observed in the solid state.

2. Synthesis and characterisation of new homopolyatomic cations

All the known methods of preparation of these materials proceed in highly acidic/very weakly basic conditions and employ non-oxidisable, complex anions permitting the isolation of crystalline salts of the homopolyatomic cations [6–12]. The three main synthetic routes proceed in super acidic media [10], acidic melts [7,10] and SO_2 (and related, nonprotic solvents) [11,14]. Oxidation of the elements is achieved either by a higher elemental halide and subsequent halide ion abstraction with a strong halide ion acceptor (e.g. $AlCl_3$, transition metal halides), or by the reaction with a strong one electron oxidiser such as MF_6 (M = Pt, W, Re, Os, Ir), $SO_3F^{\bullet}$ radicals (from $S_2O_6F_2$) and WCl_6 or two electron oxidisers such as MF_5 (M = As, Sb) in a suitable solvent. A detailed summary of these preparative routes is included in our 1989 review [11], and the interested reader is referred to this source. However, the preparation of homopolyatomic chalcogen cations by chemical vapour transport methods [13] is comparatively new and detailed in the following section. Advances have been made in the understanding of the kinetics of the halogen facilitated oxidation of the chalcogens by AsF_5 and SbF_5 [43]. Subsequently, we will introduce the preparation and characterisation of the new homopolyatomic chalcogen and halogen cations published since 1989. At present, all available data are summarised in Tables 1–4 (solid state) and Tables 5 and 6 (solution).

We have not included oxygen homopolyatomic cations, as none other than O_2^+, which we have reviewed [11], has been prepared. One of us (J. Passmore) reported attempts to prepare $O_3^+PtF_6^-$ [44], and O_4^+ is of importance in atmospheric ion chemistry [45a]. It [45] and others [46] related to homopolyatomic cations of Groups 16 and 17 in the gas phase have been the subject of theoretical and experimental investigations and will not be included here.

2.1. New selenium and tellurium cations

The last 10 years have provided one new selenium and 11 new tellurium homopolyatomic cations with hitherto unprecedented solid state structures prepared mostly by Beck et al. [13] using the techniques of solid state chemistry.

2.1.1. General preparation

Typically, the desired species are formed in a chemical vapour transport reaction [13]. The element, an elemental halide and a (usually transition-) metal halide or oxohalide are sealed in an evacuated glass tube and heated for periods of days to weeks at temperatures between 100 and 300°C. Applying a small temperature gradient (commonly 10–20°C) leads to a transport reaction and to the crystallisa-

Table 1
Summary of the presently known halogen cations [a] and method of characterisation in the solid state

Cation	Colour	Counterion			
		X-ray	Raman and IR	Chemical analysis	Magnetic susceptibility
I_2^+	Blue	$Sb_2F_{11}^-$ [47b,c]	$Sb_2F_{11}^-$ [47b,c,d]	$Sb_2F_{11}^-$ [47a] $Ta_2F_{11}^-$ [47a]	$Sb_2F_{11}^-$ [47a,d]
I_3^+ [b]	Brown/black	AsF_6^- [48a]		AsF_6^- [48b]	
I_4^{2+} [c]	Black	AsF_6^- [49] $SbF_6^-/Sb_3F_{14}^-$ [49,50]	AsF_6^- [49a,b] SbF_6^- [49a,b]		AsF_6^- [49,51] SbF_6^- [49]
		SbF_6^- [49b]	$SbF_6^-/Sb_3F_{14}^-$ [49b]		$SbF_6^-/Sb_3F_{14}^-$ [49]
I_5^+ I_7^+ [b]	Green/black	AsF_6^- [52]		AsF_6^- [52]	
I_{15}^{3+}	Black	SbF_6^- [53]			
Br_2^+	Red [54]	$Sb_3F_{16}^-$ [55]	$Sb_3F_{16}^-$ [55] OsF_6^- [56]		$Sb_3F_{16}^-$ [55]
Br_3^+	Dark brown [57a]	AsF_6^- [57b]	AsF_6^- [57a,b] $Au(SO_3F)_4^-$ [57c]	$Pt(SO_3F)_6^{2-}$ [58]	$Pt(SO_3F)_6^{2-}$ [58]
Br_5^+	Red–grey green Dark brown	AsF_6^- [59] SbF_6^- [59]	AsF_6^- [59,60] $Au(SO_3F)_4^-$ [57c]		
Cl_3^+	Yellow	AsF_6^- [61] SbF_6^- [61] $Sb_2F_{11}^-$ [61] $Sb_3F_{16}^-$ [61]	AsF_6^- [62,63] SbF_6^- [64]		

[a] ISO_3F formally containing I^+ is dimeric in the solid state containing iodine atoms in the +III and −I oxidation states [i.e. $(FO_2SO)_2I$–I] [65].

[b] Melting point of $[I_n][SO_3F]$; $n = 3, 7$ [66].

[c] NQR of $[I_n][AlCl_4]$; $n = 3, 5$ [67].

N.B.: $[Br_2^+][AsF_6^-]$ was claimed to have been synthesised as dark red crystals, experimental details are described although no method of characterisation is given [54]. A preliminary report of $[Cl_4^+][IrF_6^-]$ has been given by Seppelt [68b].

Table 2
Summary of the presently known sulphur cations and the method of characterisation in the solid state

Cation	Colour	Counterion			
		X-ray	Raman	IR	Chemical analysis
S_4^{2+}	Colourless [b]	AsF_6^- [17,68a] in $[(S_7X^+)_4(S_4^{2+})(AsF_6^-)]$, X = Br, I [68a,69] [c] [70]	AsF_6^- [68c,71a] $Sb_2F_{11}^-$ [68c] SO_3F^- [72,89d] $S_2O_6F^-$ [89d]	AsF_6^- [68c] $Sb_2F_{11}^-$ [68c] SO_3F^- [89d]	AsF_6^- [68c] $Sb_2F_{11}^-$ [68c] SO_3F^- [72,89d] $S_2O_6F^-$ [89d]
S_8^{2+} [a]	Blue [73a] Grey/blue [70]	AsF_6^- [16,72b,73a] [d] [70]	AsF_6^- [16]	AsF_6^- [72b,73b] $Sb_2F_{11}^-$ [72b]	AsF_6^- [72b,73b,96] $Sb_2F_{11}^-$[72b,96]
S_{19}^{2+}	Red/brown [70]	AsF_6^- [74] SbF_6^- [70]			

[a] Also melting point of $S_8(AsF_6)_2$ and $S_8(Sb_2F_{11})_2$ [96], $S_8(AsF_6)_2$ is red in transmitted light but blue in reflected light [16].
[b] Appeared pale yellow as SO_3F^- salt [89d].
[c] $(Sb_2F_4^{2+})(Sb_2F_5^+)(SbF_6^-)_5$.
[d] $[(SbF_2^+)(SbF_6^-)_2](SbF_6^-)=(Sb_3F_{14}^-)(SbF_6^-)$.

Table 3
Summary of the presently known selenium cations and method of characterisation in the solid state

Cation	Colour	Counterion			
		X-ray	Raman	IR	Chemical analysis
Se_4^{2+}	Yellow/orange Yellow/green [75]	[a] [76] [b] [77]	AsF_6^- [36,89d] [b] [89d]	AsF_6^- [36,89d] [b] [89d]	AsF_6^- [36,96] $Sb_2F_{11}^-$ [79,96]
		$AlCl_4^-$ [89a] $HfCl_6^{2-}$ [91] $ZrCl_6^{2-}$ [91] $AlBr_4^-$ [13b] AlI_4^- [13b] $MoOCl_4^-$ [75] $HS_2O_7^-$ [78]	$AlCl_4^-$ [89d] $HS_2O_7^-$ [89d] SO_3F^- [89d] $S_2O_6F^-$ [89d]	$AlCl_4^-$ [89a,d] $HS_2O_7^-$ [89d] SO_3F^- [89d] $S_2O_6F^-$ [89d]	$HS_2O_7^-$ [79] SO_3F^- [79] $S_4O_{13}^{2-}$ [79]
Se_8^{2+}	Green/black	$AlCl_4^-$ [80,89a] [c]	AsF_6^- [16]	AsF_6^- [81] $Sb_2F_{11}^-$ [81b] $AlCl_4^-$ [89a]	AsF_6^- [81,96] $Sb_2F_{11}^-$ [81b,96]
Se_{10}^{2+}	Red/brown	SbF_6^- [82a] SO_3F^- [82b]			AsF_6^- [82a] $AlCl_4^-$ [82a]
Se_{17}^{2+}	Black [83] Dark red [84]	$NbCl_6^-$ [83] $TaBr_6^-$ [83] WCl_6^- [84]		WCl_6^- [84]	

[a] $[(Sb_2F_5^+)(SbF_6^-)_3](SbF_6^-)=(Sb_4F_{17}^-)(SbF_6^-)_3$.
[b] $(Sb_2F_4^{2+})(Sb_2F_5^+)(SbF_6^-)_5$.
[c] In $(Te_6^{4+})(Se_8^{2+})(AsF_6^-)_6(SO_2)$ [107].

Table 4
Summary of presently known tellurium cations and method of characterisation in the solid state

Cation	Colour	Counterion				
		X-ray	X-ray	Raman	IR	Chemical analysis
Te_4^{2+} [a]	Red/purple	SbF_6^- [89d]	$ZrCl_6^{2-}$ [91]	AsF_6^- [36,89d]	AsF_6^- [36,89d,94]	AsF_6^- [36,96]
	Black [85–87]	$AlCl_4^-$ [89a]	$HfCl_6^{2-}$ [91]	SbF_6^- [89d]	SbF_6^- [89d]	$Sb_2F_{11}^-$ 94[96]
	Dark blue [88]	$Al_2Cl_7^-$ [89a]	$ReCl_6^{2-}$ [13b]	$Sb_2F_{11}^-$ [94]	$Sb_2F_{11}^-$ [94]	SO_3F^- [94]
		WCl_6^- [87,88]	$Bi_2Br_8^{2-}$ [92]	$AlCl_4^-$ [89b,c,d]	$AlCl_4^-$ [89a,d]]	
		$TaCl_6^-$ [90]	$Zr_2Br_{10}^{2-}$ [93]	$Al_2Cl_7^-$ [89d,95b]	$Al_2Cl_7^-$ [89d]	
		$TaBr_6^-$ [90]	$Ta_2OCl_{10}^{2}-$ [90]			
		$MoOCl_4^-$ [85]	[d]			
		$Nb_2OCl_{10}^{2-}$ [86]				
Te_6^{2+}	Black	$AlCl_4^-$ [89a]	$NbOCl_4^-$ [90,97]		$AlCl_4^-$ [89a]	
			$WOCl_4^-$ [98]			
Te_6^{4+}	Yellow	AsF_6^- [99]	[b]			
Te_7^{2+}	Black	AsF_6^- [100]	$(WOCl_4^-)(Cl^-)$ [102]			
		$(NbOCl_4^-)(Cl^-)$ [101]	$(WOBr_4^-)(Br^-)$ [103]			
		$(NbOBr_4^-)(Br^-)$ [101]				
Te_8^{2+}	Silver [104]	$ReCl_6^{2-}$ [104]	$Bi_4Cl_{14}^{2-}$ [13b]			
	Blue/black [105]	WCl_6^- [105]	[c]			
Te_8^{4+}	Black	$VOCl_4^{2-}$ [106]				
Te_{10}^{2+}	Black	[d]				

[a] Also melting point of $[Te_4^{2+}][AsF_6^-]_2$ and $[Te_4^{2+}][Sb_2F_{11}^-]_2$ [96].
[b] Also in $(Te_6^{2+})(Se_8^{2+})(AsF_6^-)_6(SO_2)$ [107].
[c] Also in $(Te_6^{2+})(Te_8^{2+})(WCl_6)_4$ [13b].
[d] In $(Te_4)(Te_{10})(Bi_2Cl_8)_2$ [13b].

Table 5
Summary of presently known halogen cations and method of characterisation in solution [a]

Cation	Colour	Solvent/melt				
		Raman/IR	Magnetic susceptibility	Cryoscopy	UV–vis	Conductance
I_2^+	Blue	Oleum [108] HSO_3F [49b,108] SbF_5 [108] $AlCl_3$–NaCl [109] SO_2 [49b]	Oleum [47a,110] $H_2S_2O_7$ [111e] HSO_3F [112]	Oleum [111a] HSO_3F [112]	Oleum [47a,110,111a] H_2SO_4 [47a,111d] $H_2S_2O_7$ [111e] HSO_3F [47a,111d,112] HF[113] $AlCl_3$–NaCl [109]	Oleum [47a,111a] $H_2S_2O_7$ [111e] HSO_3F [112]
I_3^+	Brown/black	H_2SO_4 [63] HF [57b]	HSO_3F [112]	HSO_3F [110,112] H_2SO_4/HIO_3 [3]	H_2SO_4 [111d,114] $H_2S_2O_7$ [111e] HSO_3F [111d,112,114b] HF [113]	H_2SO_4 [114a] HIO_3/H_2SO_4 [3a] HSO_3F [110,112]
I_5^+	Green/black			HSO_3F [112] H_2SO_4/HIO_3 [3]	H_2SO_4 [114a] HF [113]	HIO_3/H_2SO_4 [3a]
I_4^{2+}	Black	65% oleum [111c] SO_2 [111b] HSO_3F [49b]	HSO_3F [50]	HSO_3F [50]	HSO_3F [50]	HSO_3F [50]
Br_2^+	Red	SbF_5–$3SO_3$–HSO_3F [115]			SbF_5–$3SO_3$–HSO_3F [116]	
Br_3^+	Brown	HSO_3F [115] SbF_5–SO_3–HSO_3F [115] $BrSO_3F$ [117] HF [57b]	HSO_3F [115]		HSO_3F [116] SbF_5–SO_3–HSO_3F [115] SbF_5 [47d]	HSO_3F [115]

[a] N.B.: The Cl_4^+ cation was tentatively proposed as an unstable intermediate at 77 K [118].

Table 6
Summary of presently known chalcogen cations as characterised in solution

Cation	Colour	Solvent/Melt					
		Raman	Cryoscopy	UV–vis (absorption)	Conductance	ESR	X-NMR (X = Se, Te)
Te_4^{2+} [a,c]	Red	H_2SO_4 [95b] HSO_3F [95a,96]	H_2SO_4 [95a] $H_2S_2O_7$[119]	H_2SO_4 [95a] HSO_3F [95a,96] $AlCl_3$–NaCl[120]	H_2SO_4 [95a] $H_2S_2O_7$ [119]		Oleum [121,122]
Te_6^{4+}	Brown						Oleum [121]
Se_4^{2+} [a]	Yellow	Oleum [95b] HSO_3F [96]	H_2SO_4 [79,123] $H_2S_2O_7$ [123] HSO_3F [79,123]	H_2SO_4 [79,96b] $H_2S_2O_7$ [123] HSO_3F [79]	H_2SO_4 [79] $H_2S_2O_7$ [123] HSO_3F [79]		Oleum [121]
Se_8^{2+}	Green		H_2SO_4 [123] $H_2S_2O_7$ [123] HSO_3F [123]	H_2SO_4 [79] $H_2S_2O_7$ [123] HSO_3F [81b,96,123]	H_2SO_4 [79] $H_2S_2O_7$ [123] HSO_3F [79]		H_2SO_4 [81a] SO_2 [81a]
Se_{10}^{2+} [f]	Red brown			H_2SO_4 [82a]			H_2SO_4 [81a] SO_2 [81a]
S_4^{2+} [a,e]	White	Oleum [95b] SO_2/AsF_5 [17]		Oleum [124a] HSO_3F [72a] SbF_5 [72a,b]		Oleum [124a]	
S_5^+	Blue			SO_2 [74]		Oleum [125] SO_2 [74]	
S_8^{2+} [d]	Blue [b]		Oleum [124a]	Oleum [124a] $H_2S_2O_7$ [126] HSO_3F [72b,73b] SO_2 [74]	$H_2S_2O_7$ [126]	Oleum [124a,127] $H_2S_2O_7$ [126]	
S_{19}^{2+}	Red			SO_2 [74]		Oleum [125] SO_2 [74]	

[a] Also magnetic circular dichroism in oleum [124b].
[b] Reddish brown in SO_2/SO_2ClF [16].
[c] Magnetic susceptibility in H_2SO_4 [95a] and $H_2S_2O_7$ [119].
[d] Magnetic susceptibility in HSO_3F [72b,73b].
[e] UV–vis of S_4^{2+} also in $AlCl_3$–NaCl [128].
[f] Se_{10}^{2+} disproportionates in solution giving Se_{17}^{2+} and other species [81a]. N.B.: identification of Se_2^{2+}, Se_4^{2+}, Se_8^{2+}, Se_{12}^{2+} and Se_{16}^{2+} [129] and Te_4^{2+}, Te_6^{2+} and Te_8^{2+} [130] claimed in 63% $AlCl_3$: 37% NaCl by potentiometric and spectrophotometric methods.

tion of the homopolyatomic cations towards the cooler end of the ampoule. The dimensions of the crystals formed in the reaction grow as large as $5 \times 5 \times 5$ mm. A typical reaction is given in Eq. (1) [106].

$$4Te + 2VOCl_3 \xrightarrow{200°C} 2VOCl_2 + Te_3Cl_2 + Te \xrightarrow{270°C} 0.5[Te_8^{4+}][VOCl_4^{2-}]_2 \quad (1)$$

Alternatively, one electron oxidisers such as WCl_6 [105] or $WOCl_4$ [98] have been employed:

$$8Te + 2WCl_6 \rightarrow [Te_8^{2+}][WCl_6^{-}]_2 \quad (2)$$

$$6Te + 2WOCl_4 \xrightarrow{210-230°C} [Te_6^{2+}][WOCl_4^{-}]_2 \quad (3)$$

All of the new homopolyatomic cation salts were characterised by single-crystal X-ray crystallography, some additionally by magnetic measurements (in order to establish the oxidation state of the transition metal present in the counterion, e.g. $[Te_7^{2+}][(NbOCl_4^{-})(Cl^{-})]$; $[Te_8^{2+}][ReCl_6^{2-}]$) [101,104]. Spectroscopic methods were only occasionally employed {e.g. IR in the case of $[Se_{17}^{2+}][WCl_6^{-}]_2$} [84].

2.1.2. Square planar E_4^{2+} ($E = Se$, Te)

Numerous new examples of salts containing the well established square planar, 6π aromatic Se_4^{2+} and Te_4^{2+} dications were prepared utilising the routes delineated in Eqs. (1) and (2) or Eq. (3) (Tables 3 and 4). A dependence of the E–E bond lengths in E_4^{2+} on the nature of the counterion has been noted [13], with the less basic, fluoride-based anions giving rise to shorter E–E bond distances and the more basic, chloride and bromide-based ions leading to slightly longer E–E bond lengths.

2.1.3. Se_{17}^{2+}

Salts of the Se_4^{2+}, Se_8^{2+} and Se_{10}^{2+} dications have been prepared previously. The unknown Se_{17}^{2+} dication was synthesised using a chemical vapour transport reaction of elemental selenium and WCl_6 forming $[Se_{17}^{2+}][WCl_6^{-}]_2$ [84]. The corresponding $NbCl_6^{-}$ and $TaBr_6^{-}$ salts [83] have also been prepared. We note that Se_{17}^{2+} had been proposed previously by Schrobilgen et al. [81a] as a low temperature disproportionation product of Se_{10}^{2+}, based on ^{77}Se-NMR studies. The structure of Se_{17}^{2+} is closely related to that of S_{19}^{2+} [70,74] and $Se_7Se_2Cl^{+}$ [131] and consists of two seven-membered rings in the chair conformation linked by a three-membered selenium chain. Se_{17}^{2+} contains two three-coordinated Se atoms, which formally bear a positive

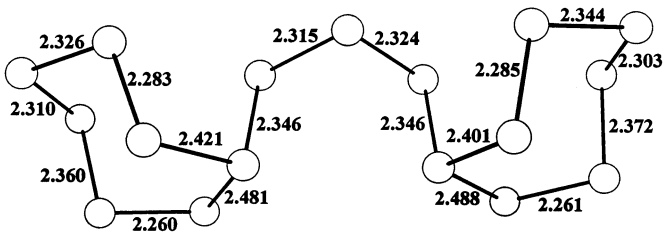

Fig. 1. Solid state structure of the Se_{17}^{2+} dication in $[Se_{17}^{2+}][WCl_6^{-}]_2$ [84]. Bond lengths are given in (Å).

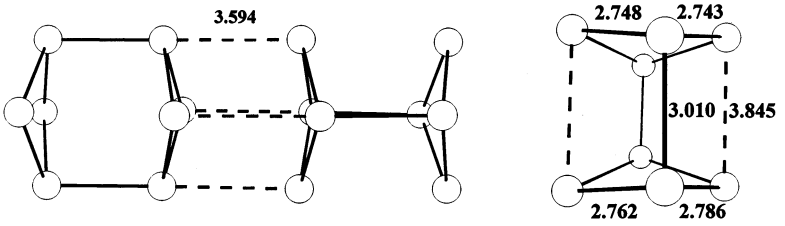

Fig. 2. Solid state structure of the Te_8^{4+} cation in $[Te_8^{4+}][VOCl_4^{2-}]_2$ [106]. Bond lengths are given in (Å).

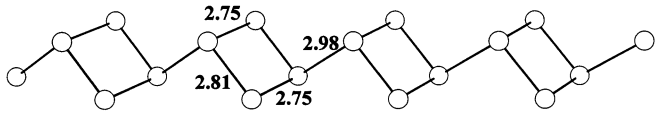

Fig. 3. The polymeric $(Te_4^{2+})_n$ cation in $[Te_4^{2+}][Te_{10}^{2+}][Bi_2Cl_8^{2-}]_2$ [13b]. Distances are given in (Å).

charge. Marked Se–Se bond length alternations are observed within the seven-membered rings. Se–Se distances range from 2.261 to 2.488 Å (see Fig. 1).

2.1.4. From monomeric Te_4^{2+} to dimeric $(Te_4^{2+})_2 = Te_8^{4+}$ and polymeric $(Te_4^{2+})_n$

A new approach to the preparation of homopolyatomic chalcogen cations was established recently by two of us (J. Passmore, I. Krossing [132]). The metathesis reaction of $Ag[Sb(OTeF_5)_6]$ with a 7:1 mixture of Te and $TeBr_4$ in SO_2 proceeds smoothly to give $[Te_4^{2+}][Sb(OTeF_5)_6^-]_2$ as the only species observed in the ^{125}Te-NMR spectrum.

$$7Te + TeBr_4 + 4Ag[Sb(OTeF_5)_6] \overset{SO_2,\ r.t.}{\rightarrow} 2[Te_4^{2+}][Sb(OTeF_5)_6^-]_2 + 2AgBr \qquad (4)$$

This intensely red coloured, square planar Te_4^{2+} dication is well known in a variety of salts and was shown by ^{125}Te-NMR spectroscopy [121,122], UV–vis- [95a,96,120] MCD- [124b], IR- and Raman spectroscopy [95ab,96] to retain this geometry in solution. However, if elemental tellurium and $VOCl_3$ are heated at 200°C, green $VOCl_2$ and Te_3Cl_2 are formed and react at 270°C in a Lewis-acid–base process to give $[Te_8^{4+}][VOCl_4^{2-}]_2$ which contains the polymeric $[VOCl_4^{2-}]_n$ anion chain (see Eq. (1)) [106]. The structure of the Te_8^{4+} cation can be visualised as being derived from a cube by elongating two sides to 3.85 Å, and can be viewed as a dimer of two square planar Te_4^{2+} dications (Fig. 2). The Te_8^{4+} units associate weakly along a fourfold screw axis in the solid state (3.59 Å).

The reaction of a mixture of tellurium, $TeCl_4$ and $BiCl_3$ at 170°C gives $[Te_4^{2+}][Te_{10}^{2+}][Bi_2Cl_8^{2-}]_2$, which contains infinite chains of a polymeric Te_4^{2+} dication fulfilling the requirements of a Zintl precise structure [13b]. The Te–Te bonds connecting the four-membered rings are longer (2.98 Å) than those found within the ring (2.75–2.81 Å) which are within the normal range found for single Te–Te bonds. This polymeric $(Te_4^{2+})_n$ can be regarded as a classical analogue to the non-classical, 6π aromatic Te_4^{2+} monomer (Fig. 3).

2.1.5. The boat shaped Te_6^{2+}

The solid state structure of the trigonal prismatic Te_6^{4+} cation was established in 1979 [99]. The formal addition of two electrons gives the reduced Te_6^{2+} dication which was first prepared in 1995 [98] by the one electron oxidation of elemental tellurium using $WOCl_4$ and giving $[Te_6^{2+}][WOCl_4^-]_2$ (see Eq. (3)) and also later [97] prepared from Te_3Cl_2 and $NbOCl_3$ (Eq. (5)).

$$3Te_3Cl_2 + 2NbOCl_3 \overset{220°C}{\rightarrow} [Te_6^{2+}][NbOCl_4^-]_2 + \ \ldots \quad (5)$$

The discrete, monomeric Te_6^{2+} dication consists of a boat shaped six-membered ring which in turn can be derived from the trigonal prismatic Te_6^{4+} structure by the shrinkage of two of the long bonds linking the Te_3^{2+} units from about 3.12 Å in Te_6^{4+} to normal Te–Te single bond lengths of 2.74 Å (av.), but increasing the length of one of the long bonds to 3.66–3.68 Å (see Fig. 4). A short–long–short bond length alternation is observed (starting at Te1).

The two transannular pairs of tellurium atoms Te3–Te5 and Te2–Te6 are separated only by 3.21–3.38 Å indicating a delocalisation of the positive charge over at least four atoms (sum of the van der Waals radii of Te: 4.30 Å).

2.1.6. Polymeric Te_7^{2+}

Two isomers of the previously unknown polymeric, heptatellurium dication were synthesised recently. The first isomer was obtained from elemental tellurium, tellurium halides and the transition metal oxohalides $NbOX_3$ [101] and WOX_4 (X = Cl, Br) [102,103] and was characterised structurally in the $[Te_7^{2+}]$-$[(MOX_4^-)(X^-)]$ (M = Nb, W; X = Cl, Br) salts. The repeating structural motif consists of a planar, centrosymmetric Te_7^{2+} unit in which one square planar, tetracoordinated tellurium atom is a common member of two four-membered rings. These units are further linked by four long Te–Te bonds (2.878 Å) to the next two Te_7^{2+} units forming an endless folded band (see Fig. 5). The Te–Te bond lengths around the tetracoordinated Te atoms are relatively long (2.93–2.97 Å) while those around the dicoordinated Te atoms are within the range found for normal Te–Te single bonds (2.75–2.77 Å).

The structure has been rationalised as containing one square-planar, tetracoordinated Te^{2-} and four tricoordinated Te^+ atoms in comparison to similar structural elements found within the polytellurium anions Te_5^{6-} and Te_7^{2-} [133]. Following

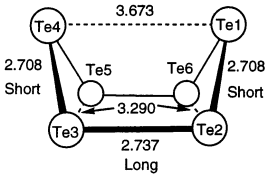

Fig. 4. The solid state geometry of Te_6^{2+}, averaged assuming local C_{2v} symmetry. The experimental bond lengths [Å] in $[Te_6^{2+}][MOCl_4^-]_2$ (M = W, Nb) range from 2.701 to 2.717 Å (Te1–Te2 and equiv., av. 2.708 Å), 2.733 to 2.742 Å (Te2–Te3 and equiv., av. 2.737 Å), 3.209 to 3.383 Å (Te2–Te6 and equiv., av. 3.290 Å) and from 3.655 to 3.683 Å (Te1–Te4 and equiv., av. 3.673 Å) [97,98].

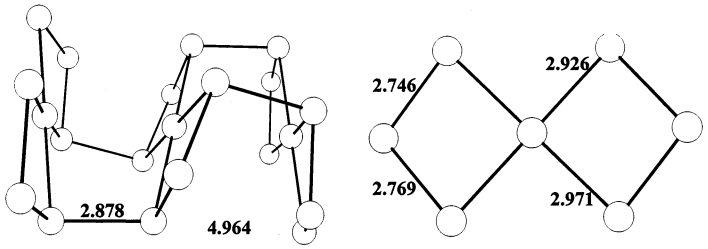

Fig. 5. Solid state structure of the polymeric $[Te_7^{2+}]_n$ dication in $[Te_7^{2+}][(WOCl_4^-)(Cl^-)]$ [102]. Distances are given in (Å).

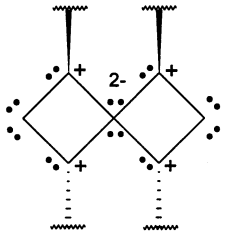

Fig. 6. Lewis structure of polymeric Te_7^{2+} [102].

this assignment, the structure of $[Te_7^{2+}]_n$ can be regarded as being electron precise and was described [102] by the Lewis-structure shown in Fig. 6.

The second Te_7^{2+} isomer was discovered in 1996 [100], prepared by the reaction of $Te_4(AsF_6)_2$ and $Fe(CO)_5$ in liquid SO_2. The precise role of the iron carbonyl is not clear, but one can conjecture that it presumably reduces the Te_4^{2+} to the Te_7^{2+} cation. Its structure is closely related to that of the known, polymeric Se_6I^+ cation [12,14,134a]. Six-membered Te_6 rings in the chair conformation are connected in the 1 and 4 positions to one bent, bridging tellurium atom, giving rise to endless $[(Te–Te_6)^{2+}]_n$ chains in $[Te_7^{2+}][AsF_6^-]_2$. This structure contains two three-coordinated tellurium atoms for each Te_7^{2+} unit that formally bear the positive charge. All the Te atoms in this Te_7^{2+} dication exhibit stabilising Te–F contacts which suggests that the positive charge is delocalised over all atoms (Fig. 7).

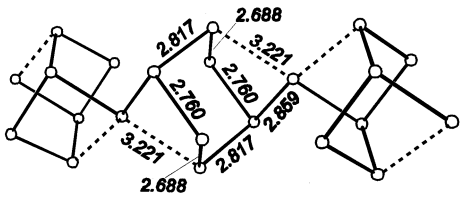

Fig. 7. The solid state structure of the polymeric $[(Te–Te_6)^{2+}]_n$ dication in $[Te_7][AsF_6]_2$ [100]. Distances are given in (Å).

2.1.7. Four isomers of Te_8^{2+}

The heavier tellurium homologue of the well established S_8^{2+} and Se_8^{2+} dications was prepared finally in 1990 [13b,104,105]. In fact, four different isomers are now characterised in the solid state, two of which adopt structures which are not even related to the first. The first form of Te_8^{2+} (which is isostructural to S_8^{2+} and Se_8^{2+}) was prepared by the reaction of 15Te, TeC and $2ReCl_4$ at 200°C giving $2[Te_8^{2+}][ReCl_6^{2-}]$ [104]. The central transannular Te–Te distance in the folded eight-membered ring in the *exo–endo* conformation is 3.153(1) Å, i.e. about 0.30 Å longer than those found for the (lighter) sulphur and selenium homologues. Cross ring distances in S_8^{2+} ($\sim$2.85 Å), Se_8^{2+} ($\sim$2.84 Å) and Te_8^{2+} ($\sim$3.25 Å) are about 0.80, 0.50 and 0.41 Å greater than the sum of their corresponding covalent radii and the lengths of the cross-ring interaction relative to the single bond distance decreases down the group. The solid state structure of this first isomer is displayed in Fig. 8.

The second isomer of Te_8^{2+} was prepared by the one electron oxidation of elemental tellurium with WCl_6 (see Eq. (2)). The analogous reaction of S_8 and WCl_6 gives a solid in which isolated sulphur and WCl_6 molecules cocrystallise without oxidation. Elemental selenium forms $[Se_{17}^{2+}][(WCl_6^-)_2]$ [84] and the more readily oxidised tellurium gives the $[Te_8^{2+}][WCl_6^-]_2$ salt [105]. The X-ray crystal structure of this compound is related to the previous one, although it has a more pronounced bicyclic nature: Two five-membered rings in the envelope conformation share one long side (2.99 Å), the centre of which incorporates a two fold rotational axis perpendicular to the bond. However, these Te_8^{2+} units associate forming an undulated chain containing four long Te–Te contacts per unit (3.43 Å, the sum of the tellurium van der Waals radii is 4.30 Å), shown in Figs. 9 and 10.

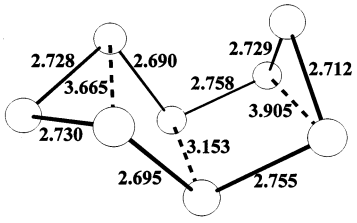

Fig. 8. Solid state structure of the isolated, discrete Te_8^{2+} dication as found in $[Te_8^{2+}][ReCl_6^{2-}]$ [104]. Distances are given in (Å).

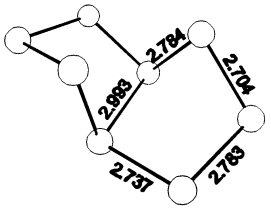

Fig. 9. Solid state structure of the C_2 symmetric Te_8^{2+} in $[Te_8^{2+}][WCl_6^-]_2$ [105]. Distances are given in (Å).

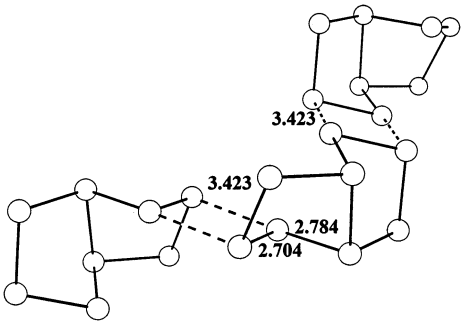

Fig. 10. Solid state structure of polymeric Te_8^{2+} in $[Te_8^{2+}][WCl_6^-]_2$ [105]. Distances are given in (Å).

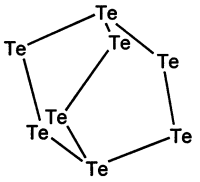

Fig. 11. Te_8^{2+} in a bicyclo[2.2.2]octane geometry in $[Te_6^{2+}][Te_8^{2+}][WCl_6^-]_4$ [13b].

The third isomer was prepared by a solvothermal reaction between Te and WCl_6 and also from Te, $TeCl_4$ and $NbCl_5$ in $SnCl_4$ at 150°C yielding the mixed $[Te_6^{2+}][Te_8^{2+}][MCl_6^-]_4$ (M = W, Nb) [13b] salts which contain the discrete boat shaped Te_6^{2+} dication and Te_8^{2+} having a bicyclo[2.2.2]octane geometry. The latter geometry was found previously in the $Te_2Se_6^{2+}$ interchalcogen cation in $[Te_2Se_6^{2+}]$-$[Te_2Se_8^{2+}][AsF_6^-]_4$ [135]. This Te_8^{2+} isomer has a classical, Zintl precise structure and possesses two tricoordinated Te atoms bearing the formal positive charge shown in Fig. 11.

The last of the four isomers of Te_8^{2+} is found to have a structure closely related to that of Se_6I^+ [134b,c] and one of the Te_7^{2+} structures. It was obtained by a chemical vapour transport reaction from Te, $TeCl_4$ and $BiCl_3$ giving $[Te_8^{2+}][Bi_4Cl_{14}^{2-}]$ which contains the polymeric $Bi_4Cl_{14}^{2-}$ counterion [13b]. This Te_8^{2+} solid state geometry consists of six-membered Te_6 rings in the boat conformation that are linked in the 1,4 position by a two-membered Te–Te bridge forming an endless chain. This arrangement is formally electron precise and fulfils the requirements of the Zintl rules (see Fig. 12).

2.1.8. Polymeric Te_{10}^{2+}

A dication containing 10 sulphur atoms is, presently, not known, although the solid state structure of the heavier Se_{10}^{2+} homologue was determined in 1980 [82]. A polymeric Te_{10}^{2+} salt with a very different geometry to that of the monomeric Se_{10}^{2+} dication was recently synthesised from Te, $TeCl_4$ and $BiCl_3$ at 170°C [13b]. It is found in the mixed $[Te_4^{2+}][Te_{10}^{2+}][Bi_2Cl_8^{2-}]_2$ salt (see Section 2.1.4). The solid state structure of this polymeric Te_{10}^{2+} cation is related to one of the previously described

Te_7^{2+} geometries (see Fig. 5) and consists of two tetracoordinated, six tricoordinated and two dicoordinated tellurium atoms. The two tetracoordinated Te atoms are members of two adjacent planar four-membered rings and the six tricoordinated centres link the planar Te_{10}^{2+} units giving an infinite folded band. A similar interpretation of the structure to that of the related Te_7^{2+} cation yields the two tetracoordinated Te atoms as (first order) Te^{2-} units but the six tricoordinated atoms as Te^{+} units giving an overall charge of $+2$. The resulting Lewis structure is similar to that proposed for Te_7^{2+} in Fig. 6. Fig. 13 shows a section of the solid state structure of the Te_{10}^{2+} dication.

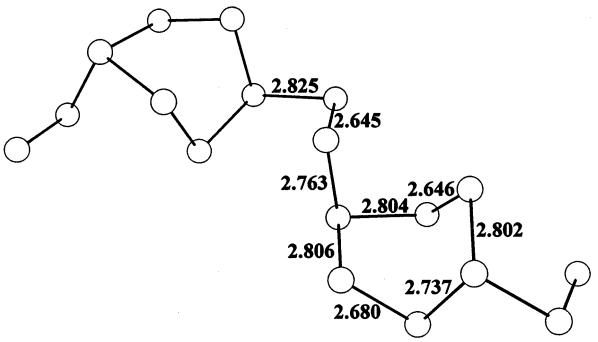

Fig. 12. Solid state structure of polymeric $[(Te–Te_6–Te)^{2+}]_n$ in $[Te_8^{2+}][Bi_4Cl_{14}^{2-}]$ [13b]. Distances are given in (Å).

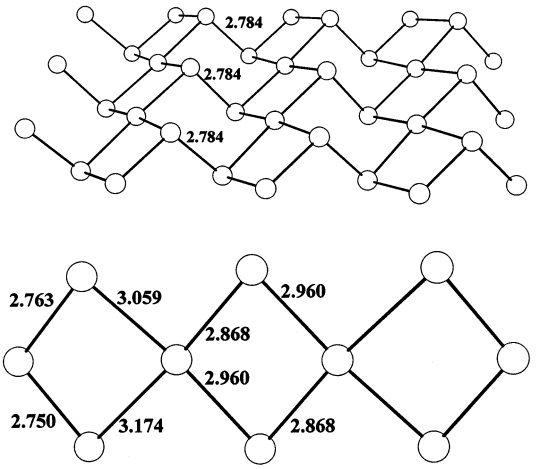

Fig. 13. A section of the solid state structure of $(Te_{10}^{2+})_n$ in $[Te_4^{2+}][Te_{10}^{2+}][Bi_2Cl_8^{2-}]_2$ [13b]. The planar, centrosymmetric Te_{10}^{2+} units are shown in the lower representation. Distances are given in (Å).

2.2. New homopolyatomic halogen cations

Some recent advances have been made in the determination of the solid state structures containing chlorine and bromine cations, however no new iodine cations have been prepared since the 1989 review [11].

2.2.1. Chlorine cations

There are reports of salts of Cl_2^+, presented at conferences and in PhD theses supervised by N. Bartlett [136] that show that Cl_2 reacts at very low temperatures (10 K) with IrF_6 giving a blue salt. This was assigned, by Raman spectroscopy, to be $[Cl_2^+][IrF_6^-]$. This blue material decomposes at low temperatures (193 K) to give yellow $[Cl_3^+][IrF_6^-]$ which further decomposes upon warming up to room temperature (r.t.) with the loss of Cl_2 and ClF to give IrF_5. Very recently, the preliminary X-ray crystal structure of the rectangular Cl_4^+ cation was reported by K. Seppelt in $[Cl_4^+][IrF_6^-]$ [68b] (obtained by the reaction of IrF_6 with Cl_2).

When Cl_2 was reacted with $[O_2^+][MF_6^-]$ (M = As, Sb) in anhydrous HF, a violet, a blue, and a yellow solution was formed; subsequently crystals from the violet solution were identified structurally by Seppelt et al. as the SbF_6^- and $Sb_2F_{11}^-$ salts of $Cl_2O_2^+$ [61]. By warming the aforementioned solutions in the presence of excess chlorine to r.t. the Cl_3^+ cation was synthesised recently and characterised structurally in its AsF_6^-, SbF_6^-, $Sb_2F_{11}^-$ and $Sb_3F_{16}^-$ salts [61]. The Cl_3^+ cation has C_{2v} symmetry, with Cl–Cl bond distances that range from 1.972 (1) to 1.994 (1) Å, and Cl–Cl–Cl bond angles between 104.5(1) and 105.62(7)°. Prior to this work, this cation was characterised in its $[Cl_3^+][SbF_6^-]$ [64] and $[Cl_3^+][AsF_6^-]$ [62] salts using low temperature Raman spectroscopy.

2.2.2. Bromine cations

The well known Br_2^+ cation was characterised previously by means of Raman spectroscopy [116] and by a single-crystal X-ray structure analysis of its $Sb_3F_{16}^-$ salt [55]. The Br_3^+ cation was first characterised in solutions of Br_2 and $S_2O_6F_2$ in either HSO_3F or SbF_5–$3SO_3$–HSO_3F in the late 1960s [116]. Br_3^+ was also identified in the solid state as the AsF_6^- salt [57a] by UV–vis, IR and mass spectroscopy, and was prepared from Br_2 and either $[O_2^+][AsF_6^-]$ or $[BrF_2^+][AsF_6^-]$, or from Br_2, BrF_5 and AsF_5 [57a,b]. However, the crystal structure of $[Br_3^+][AsF_6^-]$ was not determined until 1991 [57b], and consists of discrete AsF_6^- and Br_3^+ ions, the cation possessing C_{2v} symmetry and having an average Br–Br bond length of 2.270(5) Å and a Br–Br–Br bond angle of 102.5(2)°. Br_3^+ exhibits cation–anion interactions which serve to distort the geometry of the octahedral AsF_6^-.

Br_5^+ was first prepared as the $[Au(SO_3F)_4]^-$ salt from the reaction of $[Br_3^+][Au(SO_3F)_4]^-$ with excess bromine at 70°C and characterised by Raman spectroscopy [57c]. $[Br_5^+][AsF_6^-]$ was also prepared as a by-product in the synthesis of $[Br_3^+][AsF_6^-]$ from $[BrF_2^+][AsF_6^-]$ and Br_2 [57b]. Crystals of $[Br_5^+][MF_6^-]$ (M = As, Sb) were obtained from the reaction of Br_2 with $[XeF^+][MF_6^-]$ [59] and contain the planar, centrosymmetric Br_5^+ cations having central and terminal Br–Br bond distances in the AsF_6^- $[SbF_6^-]$ salts of 2.512(1) [2.514 (1)] Å and 2.275 [2.268(2)] Å,

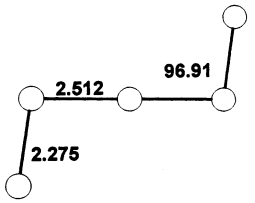

Fig. 14. The solid state structure of the Br_5^+ cation in $[Br_5^+][AsF_6^-]$ [59]. Distances are given in Å.

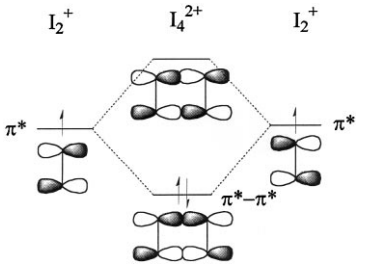

Fig. 15. MO representation of the four centre two electron π*–π* bond in I_4^{2+} (qualitative relative energies only, here and elsewhere).

respectively. The central Br atom is almost coordinated linearly by two Br atoms [Br–Br–Br = 178.1(2)°], and the terminal Br–Br–Br bond angles were found to be 96.91(4) and 97.69(5)° for the AsF_6^- and SbF_6^- salts, respectively. The central Br–Br–Br bond angle has been calculated to be 168.6°, using the local density functional approximation [60], and our recent MPW1PW91/3-21G* calculations result in an angle of 180.0° (Fig. 14).

3. Bonding in the homopolyatomic cations

Many of the geometries of the homopolyatomic cations of the chalcogens and the halogens are not readily explained by a classical electron precise Lewis approach. One of us (J. Passmore) proposed [11,14] that structures in which positive charges are localised on one atom are not adopted. Rather positive charge is delocalised over all atoms so minimising electrostatic repulsion. This leads to the observed geometries containing bond lengths alternation, np_π–np_π bonds ($n \geq 3$), long intracationic transannular interactions and cluster like geometries resulting from four centre two electron and six centre two electron π*–π* bonds (as in I_4^{2+} and S_8^{2+}). A representation of a four centre two electron π*–π* bond is shown in Fig. 15 for I_4^{2+}. The electrons residing in the singly occupied π* orbital of I_2^+ overlap and form two molecular orbitals of π symmetry, one is transannularly bonding and occupied (i. e. the orbital labelled π*–π* in Fig. 15) and one is antibonding and empty. The resulting π*–π* bond in I_4^{2+} accounts for the weak interaction between the now weakly bound I_2^+ moieties [d(I–I) = 3.270(1) Å, I–I bond order: 0.5].

This arrangement delocalises the positive charges over all four atoms and is favoured relative to the Lewis structure in which the charges are localised on two adjacent iodine atoms.

This approach was qualitative and supported by model ab initio calculations. More recently, this thesis has received strong support from our ab initio calculations on E_4^{2+} and E_8^{2+} (E = S, Se, Te) [16,32]. In addition we found that the $np^2 \rightarrow n\sigma^*$ interaction ($n = 3, 4, 5$) also delocalises the positive charge [16,32]. Intermolecular $np^2 \rightarrow n\sigma^*$ interactions are well established in charge transfer complexes, e.g. $R_3N \rightarrow I_2$, and were shown by Steudel to account for the bond alternation in S_7 [137,138]. The $np^2 \rightarrow n\sigma^*$ ($n = 3, 4, 5$) interactions are more important for the heavier group members since the energy difference of the orbitals involved is smaller as n increases making this bonding more favourable as the group is descended. Such bonding is very versatile, can be inter- or intracationic, and allows the formation of many different structures which are similar in energy. It is for this reason that cations of the heavier chalogens and halogens possess a more diverse structural chemistry and also form oligo- or polymeric species. It is also the reason that intermolecular interactions amongst the Groups 16 and 17 elements increase for the heavier elements. For the lighter group members only one geometry, and thus one type of bonding, is preferred thermodynamically (e.g. square planar E_4^{2+}, E_8^{2+}; E = S, Se; Br_2^+, Br_5^+). However, such a statement does not hold for tellurium and iodine [e.g. Te_4^{2+} vs. $(Te_4^{2+})_2$ or $(Te_4^{2+})_n$; four isomers of Te_8^{2+}; I_2^+ vs. I_4^{2+}, I_5^+ vs. I_{15}^{3+}]. This may be illustrated further by comparison of the number of presently known sulphur (chlorine) cations and the respective tellurium (iodine) species (e.g. the number of different solid state geometries known to date): Whilst for sulphur (chlorine) only three (1) different homopolyatomic cations have been unambiguously identified by X-ray crystallography, at least 13 (5) different species are known for the heaviest members of their groups.

3.1. Bonding in the homopolyatomic chalcogen cations

Quantum chemical calculations of the homopolyatomic chalcogen cations have proved to be difficult because of the need to employ large and flexible basis sets as well as to provide an accurate description of the electron correlation. Accordingly, correct optimised geometries of some species were not always obtained (e.g. E_8^{2+}, E = S, Se, Te) [16] and hence no theoretically based interpretations of their bonding or thermochemistry could be given. However, evolution of new methods and greatly enhanced computational power now provide us with a number of recent, accurate determinations of geometries, energetics and bonding of the homopolyatomic chalcogen cations. This allows us to discuss the properties of E_4^{2+}, E_8^{2+} (E = S, Se, Te) and Te_6^{4+}, for which the bonding was investigated thoroughly by means of ab initio molecular orbital theory, with confidence. We will interpret the bonding in the other, not theoretically assessed, cations by analogy with the bonding in the cations which have been investigated rigorously. We will first examine the known homopolyatomic cations in the highest formal oxidation state ($+2/3$) and later discuss less highly charged species.

3.1.1. Oxidation state +2/3: E_3^{2+} (E = S, Te) and Te_6^{4+}

The trigonal prismatic Te_6^{4+} cation was rationalised as a π*–π* bonded $(Te_3^{2+})_2$ dimer [11]. We will first describe the properties of its monomer Te_3^{2+} and the closely related lighter congener S_3^{2+} before we discus the dimers. Using high level ab initio MO theory [18], it was shown that S_3^{2+} has a $^3A_1$ triplet ground state and possesses a triangular, D_{3h} symmetric geometry with a best S–S bond length of 2.03 Å. The $^1A_1$ singlet state of S_3^{2+} is 45 kJ mol^{-1} higher in energy than the triplet state [139]. S_3^{2+} is a delocalised 4π electron species, the π-orbitals of which are depicted in Fig. 16 (the same orbitals hold for Te_3^{2+}).

Overall one π-bond is formed, delocalising the positive charge and shortening the S–S bond by 0.03 Å when compared to the normal covalent S–S distance of 2.060 Å as in S_8. The heavier Te_3^{2+} dication was computed to have a Te–Te distance of 2.750 Å [140].

Good quality DFT calculations show that the elongated trigonal prism is the ground state geometry of the Te_6^{4+} tetracation [31]. This agrees with the experimental X-ray crystal structure determination (see Fig. 17) [99] but conflicts with earlier computational findings at the semiempirical Fenske–Hall and extended Hückel levels of theory [141].

The classically anticipated C_{2v} boat structure with four tricoordinated, formally positively charged Te atoms has no stationary point on the Te_6^{4+} hypersurface. However, elongation of one of the long bonds by 0.5 Å results in a bonding situation, which increases the energy by only 25 kJ mol^{-1}, see [31] (Fig. 18).

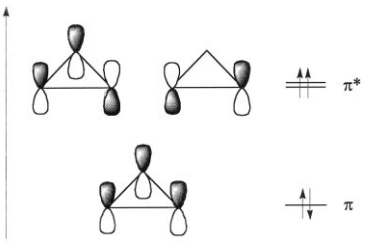

Fig. 16. The three molecular orbitals of π-symmetry in E_3^{2+} (E = S, Te).

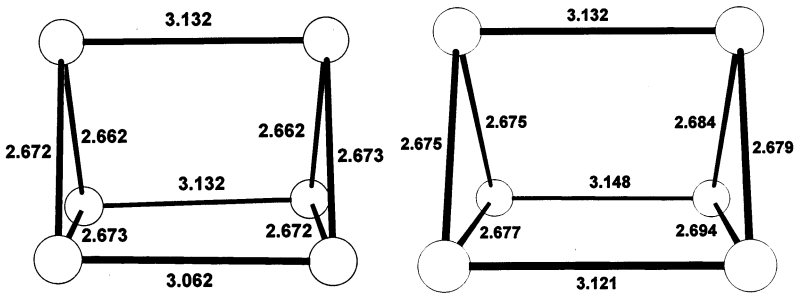

Fig. 17. The solid state geometry of Te_6^{4+} in $[Te_6^{4+}][AsF_6^-]_4{\cdot}2SO_2$ and $[Te_6^{4+}][AsF_6^-]_4{\cdot}2AsF_3$ [99]. Distances are given in Å.

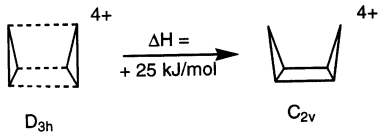

Fig. 18. Conversion of the elongated prism (D_{3h}) of Te_6^{4+} into a C_{2v} symmetric boat structure.

The interaction of the two Te_3^{2+} units in Te_6^{4+} was described [11] as a π*–π* six centre four electron bond of the two unpaired electrons residing in the π* orbitals of the Te_3^{2+} moieties (see Fig. 16). This view still prevails and is now described based on Ref. [31]. The six $5p_z$ orbitals (being parallel to the threefold axis) of the six Te atoms in Te_6^{4+} can be converted into six molecular orbitals of a_1', a_2'', e' and e'' symmetry. Two MOs are bonding within the Te_3^{2+} rings (a_1' and a_2), two are nonbonding (e') within the Te_3^{2+} moieties but bonding between the Te_3^{2+} units, and two of them are antibonding (e''). Only eight electrons reside in these six molecular orbitals resulting in bond shortening within the Te_3^{2+} units (one π-bond per Te_3^{2+} unit) and a six centre four electron bond between the two Te_3^{2+} rings, arising from the two e' orbitals, since the a_1' contribution is cancelled by the a_2'' orbital. The e' orbitals are a representation of the interaction of two singly occupied π* orbitals in Te_3^{2+} and thus the overall description of the bonding between the two Te_3^{2+} units as a six centre four electron π*–π* bond holds (compare to the E_3^{2+} orbitals above). A graphic representation for the bonding molecular orbitals is provided in Fig. 19 below.

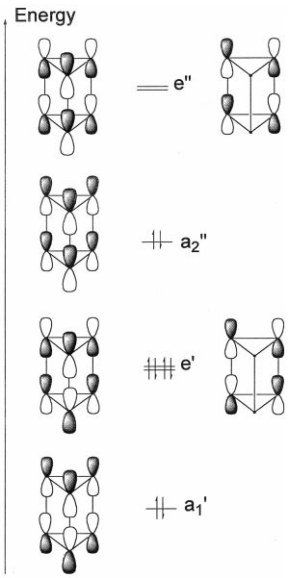

Fig. 19. Calculated molecular orbitals of the Te_6^{4+} dication at the BP88/TZ(d,p) level of theory [31].

A six-centre four electron π*–π* bond assigns a bond order of 2/3 to the longer sides of the prism in good agreement with the experimentally determined long bond distances of 3.06–3.13 Å [99] (cf. Te–Te single bond: 2.74 Å). However, in the gas phase, two equivalents of the Te_3^{2+} dication are more stable by 1046 kJ mol^{-1} than Te_6^{4+} (Eq. (6)) [142].

$$Te_6^{4+}\ (g) \rightarrow 2Te_3^{2+}\ (g)\ \Delta H = -1046\ \text{kJ mol}^{-1} \quad (6)$$

This high gas phase dissociation enthalpy arises as a result of the strong Coulomb repulsion which exists between the two doubly charged ions. In the homologous $S_6^{4+}/2S_3^{2+}$ system, an even higher gas phase dissociation energy of -1278 kJ mol^{-1} was found [143].

3.1.2. Oxidation state +0.5: E_2^+, E_4^{2+}, E_8^{4+} and $(E_4^{2+})_n$

The O_2^+ radical cation was the first homopolyatomic chalcogen or halogen cation to be characterised unambiguously [4]. A formal O–O bond order of 2.5 is expected which is in good agreement with the observed short O–O bond length (cf. O_2, 1.21 Å; O_2^+, 1.12 Å). In contrast to all the heavier homologues, no indication of the formation of a doubly charged O_2^+ dimer (=O_4^{2+}) has been found experimentally while the S_2^+, Se_2^+ and Te_2^+ radical cations associate in solution and in the solid state to form monomeric E_4^{2+} (E = S, Se, Te). The square planar E_4^{2+} species were shown to be 6π aromatic [20,33], for which the constituting π-orbitals are depicted in Fig. 20 below.

Three sets of orbitals are formed: one bonding π-orbital (A_{2u}), two nonbonding (E_g) and one antibonding (B_{2u}, unoccupied) orbitals. Overall, one π bond is delocalised over all four atoms thus giving a formal bond order of 1.25, which is in good agreement with the calculated Wiberg bond orders of 1.249–1.253 as computed for E_4^{2+} (E = S, Se) [33] and the experimentally found, relatively short E–E bonds.

Several E_4^{2+} (E = S, Se) isomers were examined recently using good quality ab initio MO descriptions [33]. This investigation showed that the square planar, D_{4h}

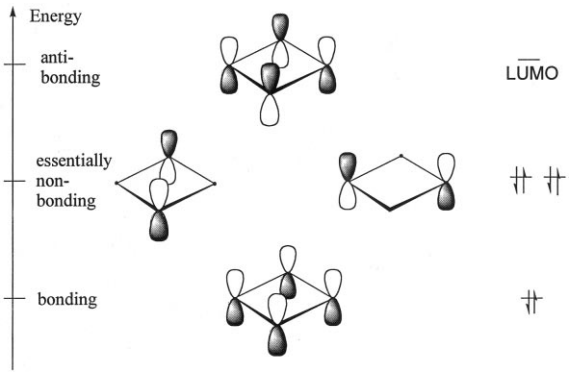

Fig. 20. Molecular orbitals of π-symmetry in E_4^{2+} [20,33].

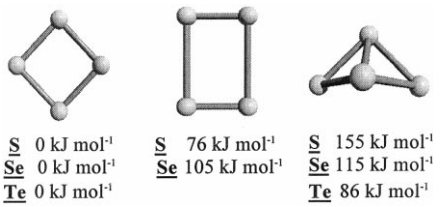

Fig. 21. Optimised D_{4h}, D_{2h} and C_{2v} geometries of E_4^{2+} (E = S, Se, Te) [33].

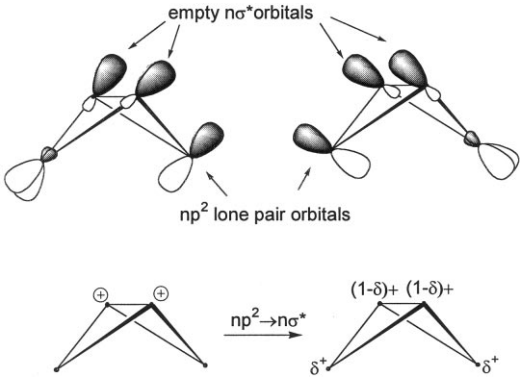

Fig. 22. $np^2 \rightarrow n\sigma^*$ bonding ($n = 3, 4, 5$) in the butterfly shaped E_4^{2+} isomer (E = S, Se, Te) [33].

symmetric E_4^{2+} isomer is the global minimum in the gas phase (as it is in the solid state). Surprisingly it was found that a D_{2h} symmetric, π*–π* bonded $(E_2^+)_2$ dimer is the second most stable isomer [E_{rel}(S): + 76 kJ mol^{-1}; E_{rel}(Se): + 106 kJ mol^{-1}], which is favoured over an all σ bonded C_{2v} symmetric bicycle [E_{rel}(S): + 155 kJ mol^{-1}; E_{rel}(Se): + 115 kJ mol^{-1}, E_{rel}(Te): + 86 kJ mol^{-1}]. The D_{2h} $(Te_2^+)_2$ dimer does not have a stationary point on the Te_4^{2+} hypersurface. All geometries are summarised in Fig. 21.

Although the butterfly shaped C_{2v} bicycle E_4^{2+} (E = S, Se. Te) is a Zintl precise species, the calculated natural charges in these dications are delocalised [bridgehead: + 0.55 to + 0.58, bridging atom: + 0.42 to 0.45]. According to a NBO analysis, this positive charge delocalisation is achieved by $np^2 \rightarrow n\sigma^*$ interactions which transfer electron density from the occupied np^2 lone pair orbitals of the dicoordinated sulphur atoms into the empty, vicinal $n\sigma^*$ orbital, as shown in Fig. 22.

The four equivalent $np^2 \rightarrow n\sigma^*$ interactions in C_{2v}–E_4^{2+} (E = S, Se, Te) lower the total energy by about 80–100 kJ mol^{-1} and transfer about 0.2 electrons from the two np^2 lone pair orbitals to the four vicinal E–E $n\sigma^*$ bonds (NBO-analysis). This reduces the formally unipositive charge on the tricoordinated atoms and lengthens the vicinal E–E bonds by 8–10 pm [33].

The structural chemistry of the Te_4^{2+} dication is more diverse due to a lower Coulomb repulsion, less stable π bonds and the more favourable $5p^2 \rightarrow 5\sigma^*$ bonding. Consistently the gaseous, π*–π* bonded D_{2h} rectangle of Te_4^{2+} is not a

minimum on the Te_4^{2+} hypersurface. With a variety of monomeric, univalent and hard counterions such as MF_6^- (M = As, Sb) or $AlCl_4^-$, the 6π aromatic square is formed, whilst the polymeric, higher charged and more basic $(VOCl_4^{2-})_n$ anion promotes the formation of a dimeric Te_8^{4+} cation [106] and a polymeric chain of $(Te_4^{2+})_n$ is observed in the mixed $[Te_4^{2+}][Te_{10}^{2+}][Bi_2Cl_8^{2-}]_2$ salt [13b].

3.1.2.1. Bonding in Te_8^{4+}. The structure of Te_8^{4+} [106] is obtained formally by a dimerisation of two equiv. of Te_4^{2+}. The long Te–Te bonds that connect the two four-membered rings (3.01 Å) in Te_8^{4+}, imply the presence of electron density within the respective antibonding σ* orbitals. The Te–Te bonds in the ring are in the range of normal Te–Te single bonds (2.74–2.77 Å). The Te_8^{4+} units are found to be weakly associated in the solid state giving an endless linear chain in which the Te_8^{4+} units are separated by 3.59 Å and are aligned along a fourfold screw axis. Such observations as these can be explained assuming an intra- and intermolecular $5p^2 \rightarrow 5\sigma^*$ interaction which delocalises the unfavourable localised positive charges formally residing on the four tricoordinated Te atoms, as is shown in Figs. 23 and 24.

The occupied $5p^2$ lone pair orbitals of the four dicoordinated Te-atoms in the Te_4 rings donate electron density into the empty, antibonding 5σ* orbitals of the two Te^+–Te^+ bonds connected to the two four-membered rings. Such an interaction serves to lengthen the two central Te–Te bonds (cf. 3.01 Å) and also allows for positive charge delocalisation over all eight tellurium atoms. Moreover, such a model allows the formation of intermolecular interactions between the Te_8^{4+} units, every second of which is canted by 90° towards the others. In this orientation, an intermolecular $5p^2 \rightarrow 5\sigma^*$ donor–acceptor interaction becomes favourable account-

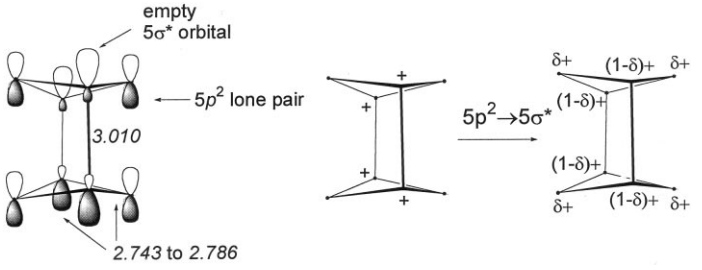

Fig. 23. Bonding in Te_8^{4+}: intramolecular $5p^2 \rightarrow 5\sigma^*$ interactions (distances are given in Å).

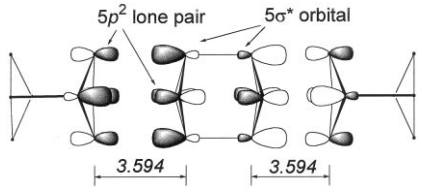

Fig. 24. Bonding in Te_8^{4+}: intermolecular $5p^2 \rightarrow 5\sigma^*$ interactions (distances are given in Å). (Reprinted with permission from [33], Copyright 2000 American Chemical Society.)

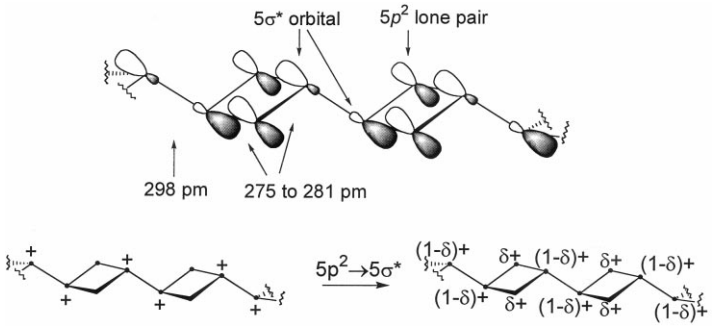

Fig. 25. $5p^2 \rightarrow 5\sigma^*$ interactions in the solid state structure of polymeric $(Te_4^{2+})_n$.

ing for the short intermolecular distance of 3.59 Å and the chain like arrangement of the cations in the solid state (see Fig. 24).

3.1.2.2. Bonding in polymeric $(Te_4^{2+})_n$. Although this species [13b] is formally a Zintl-precise cation, it is not expected to exhibit localised charges on the tricoordinated tellurium atoms. Te–Te bonds connecting the almost planar four-membered rings are comparatively long (2.98 Å) whilst the ring distances are in the range of normal Te–Te single bonds (2.75–2.81 Å). This can be understood by means of the $5p^2 \rightarrow 5\sigma^*$ interaction shown in Fig. 25.

The filled $5p^2$ lone pair orbitals of the dicoordinated Te atoms in the four-membered rings thereby donate electron density into the empty, vicinal $5\sigma^*$ orbital of the formally positively charged tricoordinated Te atoms so connecting the rings. Such an interaction lengthens the Te–Te distance between the rings (cf. 2.98 Å) whilst shortening the bonds within the ring itself and allowing the delocalisation of positive charge from the tricoordinated to the dicoordinated atoms. This implies that even the Zintl precise structure of $(Te_4^{2+})_n$ [13b] is governed by positive charge delocalisation which reduces the Coulomb repulsion between the adjacent, positively charged Te atoms connecting the rings.

3.1.3. Bonding in Te_6^{2+}

The boat shaped C_{2v} symmetric solid state structure of the Te_6^{2+} dication (in $[Te_6^{2+}][(MOCl_4)^-]_2$, M = Nb, W) [97,98] contains two weak transannular interactions between the central two pairs of Te atoms [d(Te–Te) = 3.209–3.383 Å] and exhibits a short–long–short bond alternation (starting at Te1, see Figs. 4 and 26). This geometry is reminiscent of that shown by the E_8^{2+} dications (E = S, Se, Te) [16] as examined by ab initio MO theory (see Section 3.1.5 below), and raises the question as to whether a similar approach can be used to explain the geometry of the Te_6^{2+} dication (see Fig. 4). It is reasonable to assume that electron density is removed from the $5p^2$ lone pair orbitals upon ionisation, as it is the case in E_8^{2+} [16]. Therefore the partially occupied $5p^2$ lone pair orbitals of the four central Te atoms can be converted into four molecular orbitals of π-symmetry, two are

bonding and two are antibonding. Adding six electrons to these orbitals results in a gain of one π-bond (0.5 π bond per Te_2 unit) which shortens the two central Te–Te bonds and has non-cancelled transannular contributions (see Fig. 26). The MOs of this series correspond to the representation of a $5p_\pi$–$5p_\pi$ and a four centre two electron intracationic π*–π* bond.

According to such a model one would expect a long–short–long bond length alternation (starting at Te1). However the experimental structure exhibits a short–long–short alternation with bond shortening between all adjacent Te atoms which is found to be more pronounced around the two apical Te1 and Te4 positions (see Fig. 4). Therefore, a second interaction must be considered which involves the apical atoms. This is provided by proposing an interaction between the occupied $5p^2$ lone pair orbital of the Te1 and Te4 atoms and the empty, vicinal Te2–Te3 and Te5–Te6 5σ* orbital [drawing an analogy with the similar situation in E_8^{2+} (E = S, Se, Te see below)]. This proposed $5p^2 \rightarrow 5\sigma^*$ interaction thus now shortens the bonds adjacent to Te1 and Te4 and two antibonding contributions serve to lengthen the central Te–Te bonds and counteract most of the bond shortening which arises due to the $5p_\pi$–$5p_\pi$ interaction. The net result therefore is a short–long–short bond alternation as is found experimentally [97,98] (cf. Fig. 27).

DFT calculations [31] support this picture. For Te_6^{4+} it was shown that the unoccupied *e″* orbitals (see Section 3.1.1) transform, upon lowering of the symmetry from D_{3h} to C_{2v}, into a $1b_1$ and a $2b_1$ orbital. The $1b_1$ orbital is lower in energy and so will be occupied upon reduction from Te_6^{4+} to Te_6^{2+}. This $1b_1$ orbital is

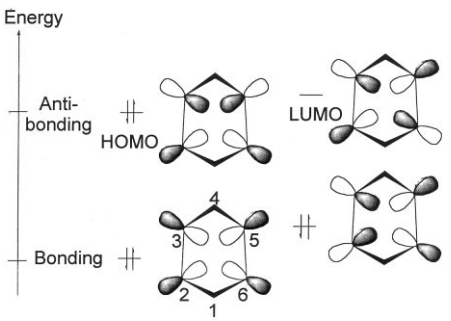

Fig. 26. $5p_\pi$–$5p_\pi$ bonding of the central four partially occupied 5p orbitals in the Te_6^{2+} dication.

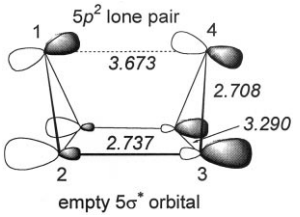

Fig. 27. $5p^2 \rightarrow 5\sigma^*$ interaction in Te_6^{2+} (distances are given in Å).

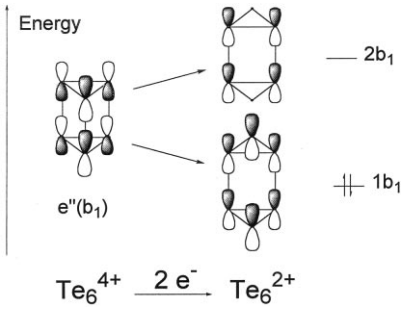

Fig. 28. Splitting of the unoccupied e'' orbital in Te_6^{4+} upon lowering of the symmetry to C_{2v} and addition of two electrons (to give Te_6^{2+}) [31].

almost identical to the proposed $5p^2$–$5\sigma^*$ interaction in Fig. 27; the splitting of the degenerate e'' orbitals in Te_6^{4+} is shown in Fig. 28.

The preference of the boat over the chair conformation can be explained by the improved overlap of the 5p orbitals constituting the $5p_\pi$–$5p_\pi$ bond in the boat isomer and a weak bonding interaction of the two partially occupied 5p lone pair orbitals at Te1 and Te4 which is not achievable within the chair conformation as is shown in Fig. 29b.

The $5p^2$ lone pair orbitals at Te1 and Te4 can be converted into two molecular orbitals, one of which is bonding and one is antibonding. Less than four electrons occupy these two orbitals and therefore a weak not bonding between Te1 and Te4 remains, in agreement with the long separation of 3.673 Å as is observed experimentally (see Fig. 29a). The 5p orbitals constituting the $5p_\pi$–$5p_\pi$ bond are orthogonal in the chair conformation, but aligned in the boat conformation so permitting good orbital overlap. Accordingly the boat conformation is preferred over the chair. The driving force behind this unusual $5p_\pi$–$5p_\pi$ bonding and the cluster like geometry of this Te_6^{2+} dication lies in the maximisation of positive charge delocalisation which minimises electrostatic Coulomb repulsion and renders π-bonding and the weak intracationic bonding more favourable than the classical σ-bonding [16].

3.1.4. Bonding in Te_7^{2+} and the closely related Te_{10}^{2+}

The bonding in the structurally closely related Te_7^{2+} and Te_{10}^{2+} cations [13b,101,102,103] was rationalised by proposing an auto-ionisation, leading to tetracoordinated Te^{2-} and tricoordinated Te^{+} units. However, although anions such as Te_5^{6-} or Te_7^{2-} [133] contain negatively charged tetracoordinate Te atoms that exhibit the same local planar geometry as the one found in Te_7^{2+}, it is not necessary to assume the presence of a localised dianionic Te atom (within the framework of a dication). The long distances around the tetracoordinate Te atoms in Te_7^{2+} and Te_{10}^{2+} can be accounted for by prescribing the following resonance structures (Fig. 30).

According to this model, the tetracoordinated Te atoms form four weak bonds of bond order 0.5 utilising its singly occupied $5p_x^1$ and $5p_y^1$ orbitals by forming two

three centre four electron bonds perpendicular to one another. Consistently, long Te–Te bond lengths of 2.93?2.97 Å around the tetracoordinated Te atoms result; a MO representation of this process is shown in Fig. 31.

The Te–Te distances around the dicoordinated Te-atoms are in the range of normal Te–Te single bonds and the Te–Te bonds connecting the planar 7-or 10-atomic units are considerably longer. These distances can be explained by a delocalised $5p^2 \rightarrow 5\sigma^*$ bonding scheme as shown in Fig. 32.

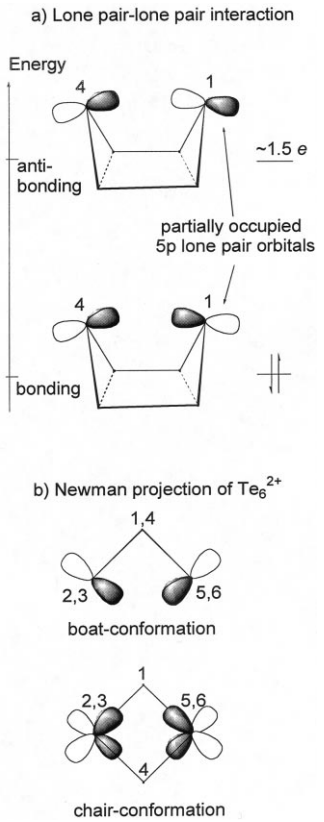

Fig. 29. Orientation of the $5p^2$ orbitals in Te_6^{2+} in boat and chair conformation, bonding interaction of the two partially occupied apical $5p^2$ lone pair orbitals.

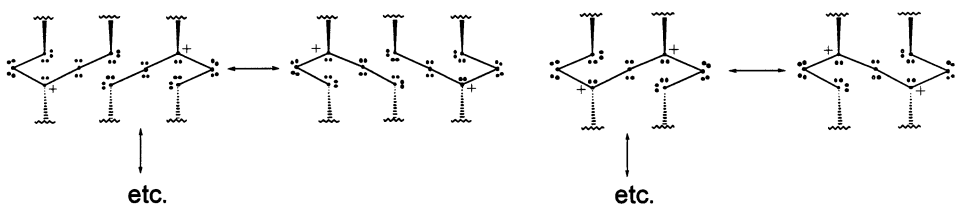

Fig. 30. Resonance structures for the Te_7^{2+} and Te_{10}^{2+} cations.

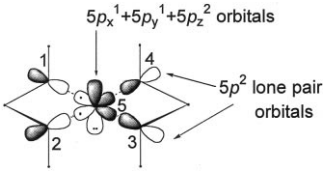

Fig. 31. Bonding of the central tetracoordinated Te atom in the polymeric Te_7^{2+} dication (and analogously in the Te_{10}^{2+} dication) [13b,101,102,103].

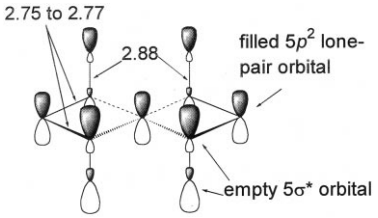

Fig. 32. $5p^2 \rightarrow 5\sigma^*$ bonding in polymeric Te_7^{2+} (and analogous in Te_{10}^{2+}), distances are given in Å [13b,101,102,103].

All $5p^2$ lone pair orbitals of the dicoordinated and tetracoordinated tellurium atoms donate electron density into the empty, antibonding 5?* orbital of the four (six) Te^+–Te^+ bonds which connect the planar units. Overall, we find long bonds in the connections (2.88 Å) and shorter bonds around the dicoordinated atoms (2.75?2.77 Å). The weak bonds between the tricoordinated and tetracoordinated Te atoms are correspondingly strengthened by donation from the $5p_z$ lone pair orbital of the tetracoordinate tellurium atom.

3.1.4.1. Bonding in $[(Te–Te_6)^{2+}]_n$. The six-membered Te_6 rings of this polymeric cation [100] (shown in Fig. 7) contain two long Te–Te bonds (2.817 Å) adjacent to the bridge, two short Te–Te bonds (2.688 Å) between the dicoordinated tellurium atoms and two normal Te–Te single bond lengths of 2.760 Å. The distance to the symmetric bridge is quite long (2.859 Å) and an additional weak contact connects one ring atom with the bridging atom. These observations can be accounted for by assuming two $5p^2 \rightarrow 5\sigma^*$ interactions as shown in Figs. 33 and 34(a).

The occupied $5p^2$ lone pair orbital of the two purely dicoordinated Te atoms within the Te_6 ring and the bridging Te atom in $[Te–Te_6)^{2+}]_n$ donate electron density into the empty vicinal antibonding $5\sigma^*$ orbital, as shown in Figs. 33 and 34(b). This lengthens the bonds which are vicinal to the dicoordinated atoms, but shortens those around the dicoordinated Te atoms. A second $5p^2 \rightarrow 5\sigma^*$ interaction explains the stacked solid state arrangement found in the cations in $[Te_7^{2+}][AsF_6^-]_2$. Electron density is transferred from the occupied $5p^2$ lone pair orbital of a ring tellurium atom into the empty, antibonding $5\sigma^*$ orbital of the ring–bridge connection. This explains the long bond to the bridging atom (2.859 Å) and the weaker contact to the second ring tellurium atom (3.221 Å). Such interactions allow the delocalisation of the positive charge over all seven atoms, which is in very good

agreement with the presence of the observed solid state Te–F contacts found to all the Te atoms in this structure.

3.1.5. Bonding in E_8^{2+} ($E = S, Se, Te$)

Solid state structures of the isostructural E_8^{2+} dications (E = S, Se, Te) [16,73a,89a,105] show the transannular proximity of the three central pairs of atoms in the folded, eight-membered rings in the *exo–endo* conformation (see experimental geometries in Fig. 35 below).

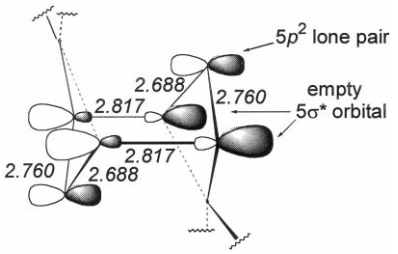

Fig. 33. $5p^2 \rightarrow 5\sigma^*$ interaction within the six-membered rings in the $[Te–Te_6)^{2+}]_n$ dication in $[Te_7^{2+}][AsF_6^-]_2$ (distances are given in Å) [100].

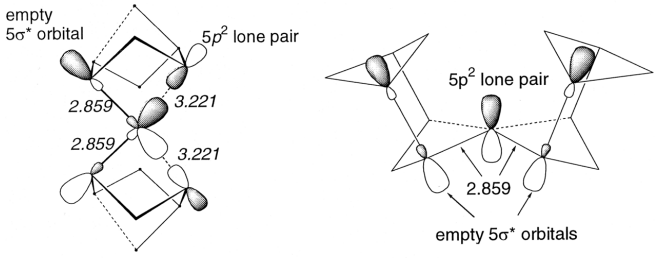

Fig. 34. $5p^2 \rightarrow 5\sigma^*$ interaction between one ring atom and the bridging Te atom in the $[Te–Te_6)^{2+}]_n$ dication in $[Te_7^{2+}][AsF_6^-]_2$ (distances are given in Å, structure is rotated by 90° vs. Fig. 33) [100].

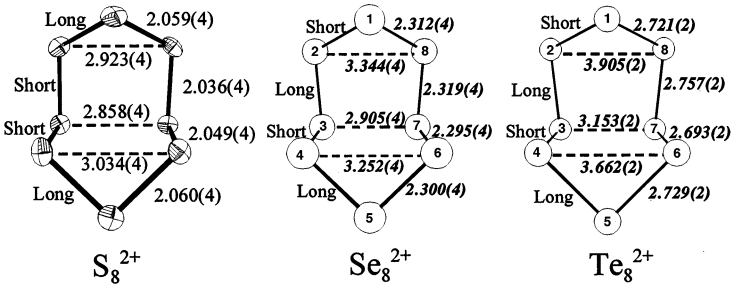

Fig. 35. Experimental bond lengths (averaged assuming local C_s symmetry) and bond alternation in the isostructural E_8^{2+} dications in $S_8(AsF_6)_2$, $(Se_8)(Te_6)(AsF_6)_6$ and $Te_8(ReCl_6)$. Distances are given in Å. (Reprinted with permission from [16], Copyright 2000 American Chemical Society.)

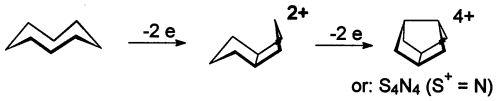

Fig. 36. Expected geometric changes upon oxidation of S_8 to S_8^{2+} and S_8^{4+}.

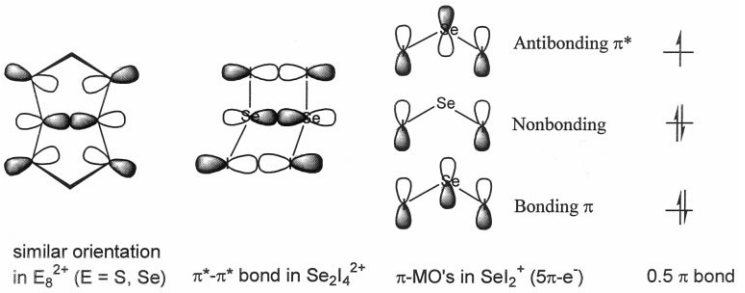

Fig. 37. Six centre two electron π*–π* bond in $Se_2I_4^{2+}$. (Reprinted with permission from [16], Copyright 2000 American Chemical Society.)

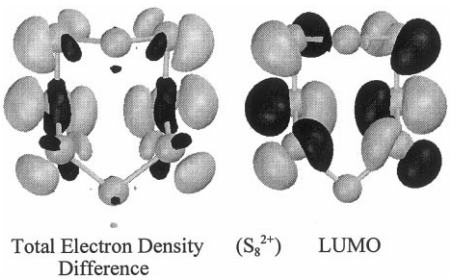

Fig. 38. The LUMO of S_8^{2+} and the total electron density difference of S_8 and S_8^{2+} (both in the C_s symmetric S_8^{2+} minimum geometry). Lighter shaded areas represent electron density left over from S_8 while the darker shaded areas represent electron density left over from S_8^{2+}. (Reprinted with permission from [16], Copyright 2000 American Chemical Society.)

The *exo–endo* conformation of S_8^{2+} was not unexpected, since it was rationalised as an intermediate between the *exo–exo* structure of S_8 crown and the cagelike *endo–endo* S_4N_4 (≡ isoelectronic to S_8^{4+}, Fig. 36) [6f,144,145].

While this model explains the overall geometry, it fails to account for the transannular bonds which are found to be much longer than usual E–E single bonds (in S_8^{2+}, 2.87–3.02 Å; in Se_8^{2+}, 2.84–3.35 Å; in Te_8^{2+}, 3.15–3.91 Å), although they are well below the sum of the respective van der Waals radii (S, 3.70 Å; Se, 3.90 Å; Te, 4.30 Å). The solid state structure of the $Se_2I_4^{2+}$ dication [146] shows a π*–π* bond formed by the π* orbitals of two SeI_2^+ moieties and exhibits a geometric arrangement similar to that found for the six central chalcogen atoms in E_8^{2+} (see Fig. 37).

Therefore the transannular bond in the Se_8^{2+} cation was also rationalised as a six-centre two electron π*–π* bond of the six atoms residing on opposite sides of

the ring (see the LUMO of S_8^{2+} in Fig. 38) [11,14,146]. A delocalisation of the positive charge over six atoms is achieved using this model and so one additional stabilising π bond is gained in total. Semiempirical CNDO and extended Hückel single point calculations have supported this view [11,147,148], but numerous attempts to fully optimise the structures of E_8^{2+} (E = S, Se, Te) have failed (one as recent as 1997) [26–28]. Very recently we did succeed in optimising the gas phase structures of E_8^{2+} (E = S, Se, Te) [16] and showed that most of the additional bonding in E_8^{2+} stems from the π interaction of the partially occupied np^2 lone pair orbitals of the central six atoms in E_8^{2+}. This is best visualised by the LUMO of E_8^{2+} (where the electrons are removed) and the total electron density difference of E_8 and E_8^{2+} (both in the C_s geometry of E_8^{2+}), depicted for E = S in Fig. 38.

The calculated Wiberg bond orders in E_8^{2+} (E = S, Se) show the presence of small bonding interactions between all transannular pairs of atoms. All eight σ bonds in the ring have higher bond orders than the one found for neutral E_8. For S_8^{2+} a long–short–short–long bond lengths alternation (starting at S1) was found experimentally and mirrored computationally, while for both Se_8^{2+} and Te_8^{2+} a short–long–short–long pattern is observed (see Fig. 35). The calculated positive charges are delocalised over all eight atoms and range from 0.2 to 0.3. This is in good agreement with evaluations of the positive charges residing on the individual atoms using I.D. Brown's methodology [16,149], which showed a nearly even delocalisation of the positive charge over all eight chalcogen atoms (E = S, Se). In the heavier homologues the charge on the two apical E1 and E2 atoms increases from +0.17 in S_8^{2+} to about +0.21 in Te_8^{2+}. Two major contributions are responsible for such observations: A np_π–np_π bond results from an interaction of the six partially filled np^2 lone pair orbitals ($n = 3, 4, 5$). These six np^2 lone pair orbitals can be converted into six molecular orbitals, two of which are bonding, two are nonbonding and two are antibonding. In total five of these six MOs are occupied giving a net result of one π bond delocalised over the six central atoms, shortening these four bonds and delocalising the positive charge over six atoms. The highest occupied A′ orbital of this series is the representation of the earlier proposed intramolecular π*–π* bond [11,14]. The transannular interactions in MO A are not cancelled and therefore they account for most of the transannular bonding (Fig. 39) and provide one π bond delocalised over the central six chalcogen atoms 2, 3, 4, 6, 7, 8.

However, according to this model (Fig. 39), one would expect the same long–short–short–long bond length alternation in all the E_8^{2+} (E = S, Se, Te) dications, which is not found to be the case. Moreover, AIM (atoms in molecules [150]) bond critical points should be found between all three transannular pairs of atoms (E2–E8, E3–E7, E4–E6) while only one was actually computed between E3 and E7 and an additional ring critical point was computed for Se_8^{2+} but not for S_8^{2+} {a bond (ring) critical point shows the presence of a bond (ring) [150]}. This ring critical point is due to a bonding interaction of the partially occupied $4p^2$ lone pair orbitals at Se1, Se4 and Se6, a MO representation of this bonding interaction is given below in Fig. 40.

This interaction is reminiscent of a closed B–B–B three centre two electron bond as is found in many polyboranes and boranates. Moreover, the experimentally

derived valency units and calculated natural charges place roughly a $+0.2$ to $+0.3$ charge on all eight chalcogen atoms. The delocalisation of the positive charge, including the two apical chalcogen atoms E1 and E5, is achieved by a $np^2 \rightarrow n\sigma^*$ ($n = 3, 4, 5$) interaction of the np^2 ($n = 3, 4, 5$) lone pair orbital at E1 and E5 with the vicinal empty antibonding σ^* orbital, as depicted in Fig. 41.

This $np^2 \rightarrow n\sigma^*$ interaction ($n = 3, 4, 5$) leads to bond shortening around the apical E1 and E5 atoms and bond lengthening around the central E3–E7 bond. This is more important for the heavier elements, since the energy gaps between the respective orbitals get smaller as the group is descended. Following this model, one would anticipate a small short–long–long–short bond lengths alternation in Se_8^{2+}, which is experimentally *not* observed (see Fig. 35). In contrast to S_8^{2+}, a third bond critical point is found in Se_8^{2+} centred within the Se1, Se4 and Se6 triangle; the transannular Se2–Se8 distance is longer than that between Se4 and Se6 [exp.: 3.344(4) vs. 3.252(4) Å], more pronounced still in Te_8^{2+} [exp.: 3.905(2) vs. 3.662(2)

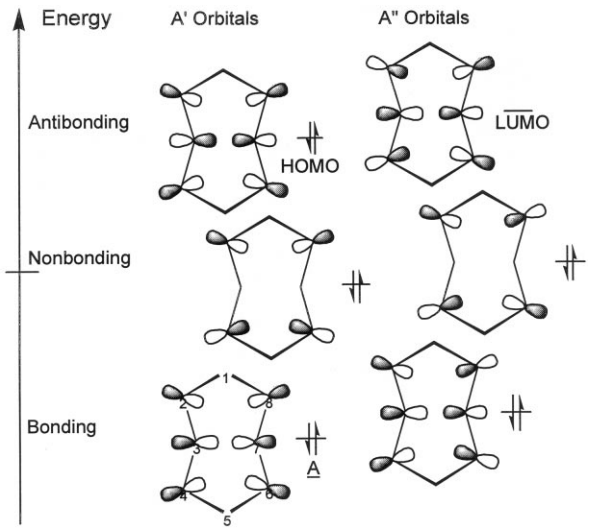

Fig. 39. The six molecular orbitals of π-symmetry in E_8^{2+} (E = S, Se, Te).

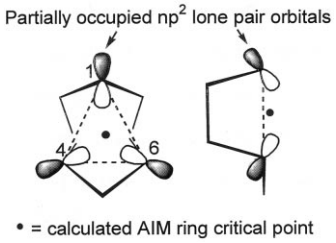

Fig. 40. Bonding interaction of the partially occupied np^2 lone pair orbitals ($n = 3, 4, 5$) at E1, E4 and E6. (Reprinted with permission from [16], Copyright 2000 American Chemical Society.)

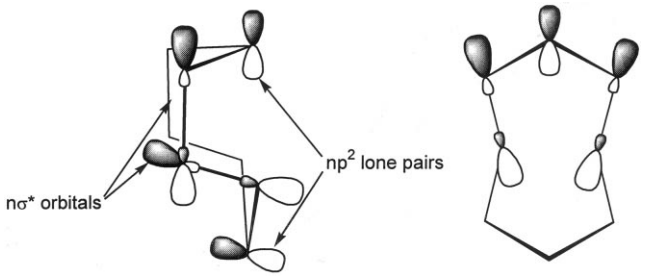

Fig. 41. $np^2 \rightarrow n\sigma^*$ bonding in E_8^{2+}.

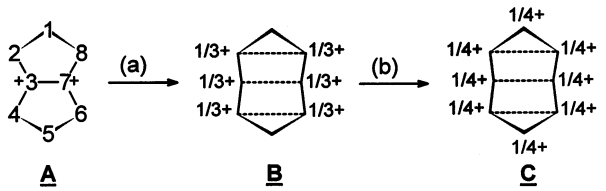

Fig. 42. Positive charge delocalisation in E_8^{2+} (E = S, Se, Te) [16].

Å, see Fig. 35]. The apical E1 atoms (E = Se, Te) bend downwards towards E4 and E6 due to an additional three centre σ-bond as shown in Fig. 40. This renders the orientation of the np^2 lone pair orbitals at E2 and E8 less favourable for np_π–np_π bonding and consistently the E2–E3 and E7–E8 bonds are the longest in the ion. This effect is more pronounced in the experimental solid state structure of Te_8^{2+}. Here the Te2–Te3 and Te7–Te8 distances are 6–7 pm longer than the adjacent Te3–Te4 and Te6–Te7 bonds which are the shortest in the ion (2.757 vs. 2.693 Å, see Fig. 35). To account for this stronger σ-bonding in Te_8^{2+} (Fig. 40), the $5p^2$ lone pair orbital at Te1 must be occupied by fewer electrons than in E_8^{2+} (E = S, Se). This is in agreement with the calculated charges of the apical E1 atoms in E_8^{2+} [S1 + 0.178; Se1 + 0.197; Te1 + 0.208]. Higher charges, and thus less electron density, reside on the heavier E1 atoms. This may be attributed to the smaller energy difference between the np^2 lone pair orbital and the empty, vicinal $n\sigma^*$ orbital as n increases, which allows the delocalisation of more electron density into the σ* orbital (as shown in Fig. 41). Therefore a four centre intramolecular π*–π* bond is found in Te_8^{2+} (and to a lesser extent in Se_8^{2+}) rather than a six centre π*–π* bond as in S_8^{2+} and consistently a short–long–short–long bond alternation is found in the Se_8^{2+} and Te_8^{2+} dications [16].

Positive charge delocalisation in E_8^{2+} (E = S, Se, Te) leads to np_π–np_π ($n \geq 3$) and weak transannular bonding by interactions of electrons in π* orbitals in opposite sides of an ring, i.e. π*–π* bonding. The classically bonded structure **A** in Fig. 42, e.g. $[E_2(CH_2)_6]^{2+}$ (E = S, Se) [151], with localised charges residing on E3 and E7 is not observed, but rather charge is delocalised to E2, E3, E4, E6, E7 and E8 (**B**) by formation of a six centre intramolecular π*–π* bond which includes weak transan-

nular interactions (Fig. 42, process (a)). This is accompanied by the formation of annular np_π–np_π bonding between E2–E3, E3–E4, E7–E8 and E6–E7. Further delocalisation takes place from the occupied np^2 lone pair orbital at E1 and E5 into the formally empty σ* orbitals corresponding to the E2–E3, E3–E4, E6–E7 and E7–E8 bonds (Fig. 42, process (b)), and is accompanied by formation of annular np_π–np_π bonding in bonds to E1 and E5, and weakening of the bonds adjacent to E3 and E7. The calculated energy differences between isomer **A** and **C** are 29 (S) and 6 (Se) kJ mol^{-1} in favour of the latter geometry [16].

Delocalisation process (b) is more favoured as the group is descended accounting for the changing bond alternation and in keeping with the decreasing $np^2 \rightarrow n\sigma^*$ energy gap in the heavier homologues. Other intracationic interactions include a three centre E1–E4–E6 interaction that increases in importance for the heavier group members. This three centre bonding is reminiscent of the closed B–B–B three centre two electron bond. The net result is a highly delocalised bonding between positively charged chalcogen atoms that gives rise to the cluster-like geometry of the E_8^{2+} dication.

3.1.5.1. Other Te_8^{2+} isomers. The more efficient $np^2 \rightarrow n\sigma^*$ bonding of the heavier elements allows for the existence of four different Te_8^{2+} isomers. Whereas for S_8^{2+} and Se_8^{2+} only one geometry is favourable thermodynamically, Te_8^{2+} realises at least four different ways in which the positive charge is delocalised and thus its overall energy is lowered. This implies that all four isomers are very similar in energy. In what follows, we will apply the models derived above to interpret the bonding in the recently characterised Te_8^{2+} isomers. In the isostructural E_8^{2+} (E = S, Se, Te) species we encounter a combination of intramolecular np_π–np_π, π*–π* and $np^2 \rightarrow n\sigma^*$ bonding. As a result of the partially occupied np^2 lone pair orbitals, np^2–np^2 lone pair–lone pair interactions are formed. The second isomer ([105], in $Te_8(WCl_6)_2$, see Fig. 9) exhibits inter- and intramolecular $np^2 \rightarrow n\sigma^*$ bonding, shown in Figs. 43 and 44.

The Zintl precise bicyclo[2.2.2]octane structure of Te_8^{2+} [13b] supports the thesis that $np^2 \rightarrow n\sigma^*$ bonding is very efficient for tellurium and is sufficient to account for delocalisation of the unfavourable localised positive charge. In this isomer, long bonds are observed around the central tricoordinated tellurium atoms and short Te–Te distances in the Te_2-bridges. This situation can be understood assuming a bonding interaction such as is shown in Fig. 45.

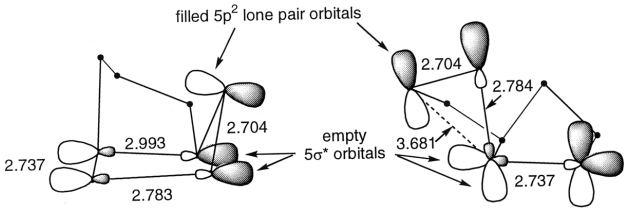

Fig. 43. Intramolecular $np^2 \rightarrow n\sigma^*$ bonding in the Te_8^{2+} dication in $[Te_8][WCl_6]_2$ [105]. Distances are given in (Å).

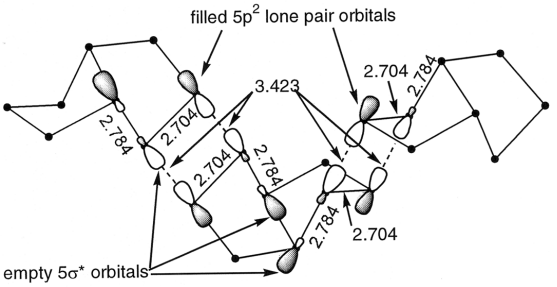

Fig. 44. Intermolecular $np^2 \rightarrow n\sigma^*$ bonding in the Te_8^{2+} dication in $[Te_8][WCl_6]_2$ [105]. Distances are given in (Å).

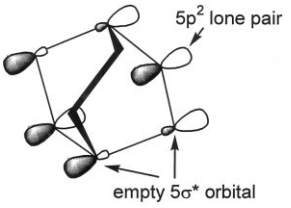

Fig. 45. MO representation of two of the six equivalent $5p^2 \rightarrow 5\sigma^*$ interactions in the bicyclo[2.2.2]octane structure of Te_8^{2+} in $[Te_6^{2+}][Te_8^{2+}][WCl_6^-]_4$ [13b].

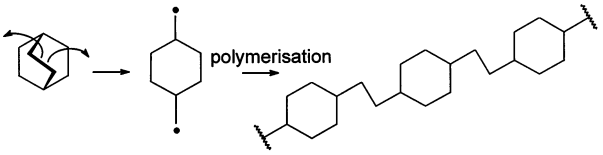

Fig. 46. Conversion of the bicyclo[2.2.2]octane structure of Te_8^{2+} into the polymeric $[Te–Te_6–Te^{2+}]_n$ structure [13b].

The six possible, equivalent interactions in Fig. 45 allow for positive charge delocalisation over all eight atoms. Similarly the polymeric $[Te–Te_6–Te^{2+}]_n$ structure can be understood as a polymeric bicyclo[2.2.2]octane species. When one of the Te–Te bridges in this monomeric Te_8^{2+} is cleaved symmetrically and the radicals are polymerised, then the resulting endless chain becomes equivalent to the fourth isomer observed (see Fig. 46 above).

Consequently positive charge delocalisation in polymeric $[Te–Te_6–Te^{2+}]_n$ is achieved by a $np^2 \rightarrow n\sigma^*$ interaction analogous to that found in the bicyclo[2.2.2]octane structure of Te_8^{2+} above.

3.1.6. Bonding in Se_{10}^{2+}

In the Se_{10}^{2+} dication (see Fig. 47), three tricoordinated selenium atoms with very long adjacent Se–Se distances of about 2.40–2.48 Å are found [cf. *d*(Se–Se) in Se_8:

2.336(2) Å] [82]. A Se_4 chain connects the six-membered ring in the boat conformation in the 1,4 positions and exhibits a pronounced long?short?long?short?short bond length alternation (commencing at a tricoordinated Se atom). Similarly, the two Se_2 bridges show a long?short?long bond length alternation (see Fig. 47).

Several weaker contacts in the range between 3.232 and 3.685 Å are found between non-neighbouring atoms [e.g. between Se4–Se5, Se2–Se7, Se2–Se10, Se7–Se10, Se3–Se6, Se6–Se9, Se3–Se9]. These observations can be accounted for by assuming several $4p^2 \rightarrow 4?^*$ and $4p^2$–$4p^2$ interactions of the partially occupied $4p^2$ lone pair orbitals.

3.1.6.1. $4p^2 \rightarrow 4\sigma^*$ interactions. Long Se–Se bond distances in Se_{10}^{2+} are observed around the tricoordinated atoms which are presumably the only atoms which only have a $4s^2$ lone pair orbital, but no $4p^2$ lone pair orbitals (see Se_8^{2+}). Therefore, the occupied $4p^2$ lone pair orbitals of the vicinal dicoordinated Se atoms donate electron density into the empty antibonding $4\sigma^*$ orbitals of the bonds around the tricoordinated Se atoms so serving to reduce the unfavourable localised formal positive charge which resides on these atoms. Since the tricoordinated Se atoms do not have a $4p^2$ lone pair orbital, they cannot compensate for this bond lengthening by the formation of a similar $4p^2 \rightarrow 4\sigma^*$ interaction and therefore the Se–Se distances adjacent to the tricoordinated Se atoms remain long whilst the vicinal bonds are short (see Fig. 48).

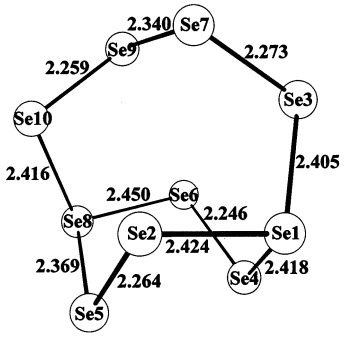

Fig. 47. The solid state structure of the Se_{10}^{2+} dication in $[Se_{10}^{2+}][SO_3F^-]_2$ [82b].

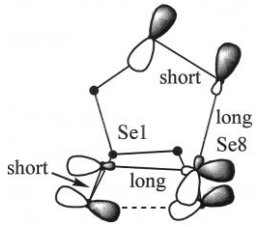

Fig. 48. $4p^2 \rightarrow 4\sigma^*$ interactions around the tricoordinated Se atoms in Se_{10}^{2+}.

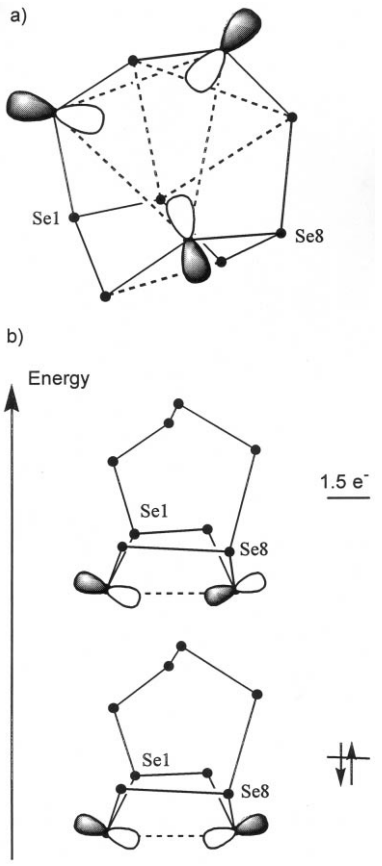

Fig. 49. $4p^2$–$4p^2$ interactions between partially occupied lone pair orbitals in Se_{10}^{2+}.

3.1.6.2. $4p^2$–$4p^2$ interactions between partially occupied lone pair orbitals. The two apical atoms in the Se_6 boat moiety in Se_{10}^{2+} are separated by only 3.232 Å, indicating weak bonding (cf. sum of the Se van der Waals radii: 3.90 Å). By assuming the existence of an interaction between the two partially occupied $4p^2$ lone pair orbitals this can be explained. The two $4p^2$ lone pair orbitals can be converted into two molecular orbitals, one being bonding and the other being antibonding. Since less than four electrons reside in these two orbitals, a small net bonding results, which is in agreement with the observed long Se–Se distance of 3.232 Å (see Fig. 49b). Two sets of weak interactions are also found between three non-neighbouring atoms which are arranged in two equilateral triangles [d(Se–Se) = 3.531–3.685 Å]. This situation is reminiscent of the bonding in Se_8^{2+} where three partially occupied $4p^2$ lone pair orbitals form a similar triangle in Se_8^{2+} and an AIM ring critical point was computed to reside in the centre of this triangle (see Fig. 40). Therefore, we assume a similar bonding interaction of the partially occupied $4p^2$ lone pair orbitals will provide an explanation of these two triangular arrangements in Se_{10}^{2+} (shown in Fig. 49a).

This situation is reminiscent of a closed B–B–B three centre two electron bond as is found in the structures of polyboranes and polyboranates. The formal positive charge is delocalised from the two tricoordinated Se^+ atoms onto six of the ten Se atoms in Se_{10}^{2+} via the $4p^2 \rightarrow 4\sigma^*$ interactions. As a consequence of the now partially occupied $4p^2$ lone pair orbitals, several weak, but stabilising $4p^2$–$4p^2$ lone pair?lone pair interactions are formed.

3.1.7. Bonding in Se_{17}^{2+} and in S_{19}^{2+}

The solid state structures of the S_{19}^{2+} [70] and Se_{17}^{2+} [83,84] dications show a marked bond length alternation within the two seven-membered rings, which decreases with increasing distance from the tricoordinated chalcogen atoms. The bond distances around the tricoordinated atoms are long, while the vicinal bond lengths are short (see Figs. 1 and 50).

The bond length alternation in S_{19}^{2+} and Se_{17}^{2+} can be understood in similar terms as the bonding of the Se_{10}^{2+} dication described above. The tricoordinated chalcogen atoms in the S_{19}^{2+} and Se_{17}^{2+} dications are, presumably, the only atoms that only possess a ns^2 ($n = 3$, 4) lone pair orbital, but no np^2 lone pair orbital. The unfavourable localised positive charge formally residing on the two tricoordinated chalcogen atoms is then delocalised by several $np^2 \rightarrow n\sigma^*$ interactions, which transfer electron density from the vicinal np^2 lone pair orbitals into the empty, antibonding $n\sigma^*$ orbital of the bonds adjacent to the tricoordinated atoms. Therefore the bonds around the tricoordinated chalcogen atoms are long. Strong interactions around the tricoordinated chalcogen atoms, in turn, induce a positive charge to reside on the vicinal chalcogen atoms which is then subsequently delocalised by the formation of further $np^2 \rightarrow n\sigma^*$ interactions. This and the bond length alternation inherent in an S_7 ring [152] lead to the bond length alternation observed throughout the seven-membered rings. The bonding in S_7 was first elucidated by Steudel et al. [137,138] who showed that the $np^2 \rightarrow n\sigma^*$ interactions as responsible for bond lengthening.

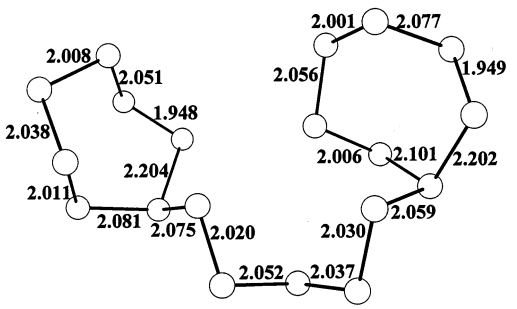

Fig. 50. Solid state structure of the S_{19}^{2+} dication in $[S_{19}^{2+}][SbF_6^-]_2$ [70]. Distances are given in Å.

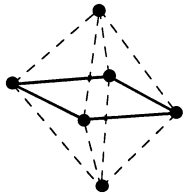

Fig. 51. E_4^{2+} (E = S, Se, Te) rationalised as an electron deficient Wade–Mingos cluster. (Reprinted with permission from [16], Copyright 2000 American Chemical Society.)

3.2. The homopolyatomic chalcogen cations rationalised as electron deficient Wade?Mingos clusters

Inspection of the graphic representations of the computed molecular orbitals of E_8^{2+} (E = S, Se) reveals the presence of at least three bonding cluster-like molecular orbitals in these ions [16]. This raises the question as to whether their structures can be rationalised as an electron deficient Wade–Mingos cluster [39?41]. Banister [153] had in fact proposed this some years ago and attempted to deduce the S_8^{2+} geometry from a cube. More recently, it was demonstrated that S_8^{2+} could be fitted by these rules in a more convincing fashion and also other geometries of the homopolyatomic cations were understood by this model [16]. The ns^2 electrons ($n = 3$, 4) of E_4^{2+} and E_8^{2+} (E = S, Se) are stereochemically inert and occupy ns^2 lone pair orbitals as shown in the NBO analysis [16,33]. It seems not to be unreasonable to assume that a similar situation exists for the heavier tellurium homologues. Therefore only the p-electrons are considered in the formation of bonding skeletal electron pairs (SEP) within the Wade–Mingos treatment. Since the parent polyhedron of a Wade–Mingos cluster [39–41] always has one corner less than the number of the SEP, one has to assume a polyhedron with (SEP-1) corners from which the structure of the cation in question has to be derived.

3.2.1. E_4^{2+} (E = S, Se, Te)

These species have 14 p-type valence electrons or seven SEP, and therefore a six cornered deltahedron has to be assumed to be the parent polyhedron. E_4^{2+} is a $n+2$ (arachno) type cluster with $n+3 =$ seven SEP. The structure of E_4^{2+} is derived from an octahedron (six corners), where both caps are omitted (Fig. 51).

3.2.2. Te_6^{2+} and Te_6^{4+}

Te_6^{2+} and Te_6^{4+} have 22 (11) and 20 (10) p-type valence electrons (SEP) [16]. A 10 and nine cornered deltahedron has to be assumed to be the parent polyhedron. Te_6^{2+} is an $n+4$ and Te_6^{4+} an $n+3$ (hypho) type cluster with $n+5=11$ and $n+4=10$ SEP. Suitable deltahedra in which to accommodate the six-membered ring in boat conformation (Te_6^{2+}) and the elongated trigonal prism (Te_6^{4+}) are to be found in a bicapped square antiprism (Te_6^{2+}: ten corners, six occupied) and a tricapped trigonal prism (Te_6^{4+}: nine corners, six occupied). A representation of these cations and their constituting parent deltahedra is given in below in Fig. 52.

3.2.3. Isostructural E_8^{2+} ($E = S$, Se, Te)

E_8^{2+} (E = S, Se, Te) has 46 valence electrons (VE). For the formation of the structure we have 30 p-type electrons ($46 - 16 = 30$ VE), or in other terms, 15 bonding skeletal electron pairs (SEP, in agreement with Banister's previous assignment [153]). This is a $n + 6$ type cluster ($n = 8$, which requires $n + 7 = 15$ SEP) and thus lies beyond the n (closo), $n + 1$ (nido), $n + 2$ (arachno) and $n + 3$ (hypho) nomenclature given by Wade and Mingos. But what is a suitable 14 cornered polyhedron? If one replaces the lower cap of an icosahedron (12 corners) by a triangle this leads to a 14 cornered polyhedron [154], which easily accommodates and explains all structural features of E_8^{2+} (see Fig. 53, the belts of the two five and one three-membered rings are indicated by circles).

What is the driving force for E_4^{2+}, Te_6^{2+}, Te_6^{4+} and E_8^{2+} to follow the Wade–Mingos rules? Each of these homopolyatomic cations is an assembly of nearly similarly charged atoms. In order to minimise the Coulomb repulsion and to maximise the positive charge delocalisation (which minimises the overall energy), it is proposed that these species occupy part of the surface of a regular polyhedron so as to maximise not only the bonding interactions but also the distances between the partially charged atoms. Strain may well be imposed when preferred bond distances, bond angles and dihedral angles within the species prevent the precise adoption of the ideal atom locations on the parent polyhedron.

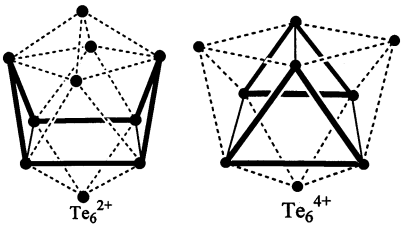

Fig. 52. Te_6^{2+} and Te_6^{4+} rationalised as electron deficient Wade–Mingos cluster. (Reprinted with permission from [16], Copyright 2000 American Chemical Society.)

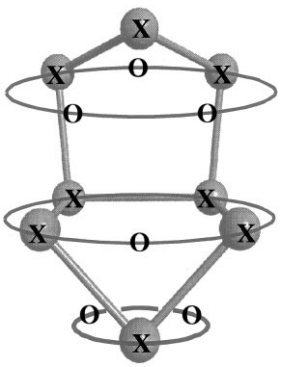

Fig. 53. The structure of E_8^{2+} (E = S, Se, Te) as an $n + 6$ type Wade–Mingos cluster incorporated in a 14 cornered polyhedron derived from an icosahedron by replacing the lower cap by a triangle. X symbolises occupied corners and O stands for unoccupied corners. (Reprinted with permission from [16], Copyright 2000 American Chemical Society.)

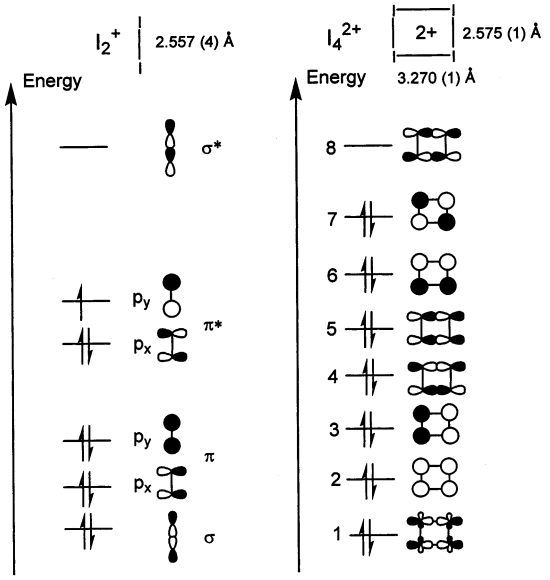

Fig. 54. The 5π MOs of I_2^+ and $[I_4]^{2+}$.

3.3. Bonding in the homopolyatomic halogen cations

New theoretical methods (hybrid Hartree–Fock/density-functional-theory) have enabled meaningful theoretical studies on structures and bonding within the homopolyatomic halogen cations. These recent advances were particularly important for iodine cations (see below) where only small basis sets are available within Gaussian 98 (3-21G*). Iodine species can now be directly studied rather than modelling these cations by substituting iodine with the lighter F, Cl or Br homologues as has been done in the past.

3.3.1. Oxidation state +1/2: X_2^+ (X = Br, I) and I_4^{2+}

The shorter bond length of 2.557 (4) Å in I_2^+ compared with the 2.666 Å in iodine is attributed to the removal of one electron from the π* antibonding HOMO of I_2 (see Fig. 54), giving a formal bond order of 1.5 [155]. This is similarly observed in Br_2^+, having a Br–Br bond length of 2.15(1) Å compared with 2.28 Å in Br_2 [43].

For rectangular I_4^{2+}, the observed short [2.575(1) Å] and long [3.270(1) Å] bond lengths (AsF_6^- salt) [49] have been described as a weak four-centre two-electron π*–π* bond formed between the singly occupied antibonding π* MOs of the two I_2^+ monomers [11,49a,156]. This was supported using Cl_4^{2+} as a model for I_4^{2+} [157].

Our recent MPW1PW91/3-21G* calculations on X_4^{2+} (X = Cl, Br, I) [191] have for the first time mirrored the observed planar rectangular geometry of I_4^{2+} [49] as stationary point structures. This contrasts with earlier studies on F_4^{2+} and Cl_4^{2+} [158], and on Cl_4^{2+} (which was used to model I_4^{2+}) [157], all of which resulted in bent nonplanar chain structures in cases where the bond angles and dihedral angles

were not restrained to enforce a planar rectangular geometry. In addition, our MPW1PW91/3-21G* calculations show the σ-bonded bent chain structure to be a stationary point structure for X = I, only 4 kJ mol^{-1} higher in energy than the optimised rectangular I_4^{2+} geometry [191]. The seven occupied MOs of π symmetry in I_4^{2+} shown in Fig. 54 are constructed from π and π* MOs of the two I_2^+ dimer units, containing 14 p-electrons, and are similar to our previously published MOs of Cl_4^{2+} calculated at the STO-3G level [157]. Two molecular orbitals that have σ bonds within the dimers have been omitted. Of the MOs shown, four (1, 2, 4, 6) are π bonding between the I_2^+ units, and four (3, 5, 7, 8) are antibonding with one (8) unoccupied. Within the I_2^+ units, four MOs (1, 2, 3, 5) are bonding and four (4, 6, 7, 8) are antibonding with one (8) unoccupied. The net result is one π- and one intradimer π*–π* bond per I_4^{2+}, confirming our earlier model prediction which used Cl_4^{2+} to model I_4^{2+} [11,157].

3.3.2. Oxidation state +1/3: X_3^+ (X = Cl, Br, I)

The crystal structures of the X_3^+ cations (X = Cl, Br, I) have all been determined (see Table 1) and contain a bent, C_{2v} symmetric X_3^+ cation with a X–X–X bond angle of ca. 102–105°. The average bond length in I_3^+ ($[AsF_6]^-$ salt) of 2.665 Å [48] is nearly identical to that in I_2 gas (2.666 Å) [4e], indicating a bond order of 1. The same holds true for the bond lengths in Cl_3^+ and Br_3^+ {Cl_3^+: 1.980 (1) Å in the $[AsF_6]^-$ salt, 1.98 Å in Cl_2 [55], Br_3^+: (2.271 Å (average), 2.28 Å in Br_2 [6e]}. The positive charge in X_3^+ is delocalised over all three atoms as shown by the recent calculated charge distribution (NBO analysis) for I_3^+ that places charges of +0.56 on the central atom and +0.22 on the terminal atom. The positive charge is distributed through two equivalent $5p^2 \rightarrow 5\sigma^*$ interactions (see Fig. 55), worth 52 kJ mol^{-1}, transferring about 0.15 electrons from the $5p^2$ lone pair orbitals to the 5σ* bonds. This is in agreement with earlier calculations that used point charges to model the external environment around the cation (+0.50, +0.25) [159], and experimental NQR measurements of $[I_3^+][AlCl_4^-]$ (+0.50 for the central, +0.24 and +0.21 for the terminal iodine atoms) [67b]. These charges are reflected in the observed I–F contacts: the central, higher charged iodine atom exhibits two I–F contacts between 3.01 and 3.07 Å, while there are only single contacts to the terminal iodine atoms in the range between 2.73 and 2.96 Å [48].

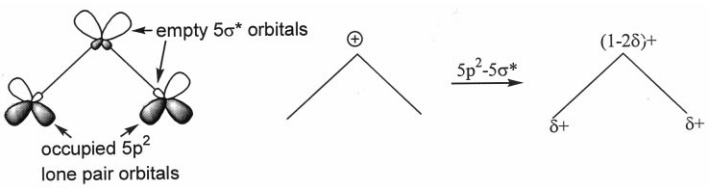

Fig. 55. $5p^2$–5σ* bonding in I_3^+.

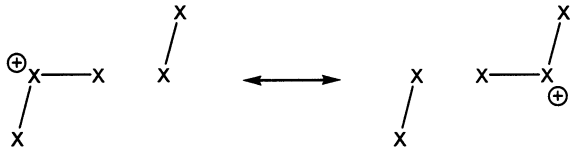

Fig. 56. Valence bond representation of the bonding in X_5^+.

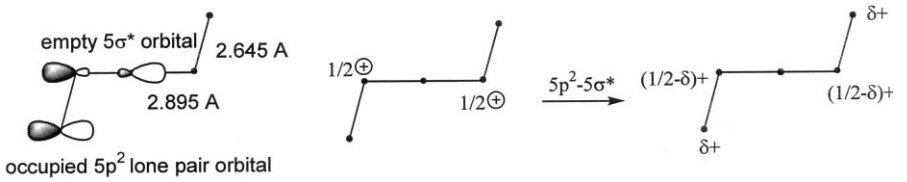

Fig. 57. $5p^2 \rightarrow 5\sigma^*$ interaction in I_5^+ (a similar model holds for Br_5^+).

3.3.3. Oxidation state $+1/5$: X_5^+ ($X = Br$, I)

The crystal structures of the X_5^+ cations (X = Br, I) have been determined and contain a planar, centrosymmetric cation with terminal bond lengths corresponding to a bond order of 1 [2.645(1) compared to 2.666 Å for I_2; 2.275(1) as compared to 2.28 Å for Br_2], and central bond lengths of bond order 0.5 (2.895 (1) Å for I_5^+, 2.512(1) Å for Br_5^+). The bonding in X_5^+ (X = Br, I) can be described in terms of simple valence bond structures (see Fig. 56) showing the formal bond orders of 1.0 and 0.5 for the terminal and central X–X bonds, respectively; the central bonds may be regarded as three-centre four-electron bonds [52].

This is in agreement with our calculated Wiberg bond orders [191], e.g. 1.01 and 0.51 for I_5^+. In addition, our recent MPW1PW91/3-21G* calculated charge distribution (NBO analysis) agrees well with the valence bond model and the observed I–F contacts [52]. The charge is distributed through $5p^2 \rightarrow 5\sigma^*$ interactions, of which one is depicted in Fig. 57, worth some 18 kJ mol^{-1} per interaction and transferring about 0.15 electrons from the $5p^2$ lone pair orbitals on each terminal iodine to the $5\sigma^*$ bonds.

Previous calculations on I_5^+ [160] have correctly described the structure but the calculated charges (using Bader's theory of Atoms in Molecules [150]) were quite poor, showing the most positive charge to reside on the central iodine atom. Earlier calculations that used Cl_5^+ to model I_5^+ also incorrectly assigned the computed charges, but it was pointed out that they were almost certainly incorrect at the level of theory used in that study [52]. Our recent calculated natural charges (MPW1PW91/3-21G* NBO population analysis) correctly reflect the observed I–F contacts, with point charges of $+0.15$ on the terminal iodine atoms (one contact at 3.06 Å), $+0.34$ on the middle iodine atoms (two contacts at 2.98 and 3.27 Å), and only $+0.02$ on the central iodine atoms (no contacts). A similar trend is observed for Br_5^+, for which the most recent published calculated charges [60] have correctly modelled the observed cation–anion contacts.

4. Methods to estimate thermodynamic properties

4.1. Lattice potential energy estimations

Thermochemical studies of any salt require the calculation or estimation of its lattice potential energy, U_{POT}, and often it is useful to estimate the lattice potential enthalpies of hypothetical species which have not yet been prepared or structurally characterised. In the latter case, full-scale calculation of lattice potential energies based on X-ray crystal structural data is not possible and an estimation has to be made. The traditional approach is to achieve this by using the Kapustinskii equation (Eq. (7)) [161]:

$$U_{POT} = \frac{121.4 z_+ z_- v}{(r_+ + r_-)}\left(1 - \frac{0.0345}{(r_+ + r_-)}\right) \quad [\text{in kJ mol}^{-1}] \tag{7}$$

where z_+ and z_- are the charges of the cation and anion, r_+ and r_- are the thermochemical radii of the cation and anion in nm and v is the number of ions in the salt formula. Estimation based upon the Kapustinskii equation relies either upon knowing the thermochemical radii of both the cation and the anion, or the knowledge of the internuclear distance (taken to be equal to $r_+ + r_-$) of the cation and the anion usually obtained from crystal structure data. Until recently, such parameters were unknown for many of the cations and complex anions covered in this review.

Bartlett et al. [162] later found a correlation between the molecular (unit formula) volume of (1:1) AB salts, obtained from crystal structure data, and the lattice enthalpy, ΔH_L, in the form of Eq. (8);

$$\Delta H_L = \frac{232.8}{\sqrt[3]{V}} + 110 \text{ kJ mol}^{-1} \tag{8}$$

where V is the molecular (formula unit) volume in nm^3. This correlation provides an estimation of the lattice enthalpies of (1:1) AB salts from minimal structural data, further developed by apportioning volumes to selected ions such as AsF_6^- ($= 0.105$ nm^3) [162]. Passmore et al. [11] employed this approach to study hypothetical cations by coupling known species with Bartlett's AsF_6^- volume.

We [15b] later made a correlation between the lattice potential energy and the molecular (unit formula) volume of (1:1) AB, (1:2) AB_2 and (2:1) A_2B salts and derived Eq. (9) that allows estimation of the lattice potential energy of any A_xB_y salt;

$$U_{POT} = |z_+||z_-|v\left(\frac{\alpha}{\sqrt[3]{V}} + \beta\right) = 2I\left(\frac{\alpha}{\sqrt[3]{V}} + \beta\right) \text{ kJ mol}^{-1} \tag{9}$$

where $\alpha = 138.7$ kJ mol^{-1} nm, $\beta = 27.6$ kJ mol^{-1}, z_+ and z_- are the respective charges on the cations and anions, v is the number of ions per molecule and I (defined as $1/2\Sigma\, n_i z_i^2$, where n_i is the number of ions of type i per formula unit, each bearing the charge z_i, with the summation extending over all ions of formula unit) is an ionic strength related item. More accurate constants for lattice potential

energy estimations of MX (1:1) salts are: $\alpha = 117.3$ kJ mol^{-1} nm and $\beta = 51.9$ kJ mol^{-1}, of MX_2 (1:2) salts: $\alpha = 133.5$ kJ mol^{-1} nm and $\beta = 60.9$ kJ mol^{-1} and of M_2X (2:1) salts: $\alpha = 165.3$ kJ mol^{-1} nm and $\beta = -29.8$ kJ mol^{-1}. This generalised equation provides an estimate of the lattice potential energy for any A_xB_y salt given minimal structural data. A comprehensive list of ion volumes (over 400) has been generated [15b] and these provide reliable estimates of the lattice potential energy of salts for which no structural data are available.

4.2. Fluoride ion affinities (FIA)

The fluoride ion affinity (FIA) represents the enthalpy of the reaction of a gaseous metal halide MX_n with the gaseous fluoride ion F^- to give MX_nF^- and thus usually comprises a negative value (exothermic reaction). However, FIA values used in the literature are generally given as positive numbers and we will follow this convention in here. Recent lattice potential energy calculations and theoretical investigations have led to improved values for the fluoride ion affinities (FIA) of AsF_5 (g), SbF_5 (g) and of $2SbF_5$ (l). The FIA of AsF_5 was estimated from lattice energy calculations of $[NF_4^+][BF_4^-]$, $[NF_4^+][AsF_6^-]$ and $[NF_4^+][SbF_6^-]$ which led to an enthalpy of formation of gaseous AsF_6^- of -1919 ± 43 kJ mol^{-1}. Subtracting therefrom $\Delta_f H$ (g) of F^- (-255 kJ mol^{-1}) and AsF_5 (-1234 kJ mol^{-1}) gives the FIA(AsF_5) as 433 ± 43 kJ mol^{-1}. This value is in very good agreement with two recent theoretical investigations which predict a FIA (AsF_5) of 431 and 443 kJ mol^{-1} [16,163]. In the following schemes we will use this thermochemically obtained FIA of AsF_5 of 433 kJ mol^{-1}. A similar lattice enthalpy treatment of salts of SbF_6^- leads to a thermochemical value of the FIA(SbF_5) of 521 kJ mol^{-1}. Recently, the FIA of SbF_5 was also examined by theoretical methods in an isodesmic reaction ($SbF_6^- + COF_2 \rightarrow COF_3^- + SbF_5$) and found to be FIA($SbF_5$ (g)) = 502 kJ mol^{-1} [163], in good agreement with the thermochemical value of 521 kJ mol^{-1}. From lattice potential energy calculations the FIA of $2SbF_5$ (l) was estimated to be greater than 582 ± 87 kJ mol^{-1}.

5. Energetics of the homopolyatomic halogen and chalcogen cations

The first pure salt containing a homopolyatomic cation of Groups 16 and 17 was $[O_2^+][PtF_6^-]$ which was obtained by the direct oxidation of oxygen with platinum(VI) hexafluoride [4,164]. A consideration of the energetics of this reaction led to the synthesis of the first xenon compound and subsequently xenon chemistry was rapidly developed. More recently the thermochemistry of the other homopolyatomic cations of Groups 16 and 17 has received more attention [11,12,14]. The now newly available data and methods to obtain reliable thermochemical estimates of gas phase species were employed in a number of very recent investigations of the thermodynamics of salts of homopolyatomic cations of the chalcogens [16,17] and the halogens [15a,b,c]. This knowledge of thermodynamic data and the ability to make good estimates enables us then to judge the stability of 'Mad magazine'

compounds i.e. salts of the chalcogen or halogen monocations, with greater accuracy than hitherto (see [11]). These hypothetical EX species (E = chalcogen, X = univalent anion) are the inversion of very common salts such as sodium chloride NaCl where the electronegative element E always acts as the anion (and not as the cation as above). We will first review the energetics of the halogen cations and then the respective chalcogen species. The following abbreviations are used frequently: (ss) standard state (of an element or molecule), (g) gas phase, (l) liquid phase, (c) crystalline.

5.1. Thermodynamic study of the halogen cations

Currently five iodine cations exist as crystalline salts (I_2^+, I_3^+, I_4^{2+}, I_5^+, and I_{15}^{3+}), all of which were structurally characterised in at least one of their salts (see Table 1). The thermochemistry of some of their $AlCl_4^-$ salts and that of the hypothetical I^+, I_7^+ (however, for melting point evidence of I_7SO_3F see [66]) and I_9^+ cations was examined recently [15]. Only three bromine (Br_2^+, Br_3^+, Br_5^+) and one chlorine (Cl_3^+) cation were characterised by X-ray crystallography (see Table 1; however, a preliminary crystal structure of $[Cl_4^+][IrF_6^-]$ was presented recently by Seppelt [68b]). In the following, the thermodynamics of existing and hypothetical X_n^+ cations (X = F, Cl, Br, I; $n = 1$–9) as hexafluoroarsenate, undecafluorodiantimonate and in some cases as tetrachloroaluminate salts is investigated. Corresponding Born–Fajans–Haber cycles and thermochemical data employed in previously unpublished sections can be found in reaction order in the Appendix.

5.1.1. The X^+ and X_2^+ cations as $Sb_2F_{11}^-$ salts

The hexafluoroarsenate salts of the X^+ and the X_2^+ halogen cations were examined in an earlier thermochemical study by one of us (J. Passmore) [11]. Their stabilities depend (i) on the size of the anion [$U_{POT} \propto 1/(r_{cat.} + r_{an.})$] and (ii) the halide ion affinity of the anion starting materials. Small anions give rise to large lattice potential energies and so these contribute favourably towards the stabilisation of the salt, but larger negative halide ion affinities also contribute favourably towards the stabilisation of the X^+ and the X_2^+ cations. Estimation of the fluoride ion affinities (FIA) of several species showed the FIA of $2SbF_5$ liquid to be the highest, [FIA($2SbF_5$ (l)) $> 582 \pm 87$ kJ mol^{-1}] [15c], greater than the fluoride ion affinity of arsenic pentafluoride (433 ± 43 kJ mol^{-1}) [15c] which was used in the preceding study [11]. This highest fluoride ion affinity known, FIA($2SbF_5$ (l)), has the potential to provide the highest stabilisation of electrophilic cations, if the size factor does not offset the effect of the higher FIA. [$3SbF_5$ (l) has an even higher FIA which is presently being evaluated.] Consequently we studied the thermodynamics of the highly electrophilic halogen cations X^+ and X_2^+, as salts of the very weakly Lewis basic $Sb_2F_{11}^-$ anion [165]. The reaction pathways listed in Table 7 are considered for the possible syntheses of the $[X^+][Sb_2F_{11}^-]$ and $[X_2^+][Sb_2F_{11}^-]$ salts (X = F, Cl, Br, I) together with the corresponding thermochemical data and the reaction enthalpies of the respective AsF_6^- salts as obtained by the preceding investigation [11]. Only $[I^+][Sb_2F_{11}^-]$ should be stable with respect to the reactants

Table 7
Estimated reaction enthalpies for the preparation of the halogen salts $[X^+][Sb_2F_{11}^-]$ and $[X_2^+][Sb_2F_{11}^-]$ (AsF_6^- salts from Ref. [11] in parenthesis) according to Eqs. (10)–(15), $\Delta_f H$ (g) of X^+ and X_2^+ and lattice potential energies of $[X^+][Sb_2F_{11}^-]$ and $[X_2^+][Sb_2F_{11}^-]$ [a]

Reaction pathways considered (kJ mol^{-1})	X =	F	Cl	Br	I
(10) X_2 (ss) + $5SbF_5$ (l) → $2[X][Sb_2F_{11}]$ (c) + SbF_3 (c)	$\Delta_r H$ (Eq. (10)) =	< 648 (632)	< 266 (255)	< 153 (138)	< 19 (8)
(11) XF (ss) + $2SbF_5$ (l) → $[X][Sb_2F_{11}]$ (c)	$\Delta_r H$ (Eq. (11)) =	< 443 (423)	< 115 (105)	< 6 (25)	< −92 (42)
(12) $1/5XF_5$ (ss) + $2/5X_2$ (ss) + SbF_5 (l) → $[X][Sb_2F_{11}]$ (c)	$\Delta_r H$ (Eq. (12)) =	–	< 108	< 39 (25)	≤ −10 (−29)
	$\Delta_f H(X^+, g)$ =	1760	1372	1252	1115
	$U_{POT}([X^+][Sb_2F_{11}^-])$ =	487 (623)	481 (611)	474 (607)	471 (602)
(13) $2X_2$ (c) + $5SbF_5$ (l) → $2[X_2][Sb_2F_{11}]$ (c) + SbF_3 (c)	$\Delta_r H$ (Eq. (13)) =	< 400 (397)	< 6 (8)	< −44 (−38)	< −115 (−113)
(14) XF (ss) + $1/2X_2$ (ss) + $2SbF_5$ (l) → $[X_2][Sb_2F_{11}]$ (c)	$\Delta_r H$ (Eq. (14)) =	< 194 (188)	< −145 (−142)	< −191 (−155)	< −226 (−163)
(15) $1/5XF_5$ (ss) + $9/10X_2$ (ss) + $2SbF_5$ (l) → $[X_2][Sb_2F_{11}]$ (c)	$\Delta_r H$ (Eq. (15)) =	–	< −152	< −158 (−155)	< −144 (−151)
	$\Delta_f H(X_2^+, g)$ =	1515	1108	1046	969
	$U_{POT}([X_2^+][Sb_2F_{11}^-])$ =	486 (611)	474 (590)	462 (582)	455 (569)

[a] See Appendix for the corresponding Born–Fajans–Haber cycles.

according to these estimates. However, it could disproportionate to give $[I_2^+][Sb_2F_{11}^-]$ and $[IF_2^+][Sb_2F_{11}^-]$ (see below). The only $[X_2^+][Sb_2F_{11}^-]$ salt not preparable is predicted to be that of fluorine. However, only the formation of solid SbF_3 could be considered, although this compound usually forms solid adducts of the type $xSbF_3 \cdot ySbF_5$ and related materials [166]. The thermodynamic data of the latter adducts are unknown. Adduct formation will favour all reactions and make the reaction enthalpies in Table 7 even more favourable than the numbers suggest.

The above thermochemical estimations are consistent with the following experimental data:

1. $[I_2^+][Sb_2F_{11}^-]$ was prepared and fully characterised [47b,c].
2. $[Br_2^+][Sb_3F_{16}^-]$ was prepared and fully characterised [55]. An excess of the Lewis acid, SbF_5, is present in the reaction mixture and so inhibits the formation of the $Sb_2F_{11}^-$ salt. In excess SbF_5 the thermodynamically favoured salt is $[Br_2^+][Sb_3F_{16}^-]$.
3. $[Cl_2^+][Sb_2F_{11}^-]$ has not been conclusively prepared to date but may be accessible using either of Eqs. (14) or (15) [136].
4. There are no reports of the fluorine salt $[F_2^+][Sb_2F_{11}^-]$.

The only $[X^+][Sb_2F_{11}^-]$ salt predicted to be stable is that of iodine, however, there are no reports of the monocation I^+ existing as this salt. The compound ISO_3F is not ionic (in the form of $I^+SO_3F^-$) but exists in the solid state as dimeric $(FO_2SO)_2I$–I. The iodine atoms in this compound are in the formal $+III$ and $-I$ oxidation states [65].

5.1.1.1. The disproportionation of $[I^+][Sb_2F_{11}^-]$. We have shown above that $[I^+][Sb_2F_{11}^-]$ is thermodynamically accessible by routes 9, 10 or 11. Salts of I_2^+ have been prepared [47] and IF_2^+ is reasonable (cf. BrF_2^+, ClF_2^+ [180,181]); therefore we considered a disproportionation reaction of $[I^+][Sb_2F_{11}^-]$ to give $[IF_2^+][Sb_2F_{11}^-]$ and $[I_2^+][Sb_2F_{11}^-]$ to examine the stability of the hypothetical $[I^+][Sb_2F_{11}^-]$ salt.

$$[I^+][Sb_2F_{11}^-]\ (c) \rightarrow 1/5[IF_2^+][Sb_2F_{11}^-]\ (c) + 2/5[I_2^+][Sb_2F_{11}^-]\ (c) + 4/5SbF_5\ (l) \quad (16)$$

The enthalpy of Eq. (16) was estimated to be exothermic by about 78 kJ mol^{-1} [see $\Delta H(16)$ in Appendix]. Since entropy favours the decomposition of $[I^+][Sb_2F_{11}^-]$ according to Eq. (16) this implies that $[I^+][Sb_2F_{11}^-]$ cannot be prepared unless synthesised under conditions where it is metastable. This disproportionation is reminiscent of that found for $(ISO_3F)_2$ (see above).

5.1.2. I_2^+, I_4^{2+} and I_3^+ cations as $AlCl_4^-$ salts

Corbett showed that $[I_3^+][AlCl_4^-]$ can be prepared from I_2, ICl and $AlCl_3$ in a sealed container but that it is unstable if left open in a drybox [67]. No experimental reports of $[I_2^+][AlCl_4^-]$ or its dimer $[I_4^{2+}][AlCl_4^-]_2$ are known. The underlying thermochemistry of these reactions was the focus of a recent study [15] and is briefly outlined here. In agreement with the experimental findings, the formation of $[I_2^+][AlCl_4^-]$ according to Eq. (17) was shown to be endothermic:

$$1/2I_2\ (c) + AlCl_3\ (c) + ICl\ (c) \rightarrow [I_2^+][AlCl_4^-]\ (c)\ \Delta H = +10\ kJ\ mol^{-1} \quad (17)$$

$[I_2^+][AsF_6^-]$ associates in the solid state giving the I_4^{2+} salt (Eq. (18), $[A^-] = [AsF_6^-]$), determined to be favourable by 29 kJ mol^{-1} [see $\Delta H(18)$ in the Appendix]. This has not been shown experimentally with the $Sb_2F_{11}^-$ anion, for which the corresponding dimerisation (Eq. (18), $[A^-] = [Sb_2F_{11}^-]$) was determined to be unfavourable by 29 kJ mol^{-1}. Therefore the thermodynamics of the dimerisation (Eq. (18)) for $[A^-] = [AlCl_4^-]$ was assessed too and was also found to be slightly endothermic.

$$2[I_2^+][A^-]\ (c) \rightarrow [I_4^{2+}][A^-]_2\ (c)\ \Delta H = +13\ kJ\ mol^{-1} \quad (18)$$

Therefore, neither $[I_2^+][AlCl_4^-]$ nor $[I_4^{2+}][AlCl_4^-]_2$ can be synthesised, which is in good agreement with Corbett's experimental findings [67]. $[I_3^+][AlCl_4^-]$ is marginally stable at room temperature as shown in Eq. (19).

$$ICl\ (c) + I_2\ (c) + AlCl_3\ (c) \rightarrow [I_3^+][AlCl_4^-]\ (c)\ \Delta H = -62\ kJ\ mol^{-1} \quad (19)$$

However, the vapour pressure of I_2 (c) and ICl (c) is relatively high at r.t. and therefore the stability of the product of Eq. (19) has to be judged by its free energy. Entropy will favour the decomposition of $[I_3^+][AlCl_4^-]$ (c) and consequently this salt is stable in a closed system but not in an open system such as a drybox in which gaseous I_2 and ICl can evolve and the left hand side of Eq. (19) is favoured.

5.1.3. X_3^+ and X_5^+ cations as AsF_6^- salts

The X_3^+ and X_5^+ halogen cations (X = Cl, Br, I) are studied thermochemically as AsF_6^- salts, since this anion is common to all the known halogen cations X_3^+ and X_5^+ (i.e. no Cl_5^+). Ab initio calculations and thermochemical studies [15c] estimate the average I–I bond energy in the I_3^+ cation to be 230 kJ mol^{-1}. The remaining X_3^+ and X_5^+ cation bond energies have not yet been assigned. In the following we use experimental results to estimate these parameters and provide information about the X_3^+ and X_5^+ cation salt stabilities. All derived estimates are listed later in Table 8.

5.1.3.1. Estimation of X_3^+ and X_5^+ bond energies. $[Br_3^+][AsF_6^-]$ was synthesised according to Eq. (20) by Christe et al. [57b] and contains some $[Br_5^+][AsF_6^-]$ as by-product.

$$(x+y)[BrF_2^+][AsF_6^-]\ (c) + (2x+3y)Br_2\ (g) \rightarrow x[Br_3^+][AsF_6^-]\ (c) + 2(x+y)BrF\ (g) + y[Br_5^+][AsF_6^-]\ (c) \quad (20)$$

From Eq. (20) we obtain [see $\Delta H(20)$ in Appendix] an estimate of the bond enthalpy of Br_3^+, $BE(Br_3^+\ (g))$, to be greater than 259 kJ mol^{-1}. Other experiments of bromine and iodine cations in solution and the solid state suggest the X_5^+ cation to be more stable than the respective X_3^+ cation. We therefore assume the following:

$$[X_3^+][AsF_6^-]\ (c) + X_2\ (ss) \rightarrow [X_5^+][AsF_6^-]\ (c)\ (\text{for } X = Br, I) \quad (21)$$

With this assumption [Eq. (21)] we obtain estimates for the bond energies of the gaseous I_5^+ and Br_5^+ cations as [see $\Delta H(21)$ in Appendix]: BE(I_5^+ (g)) > 177 kJ mol^{-1} and BE(Br_5^+ (g)) ≈ 192 kJ mol^{-1}. Using this bond energy, the thermochemistry of the preparation of $[Br_5^+][AsF_6^-]$ and $[I_5^+][AsF_6^-]$ from $[O_2^+][AsF_6^-]$ and X_2 (ss), is studied according to Eq. (22).

$$[O_2^+][AsF_6^-]\ (c) + 5/2X_2\ (ss) \rightarrow [X_5^+][AsF_6^-]\ (c) + O_2\ (g) \quad (22)$$

In the experimental preparation of $[Br_5^+][AsF_6^-]$ via Eq. (22) some $[Br_3^+][AsF_6^-]$ was observed as by-product. The enthalpy change estimated for Eq. (22) where X = Br is approximately −139 kJ mol^{-1} [see $\Delta H(22)$ in Appendix]. $[Br_3^+][AsF_6^-]$ in Eq. (20) was prepared using excess bromine. Therefore one would expect $[Br_5^+][AsF_6^-]$ to be the main product of Eq. (20), however, the latter salt is formed only as a by-product and the major salt prepared is $[Br_3^+][AsF_6^-]$. This implies that Eq. (20), for which no reaction enthalpy was defined, is thermodynamically less favourable in the preparation of $[Br_5^+][AsF_6^-]$ than is Eq. (22). Hartl et al. [59] reported the syntheses of the Br_5^+ cation in both the $[Br_5^+][AsF_6^-]$ and the $[Br_5^+][SbF_6^-]$ salts, from $[XeF^+][MF_6^-]$ (M = As, Sb) and excess bromine. The Br_3^+ cation was detected in the reaction mixture as an intermediate. These observations suggest that in the presence of excess bromine gas, the Br_3^+ cation is formed initially, but is slightly unstable with respect to the Br_5^+ cation. The synthetic route (Eq. (22)) could also be employed to synthesise the $[I_5^+][AsF_6^-]$ salt. The corre-

Table 8
Estimated $\Delta_r H$ for the preparation of $[X_3^+][AsF_6^-]$ and $[X_5^+][AsF_6^-]$ according to Eqs. (22), (26) and (27), $\Delta_f H$ (g) of X_3^+ and X_5^+, bond energies of X_3^+ and X_5^+ and $\Delta_r H$ of decomposition of $[X_3^+][AsF_6^-]$ according to Eqs. (21), (24) and (28)

Reaction pathways to AsF_6^- salts of X_3^+ and X_5^+ (kJ mol^{-1})	X =	Cl	Br	I
(26) $3X_2$ (ss) + $3AsF_5$ (g) → $2[X_3][AsF_6]$ (c) + AsF_3 (l)	$\Delta_r H(26)$ =	61 [a]	<25	−44
	$\Delta_f H(X_3^+$ (g)) =	<1020	<958	869
	av. BE(X_3^+) =	>298	>259	230
(27) $5X_2$ (ss) + $3AsF_5$ (g) → $2[X_5][AsF_6]$ (c) + AsF_3 (l)	$\Delta_r H(27)$ =	>60	<25	< −44
(22) $O_2[AsF_6]$ (c) + $5/2X_2$ (ss) → $[X_5][AsF_6]$ (c) + O_2 (g)	$\Delta_r H(22)$ =	–	< −139	< −208
	$\Delta_f H(X_5^+$ (g)) =	>996	≈932	<835
	av. BE(X_5^+) =	<216	≈192	>177
(24) $[Cl_3][AsF_6]$ (c) → Cl_2 (g) + AsF_5 (g) + ClF (g)	$\Delta_r H(24)$ =	>138 [b]	–	–
(28) $[X_3][AsF_6]$ (c) → $[X_5][AsF_6]$ (c) + AsF_5 (g) + XF (g)	$\Delta_r H(28)$ =	>136	>171	<204
(21) $[X_3][AsF_6]$ (c) + X_2 (ss) → $[X_5][AsF_6]$ (c)	$\Delta_r H(21)$ =	(>0) [c]	(<0) [c]	(<0) [c)]

[a] At 195 K.
[b] $\Delta G^{298}(24) = -74$ kJ mol^{-1}.
[c] Estimate is based on observations.

sponding reaction enthalpy is estimated to be -208 kJ mol^{-1}. The trichlorine (1 +) hexafluoroarsenate salt $[Cl_3^+][AsF_6^-]$ was prepared at -78°C by Gillespie et al. [62] (Eq. (23)).

$$[Cl_2F^+][AsF_6^-]\ (c) + xCl_2\ (l) \rightarrow [Cl_3^+][AsF_6^-]\ (c) + (x-1)Cl_2\ (l) + ClF\ (g) \quad (23)$$

Estimations of thermochemical data allow the study of Eq. (23) at r.t. An estimate of the bond enthalpy of the Cl_3^+ cation, BE(Cl_3^+ (g)), is found [see $\Delta H(22)$ in Appendix] to be greater than 298 kJ mol^{-1} (at r.t. not -78°C). The bond enthalpy estimate does not consider the entropy terms, which will favour Eq. (23) towards the left hand side and we assume that $\Delta H(23) < 0$ may not be representative of the reaction. A more accurate thermochemical description would be $\Delta G(23) < 0$, however, appropriate data for this reaction at -78°C are unavailable. At r.t. $[Cl_3^+][AsF_6^-]$ is described as being completely decomposed according to Eq. (24) [62].

$$[Cl_3^+][AsF_6^-]\ (c) \rightarrow Cl_2\ (g) + ClF\ (g) + AsF_5\ (g) \quad (24)$$

The enthalpy of this reaction is estimated [see $\Delta G(24)$ in Appendix] to be greater than 138 kJ mol^{-1}. Entropy contributions to the reaction will be very significant as one mole of solid decays to three moles of gas. At r.t., the Gibbs free energy of reaction (Eq. (24)), $\Delta G(24)$, is estimated to be greater than -74 kJ mol^{-1}. At the preparative temperature of the $[Cl_3^+][AsF_6^-]$ salt, 195 K, the entropy contribution to Eq. (24) will be less significant as one mole of solid decomposes to two moles of liquid and only one mole of gas.

$[Cl_3^+][AsF_6^-]$ was prepared in excess chlorine (Eq. (23)). In contrast to the synthesis of Br_3^+, the Cl_5^+ cation was not detected in this reaction. Various fluoroantimonate salts of the Cl_3^+ cation have been prepared recently [61], but there are no conclusive reports of the Cl_5^+ cation. This leads to the assumption indicated in Eq. (25);

$$[Cl_3^+][AsF_6^-](c) + Cl_2(l) \not\rightarrow [Cl_5^+][AsF_6^-](c) \quad (25)$$

Eq. (25) is assumed valid at -78°C; at r.t. the bond energy of the Cl_5^+ cation, BE(Cl_5^+ (g)), is estimated [see $\Delta H(25)$ in Appendix] to be less than 216 kJ mol^{-1}. This leads to the conclusion that the X_5^+ cations for X = I, Br are more stable than the respective X_3^+ cations, whereas Cl_3^+ is estimated to be more stable than the hypothetical Cl_5^+ cation. The stability of the X_5^+ and the X_3^+ cations decreases as the halogen group is ascended. However, this destabilisation is more pronounced for X_5^+ since the bond enthalpy of Cl_2 is sufficiently more favourable than those of Br_2 and I_2 [BE(X_2): X = Cl (243), Br (190), I (151) kJ mol^{-1}] [167] which enforces a disproportionation and consistently only a Cl_3^+ salt was observed experimentally.

5.1.3.2. Preparation of $[X_n^+][AsF_6^-]$ (n = 3, 5). Using all the above estimated bond enthalpies, we can now assess the thermodynamics of the direct syntheses of all $[X_n^+][AsF_6^-]$ ($n = 3$, 5) from the halogen X_2 (c) and AsF_5. Passmore et al. [48] describe the synthesis of $[I_3^+][AsF_6^-]$ according to Eq. (26) (where X = I);

$$3AsF_5{\cdot}SO_2\ (c) + 3X_2\ (ss) \rightarrow 2[X_3^+][AsF_6^-]\ (c) + AsF_3\ (l) + 3SO_2\ (g) \quad (26)$$

The thermodynamics [15c] of this reaction was studied for X = I assuming the reaction of $AsF_5{\cdot}SO_2$, with the halogen X_2 (ss) yielding $[X_3^+][AsF_6^-]$. The reaction enthalpy for X = I was estimated [see $\Delta H(25)$ in Appendix] as -44 kJ mol^{-1}. Employing the approximate bond enthalpy of Br_3^+ (BE > 259 kJ mol^{-1}), the corresponding reaction enthalpy of the synthesis of $[Br_3^+][AsF_6^-]$ via the preparative route (Eq. (26)) is shown [see $\Delta H(26)$ in Appendix] to be less than $+25$ kJ mol^{-1}. It was shown experimentally that in SO_2, bromine reacted with either SbF_5 or AsF_5 to give SO_2BrF and either SbF_3SbF_5 or AsF_3, respectively [168]. The preparation of $[Cl_3^+][AsF_6^-]$ via Eq. (26) at 195 K is estimated to be endothermic by less than 61 kJ mol^{-1} and consequently Eq. (26) is not suitable to form solid $[Cl_3^+][AsF_6^-]$.

Similarly to Eq. (26) the preparation of $[I_5^+][AsF_6^-]$ was achieved according to Eq. (27) [52];

$$3AsF_5{\cdot}SO_2\ (c) + 5X_2\ (ss) \rightarrow 2[X_5^+][AsF_6^-]\ (c) + AsF_3\ (l) + 3SO_2\ (g) \quad (27)$$

Eq. (27) was analysed including the adduct formation of AsF_5 and the SO_2 solvent [15c]. The average bond enthalpy of the I_5^+ cation was estimated to be greater than 177 kJ mol^{-1}. Therefore, the reaction enthalpy of the formation of $[I_5^+][AsF_6^-]$ will be less than -44 kJ mol^{-1}. For X = bromine ($+25$ kJ mol^{-1}) and chlorine ($+60$ kJ mol^{-1}) the corresponding reaction enthalpies become less favourable [see $\Delta H(27)$ in Appendix] as the halogen group is ascended, since we assume that for Eq. (21) $\Delta H_r(21) < 0$ for X = Br and I, $\Delta H_r(21) > 0$ for X = Cl.

The thermochemical data related to the formation of the X_3^+ and the X_5^+ cations and of their preparation as hexafluoroarsenate salts showed that for X = I, Br the X_5^+ species is more stable than the corresponding X_3^+ species while the opposite holds for X = Cl (Cl_3^+ is more stable). Eq. (28) considers the decomposition of $[X_3^+][AsF_6^-]$ to give $[X_5^+][AsF_6^-]$ for X = Cl, Br, I in the absence of excess halogen.

$$2[X_3^+][AsF_6^-]\ (c) \rightarrow [X_5^+][AsF_6^-]\ (c) + XF\ (g) + AsF_5\ (g) \quad (28)$$

The decomposition enthalpy via route (Eq. (28)) is estimated [see $\Delta H(28)$ in the Appendix] to be less than 204 kJ mol^{-1} for iodine, whilst for bromine and chlorine it is estimated to be greater than 171 and 136 kJ mol^{-1}, respectively. This is consistent with the observed trends for the stabilities of this cation series, however, decomposition via this route seems unlikely. FT-Raman spectra of $[I_3^+][AsF_6^-]$ in SO_2 solution indicate the presence of I_2^+, I_4^{2+} and possibly I_5^+ [191]. All the proceeding data are summarised in Table 8.

5.1.3.3. $[I_5^+][AsF_6^-]$ versus $[I_{15}^{3+}][SbF_6^-]_3$. Solid state structures show (see Table 1) that $[I_5^+][AsF_6^-]$ contains a monomeric I_5^+ cation whereas in $[I_5^+][SbF_6^-]$ it associates weakly giving the $[I_{15}^{3+}]$ trimer. Using the lattice potential energy approach [15], the gas phase trimerisation enthalpy for this process was estimated at 669 ± 197 kJ mol^{-1}, as given in Eq. (29).

$$3I_5^+\ (g) \rightarrow I_{15}^{3+}\ (g)\ \Delta H = 669\ \text{kJ mol}^{-1} \quad (29)$$

When the respective solid state behaviour is estimated, one would expect $[I_5^+][AsF_6^-]$ to trimerise rather than $[I_5^+][SbF_6^-]$ (i.e. due to the higher lattice potential energy of the AsF_6^- salt in the trimer: 2015 kJ mol^{-1} in $[I_{15}^{3+}][AsF_6^-]_3$ and 1996 kJ mol^{-1} in $[I_{15}^{3+}][SbF_6^-]_3$). This indicates that the solid state enthalpy of trimerisation is close to zero and the formation of a monomer or a trimer is finally governed by cation–anion interactions which favour trimerisation for the SbF_6^- salt but not for the more basic AsF_6^- salt.

5.1.4. The non-existence of $[I_n^+][AsF_6^-]$ ($n = 7, 9$)

Numerous attempts to prepare $[I_n^+][AsF_6^-]$ ($n = 7, 9$) from I_2 and AsF_5 in SO_2 always led to failure. The thermodynamics of the hypothetical preparation of $[I_7^+][AsF_6^-]$ and $[I_9^+][AsF_6^-]$ (Eq. (30)) was recently examined [15] and this showed that both compounds are unstable towards the loss of I_2.

$$3AsF_5{\cdot}SO_2\ (c) + nI_2\ (c) \rightarrow 2[I_n^+][AsF_6^-]\ (c) + AsF_3\ (l) + SO_2\ (g)$$
$$n = 7, 9,\ \Delta H > 0 \tag{30}$$

The bond enthalpies of I_7^+ (g) and I_9^+ (g) were estimated as being less than 134 (I_7^+) and 131 (I_9^+) kJ mol^{-1}. Since I_2 (I_5^+) has a bond enthalpy of 150 (177) kJ mol^{-1}, the disproportionation reactions by formation of salts of I_5^+ and solid I_2 (c) are slightly favoured. The standard enthalpies of formation of gaseous I_7^+ and I_9^+ were estimated to be equal to or greater than 951 (I_7^+) and 919 (I_9^+) kJ mol^{-1}, respectively.

5.2. Thermodynamic study of the chalcogen cations

All the known solid state structures of homopolyatomic chalcogen cations contain diamagnetic, doubly or quadruply charged species, with the exception of the salts of O_2^+. No experimental evidence for the presence of salts of radical cations has been presented to date. However, recent theoretical investigations of E_n^{2+} (E = S, Se, $n = 4, 8$) and E_6^{4+} (E = S, Te) [16,18,31–33] show that the higher charged cations are unstable in the gas phase towards a dissociation into smaller, lesser charged fragments. This is in agreement with the observation of S_5^+, S_7^+ and another radical species, in solutions containing the S_8^{2+} and S_{19}^{2+} cations, and implies that all observed E_n^{2+} and Te_6^{4+} species must be lattice stabilised in the solid state and stabilised by solvation energies in solution.

5.2.1. $[E^+][AsF_6^-]$ and $[E_2^+][AsF_6^-]$ (E = S, Se, Te)

The thermochemistry of the chalcogen X^+ and X_2^+ hexafluoroarsenate salts (X = O, S, Se, Te) was studied earlier by Passmore et al. [11,69]. Only $[Te^+][AsF_6^-]$ was predicted to be stable with respect to the starting materials, whilst all the $[X_2^+][AsF_6^-]$ salts were predicted to be stable. These $[X_2^+][AsF_6^-]$ salts, where X = S, Se and Te, later [17,36,37] were shown to be thermodynamically unstable towards the formation of the dimerised X_2^+ cation, X_4^{2+}. Here we reassessed the thermochemistry of the X^+ and the X_2^+ cations utilising the Lewis acid with highest known

FIA. With a fluoride ion affinity of FIA($2SbF_5$ (l)) > 582 kJ mol^{-1} [15c], the $Sb_2F_{11}^-$ anion should provide the largest stabilisation to salts of X^+ and X_2^+. Therefore we examine the stabilities of $[X^+][Sb_2F_{11}^-]$ and $[X_2^+][Sb_2F_{11}^-]$ according to Eqs. (10), (13), (31) and (32)) summarised in Table 9. The reaction enthalpies of the respective AsF_6^- salts were taken from Ref. [11] and are included for comparison in parentheses. Corresponding thermochemical data are listed in Table 9 and also in the Appendix. As for the halogen cations X^+ and X_2^+, only the formation of SbF_3 (c) could be considered and therefore the expected adduct formation of $xSbF_3{\cdot}ySbF_5$ will additionally favour all reactions in Table 9.

As in the case of the hexafluoroarsenate salts, the only $[X^+][Sb_2F_{11}^-]$ salt predicted to be stable is that of tellurium. Eq. (31) shows that $[X^+][Sb_2F_{11}^-]$ should be stable with respect to SbF_5 and the corresponding element X (X = S, Se, Te). All chalcogen $[X_2^+][Sb_2F_{11}^-]$ salts are predicted to be stable via either Eq. (13) or (32), with the exception of $[O_2^+][Sb_2F_{11}^-]$ (Eq. (13)). The large negative enthalpies of reaction estimated for the salts $[X_2^+][Sb_2F_{11}^-]$ reflect their stabilities in relation to the starting materials. However, for X = S, Se, Te they are unstable towards dimerisation to give square planar $[X_4^{2+}][Sb_2F_{11}^-]_2$. This reaction does not occur for X = oxygen (see below, X_4^{2+} section).

The associated thermochemical cycles for formation of the X^+ cations were examined (see Appendix) to establish what properties an anion must have in order to stabilise the X^+ chalcogen cations in the solid state. A smaller anion than $Sb_2F_{11}^-$ would provide a larger stabilising lattice enthalpy contribution, but the parent Lewis acid of the $Sb_2F_{11}^-$ anion has currently the largest known halide ion affinity ($2SbF_5$ (l)). All smaller anions have lower corresponding halide ion affinities. In the case of the X_2^+ cations, compromise of increasing anion size for increasing fluoride ion affinity favours the $Sb_2F_{11}^-$ anion over the smaller hexafluoroarsenate by ca. > 22 kJ mol^{-1}. However, for X^+ cations these contributions cancel and the resulting reaction enthalpies are essentially the same. However, one must consider that, in contrast to the FIA(AsF_5), the estimated fluoride ion affinity of ($2SbF_5$ (l)) is only a lower limit (> 582 kJ mol^{-1}).

5.2.1.1. Disproportionation of $[Te^+][Sb_2F_{11}^-]$. We showed above that $[Te^+][Sb_2F_{11}^-]$ is thermodynamically accessible by either Eq. (10) or (31). However, the oxidation of elemental Te in the presence of a trace amount of halogen leads to the Te(IV) species $[TeF_3^+][AsF_6^-]$ [36,43] and does not stop at the Te^+ stage. This raises the question as to whether the hypothetical $[Te^+][Sb_2F_{11}^-]$ salt would be stable towards a disproportionation and formation of $[TeF_3^+][Sb_2F_{11}^-]$, $[Te_4^{2+}][Sb_2F_{11}^-]_2$ and SbF_5, shown in Eq. (33).

$$[Te^+][Sb_2F_{11}^-]\ (c) \rightarrow 2/14[TeF_3^+][Sb_2F_{11}^-]\ (c) + 3/14[Te_4^{2+}][Sb_2F_{11}^-]_2\ (c) + 6/7SbF_5\ (l) \quad (33)$$

The disproportionation as to Eq. (33) was estimated [see $\Delta H(33)$ in Appendix] to be exothermic by 143 kJ mol^{-1}. Entropy will further favour this decomposition so that $[Te^+][Sb_2F_{11}^-]$ appears to be unstable with respect to disproportionation. This is in agreement with the experimental findings [43].

Table 9
Estimated $\Delta_r H$ for the preparation of $[X^+][Sb_2F_{11}^-]$ and $[X_2^+][Sb_2F_{11}^-]$ according to Eqs. (10), (13), (31) and (32), the respective values for the AsF_6^- salts are taken from the literature [11] and given in parentheses, $\Delta_f H$ (g) of X^+ and X_2^+, lattice potential energies of $[X^+][Sb_2F_{11}^-]$ and $[X_2^+][Sb_2F_{11}^-]$ (AsF_6^- salts in parentheses) [11]

Reaction pathways to $Sb_2F_{11}^-$ salts of X^+ and X_2^+	X =	O	S	Se	Te
(10) $2X\ (ss)+5SbF_5\ (l)\rightarrow 2[X^+][Sb_2F_{11}^-]\ (c)+SbF_3\ (c)$	$\Delta_r H(10)=$	<224 (435)	<183 (163)	<69 (54)	<-27 (-38)
(31) $X\ (ss)+1/2F_2\ (g)+2SbF_5\ (l)\rightarrow [X^+][Sb_2F_{11}^-]\ (c)$	$\Delta_r H(31)=$	<56	<-64	<-104	<-145
	$\Delta_f H(X^+\ (g))=$	1563	1284	1168	1066
	$U_{POT}\ ([X^+][Sb_2F_{11}^-])=$	484 (623)	476 (611)	473 (607)	467 (598)
(13) $4X\ (ss)+5SbF_5\ (l)\rightarrow 2[X_2^+][Sb_2F_{11}^-]\ (c)+SbF_3\ (c)$	$\Delta_r H(13)=$	<247 (54)	<-24 (-59)	<-137 (-84)	<-233 (-126)
(32) $2X\ (ss)+1/2F_2\ (g)+2SbF_5\ (l)\rightarrow [X_2^+][Sb_2F_{11}^-]\ (c)$	$\Delta_r H(32)=$	<-150	<-270	<-310	<-351
	$\Delta_f H(X_2^+\ (g))=$	1165	1031	985	933
	$U_{POT}\ ([X_2^+][Sb_2F_{11}^-])=$	480 (607)	466 (586)	460 (577)	449 (565)

5.2.2. Why is $E_4(AsF_6)_2$ formed rather than $E_2(AsF_6)$ (E = S, Se, Te)?

Good quality ab initio computations [32,33] show that two equivalents of the E_2^+ (g) radical cations are always favoured over the E_4^{2+} (g) dication (E = O, S, Se, Te; by 99 to 1032 kJ mol^{-1}; see Table 10). This raises the question as to why for all the heavier chalcogens only salts of the E_4^{2+} dication were identified. No experimental evidence for the existence of solid E_2^+ salts has been presented to date except for O_2^+. One factor certainly is found in the differing π and σ bond strengths. Whereas oxygen forms only weak σ bonds [BE(O–O) = 142 kJ mol^{-1}] the E–E σ-bonds (E = S, 267; Se, 172; Te, 126 kJ mol^{-1}) [169] are stronger relative to the respective π-bond energies (O, 351; S, 164; Se, 100; Te, 92 kJ mol^{-1}) [169]. When two E_2^+ radical cations are converted into square planar E_4^{2+} this results in the breaking of two π bonds, the gain of two σ bonds and the work necessary to force the two positively charged E_2^+ ions to join and form the E_4^{2+} dimer. The bond energy change is endothermic for E = O, (by 418 kJ mol^{-1}) but exothermic for E = S, Se, Te (by 206, 144 and 68 kJ mol^{-1}). The resultants of the bond energy change and the electrostatic Coulomb energy are the calculated dissociation energies of E_4^{2+} (g): E = O (−1035 kJ mol^{-1}), S (−258 kJ mol^{-1}), Se (−199 kJ mol^{-1}) and Te (−137 kJ mol^{-1}); see Table 10. Another factor is found in the different lattice potential enthalpies. This aspect was investigated recently [17] by estimating the solid state energetics of the formation of square planar E_4^{2+} (E = S, Se, Te) hexafluoroarsenate salts. The monocations E_2^+ (E = S, Se, Te) are always favoured in the gas phase, but in the solid state salts of the $E_4(AsF_6)_2$ cations are favoured by about 238–367 kJ mol^{-1} for S, Se and Te [17]. This is due to the fact that the lattice energy of a 2:1 salt [$E_4(AsF_6)_2$] is three times that of the respective 1:1 salt [$E_2(AsF_6)$]. While the lattice energy more than compensates for the unfavourable gas phase dissociation energy in the 2:1 salts of the E_4^{2+} (E = S, Se, Te) dications, this is not the case for O_4^{2+} salts and consistently only salts containing the O_2^+ radical cation are formed. The enthalpy of formation of the gaseous O_4^{2+} dimer (+3365 kJ mol^{-1} for an O_4^{2+} square) [170] is large compared

Table 10
Gas phase and solid state thermodynamics of the dissociation of E_4^{2+} [$E_4(AsF_6)_2$ (c)] to give E_2^+ [$E_2(AsF_6)$ (c)] (E = S, Se, Te)

Eq.	Dissociation reactions and $\Delta_f H^{298}$ of all reactants (kJ mol^{-1})		$\Delta_r H^{298}$
	E_4^{2+} (g) → 2 E_2^+ (g)		
(34) E = O	$\Delta_f H = 3365$	2 × 1165	−1035
(34a) E = S	$\Delta_f H = 2318$	2 × 1031	−258
(34b) E = Se	$\Delta_f H = 2207$	2 × 1004	−199
(34c) E = Te	$\Delta_f H = 2077$	2 × 970	−137
	$E_4(AsF_6)_2$ (c) → 2$E_2(AsF_6)$ (c)		
(34d) E = O	$\Delta_f H = -2039$	2 × −1327	−615
(34e) E = S	$\Delta_f H = -3104$	2 × −1433	+238
(34f) E = Se	$\Delta_f H = -3182$	2 × −1447	+288
(34g) E = Te	$\Delta_f H = -3354$	2 × −1494	+367

to that of O_2^+ (1165 kJ mol^{-1}) [198]. Therefore, the dimerisation enthalpy of two O_2^+ (g) to give O_4^{2+} (g) is very endothermic (1035 kJ mol^{-1}) [170] and favours the formation of O_2^+ salts. The thermochemical data are collected in Table 10.

$S_4(AsF_6)_2$ can only be crystallised with either $S_4(AsF_6)_2{\cdot}0.6SO_2$ or $S_4(AsF_6)_2{\cdot}AsF_3$. It was shown [17] that the loss of the solvent in Eq. (35) is endothermic by 142 kJ mol^{-1}.

$$S_4(AsF_6)_2{\cdot}AsF_3\ (c) \rightarrow S_4(AsF_6)_2\ (c) + AsF_3\ (l)\ \Delta_r H^{298} = 142\ \text{kJ mol}^{-1} \quad (35)$$

5.2.3. Is $[S_4^{2+}][AlCl_4^-]_2$ stable?

For the heavier homologues of sulphur, the X-ray crystal structures of $[Se_4^{2+}][AlX_4^-]_2$ (c) (X = Br, I) and $[Te_4^{2+}][AlCl_4^-]_2$ (c) are known (see Tables 3 and 4) and therefore the question arises as to whether S_4^{2+} salts of the $AlCl_4^-$ anion are preparable. Recently it was shown, on the basis of lattice potential enthalpy estimations and experimentally determined heats of formations [198], that the preparation of $[S_4^{2+}][AlCl_4^-]_2$ (c) from S_2Cl_2, $AlCl_3$ and S_8 is endothermic by 97 kJ mol^{-1} (Eq. (36)) showing that $[S_4^{2+}][AlCl_4^-]_2$ (c) is not accessible and would decompose according to the reverse of Eq. (36) if prepared by another route.

$$S_2Cl_2\ (l) + 2AlCl_3\ (c) + 1/4S_8\ (c) \rightarrow [S_4^{2+}][AlCl_4^-]_2\ (c)\ \Delta_r H^{298} = +97\ \text{kJ mol}^{-1} \quad (36)$$

5.2.4. S_4Cl_2 versus $[S_4^{2+}][Cl^-]_2$

One of the questions we raised in Section 1 was why a molecular, chain-like S_4Cl_2 geometry is observed and not an ionic $[S_4^{2+}][Cl^-]_2$ salt as it is found in a variety of fluoroanion salts (see Table 2). We investigated the thermodynamics for this process (Eq. (37)), the associated Born–Fajans–Haber cycle is listed in the Appendix.

$$S_4Cl_2\ (l) \rightarrow [S_4^{2+}][Cl^-]_2\ (c)\ \Delta_r H^{298} = +118\ \text{kJ mol}^{-1} \quad (37)$$

Eq. (37) is endothermic by 118 kJ mol^{-1} and shows that S_4Cl_2 (l) is more stable than the $[S_4^{2+}][Cl^-]_2$ salt. Entropy is in favour of the left hand side of Eq. (37) and therefore ΔG for Eq. (37) will be higher than ΔH. This shows that S–Cl bond formation is more favourable than the lattice potential energy gained upon salt formation.

5.2.5. Why is $E_8(AsF_6)_2$ formed rather than $E_4(AsF_6)$ (E = S, Se)?

Solutions containing the S_8^{2+} dication were shown to be paramagnetic, one of the two observed radical species was unambiguously assigned as S_5^+ [74,125] and the other tentatively assigned by one of us as S_7^+ (J. Passmore) [68a,171]. In agreement with the instability of this dissolved S_8^{2+} dication, gaseous E_8^{2+} (E = S, Se) was shown by ab initio MO methods to dissociate in a number of equilibria to give all stochiometrically possible combinations of radical cations E_n^+ (E = S, Se; $n = 2$–7) [16]. Taking the recently established enthalpies of formation of E_n^{2+} (E = S, Se, $n = 4$, 8) and the accurate experimentally determined enthalpies of formation of the gaseous polychalcogen monocations E_n^+ ($n = 2$–7) [198] the enthalpies of reaction

of possible dissociations of the E_8^{2+} dication (see Table 11 below) can be calculated. Very recently [33] we showed (in agreement with earlier photoionisation studies) [172] that the published appearance potential of S_4 (and hence the enthalpy of formation of S_4^+) is due to the fragmentation of neutral S_6 giving S_4^+ and S_2. In agreement with earlier theoretical investigations [30] we established the enthalpy of formation of gaseous S_4^+ as being 972 kJ mol^{-1}, i.e. 159 kJ mol^{-1} more favourable than the published, erroneously assigned value of 1131 kJ mol^{-1} [33]. Similarly, the ionisation potentials and enthalpies of formation of gaseous Se_3^+ and Se_4^+ are not available. Published appearance potentials arise from the fragmentation of larger neutral allotropes [173], analogous to S_4^+. Therefore the enthalpy of dissociation of Se_8^{2+} (g) to give $2Se_4^+$ (g) was calculated [174]. The enthalpy of formation of Se_3^+ was obtained at the same level [175], while the enthalpy of formation of gaseous Se_4^{2+} was derived from the published [32,33] dimerisation energy of 199 kJ mol^{-1} for the process $2Se_2^+$ (g) = Se_4^{2+} (g) and the experimental enthalpy of formation of gaseous Se_2^+ (g) of 1004 kJ mol^{-1}. The solid state behaviour of the respective gas phase dissociation Eqs. (40a,b)–(45a,b) in Table 11 were assessed by estimating the lattice potential energies of the hexafluoroarsenate salts of the respective E_n^+ monocations by using the generalised equation (vs. Section 4.1). To prove the quality of such estimates, the lattice energy of $S_8(AsF_6)_2$ was derived as follows: First the enthalpy of formation of $S_8(AsF_6)_2$ (c) was determined by fluorine bomb calorimetry as -3122 ± 12 kJ mol^{-1} [37], then the lattice potential enthalpy of $S_8(AsF_6)_2$ was derived according to:

$$\Delta H_{\text{latt.}}[S_8(AsF_6)_2] + 3RT = [\Delta_f H(S_8^{2+}\ (g)) + 2 \times \Delta_f H(AsF_6^-\ (g))] - \Delta_f H[S_8(AsF_6)_2\ (c)] \quad (38)$$

Using the thermochemically derived enthalpy of formation of gaseous AsF_6^- -1919 ± 43 kJ mol^{-1} and the gaseous enthalpy of formation of S_8^{2+} of 2150 kJ mol^{-1}, the lattice potential enthalpy of $S_8(AsF_6)_2$ according to Eq. (38) is found to be 1434 ± 55 kJ mol^{-1}. Estimation of this lattice enthalpy using the generalised equation and the unit cell volume of $S_8(AsF_6)_2$ derived from the X-ray crystal structure determination yields [16] the lattice potential enthalpy as 1455 kJ mol^{-1}, well within the standard deviation of the value derived above of 1434 ± 55 kJ mol^{-1}. Employing the enthalpies of formation of the gaseous polychalcogen radical cations E_n^+ ($n = 2$–7) [198], the derived $\Delta_f H(AsF_6^-$ (g)) [15], the lattice energies of all $E_n(AsF_6)$ (using reasonable estimates for their volume [15b,176,177]) the enthalpies of formation of solid $E_n(AsF_6)$ salts are calculated. This allows us to assess $\Delta_r H$ (c) for the equivalents of the gas phase dissociations of E_8^{2+} described above [using the experimental [37] enthalpy of formation of $S_8(AsF_6)_2$]. All values were obtained for one mol of crystalline salt and are cited below the respective formulae in Table 11.

As can be seen from Table 11 (Eqs. (39a,b)–(42a,b)), E_8^{2+}(g) (E = S, Se) is unstable towards dissociation in all the stoichiometrically possible combinations of E_n^+(g) ($n = 2$–7). All these dissociation processes are considerably less favoured for Se_8^{2+} than for S_8^{2+} and consistently, although radical cations have been observed in

Table 11
Dissociation reactions of E_8^{2+} and $E_8(AsF_6)_2$ (E = S, Se) in the gas phase and the solid state respectively in kJ mol^{-1}. (Reprinted with permission from [16], Copyright 2000 American Chemical Society.)

Eq.	Dissociation reactions and $\Delta_f H^{298}$ of all reactants (kJ mol^{-1})				$\Delta_r H^{298}$
$E_8^{2+}(g) \rightarrow 2E_4^{+}(g)$					
(39a) E = S	$\Delta_f H = 2151$	972 [a]			−207
(39b) E = Se	$\Delta_f H = 2071$	960 [a]			−151
$E_8(AsF_6)_2$ (c) $\rightarrow 2E_4(AsF_6)$ (c)					
(39c) E = S	$\Delta_f H = -3122$	−1457			+208
(39d) E = Se	$\Delta_f H = -3197$	−1447			+303
$E_8^{2+}(g) \rightarrow E_3^{+}(g) + E_5^{+}(g)$					
(40a) E = S	$\Delta_f H = 2151$	1076	939		−136
(40b) E = Se	$\Delta_f H = 2071$	1083 [a]	982		−6
$E_8(AsF_6)_2$ (c) $\rightarrow E_3(AsF_6)$ (c) + $E_5(AsF_6)$ (c)					
(40c) E = S	$\Delta_f H = -3122$	−1361	−1473		+288
(40d) E = Se	$\Delta_f H = -3197$	−1331	−1402		+464
$E_8^{2+}(g) \rightarrow E_2^{+}(g) + E_6^{+}(g)$					
(41a) E = S	$\Delta_f H = 2151$	1031	971		−149
(41b) E = Se	$\Delta_f H = 2071$	1004	996		−71
$E_8(AsF_6)_2$ (c) $\rightarrow E_2(AsF_6)$ (c) + $E_6(AsF_6)$ (c)					
(41c) E = S	$\Delta_f H = -3122$	−1433	−1427		+262
(41d) E = Se	$\Delta_f H = -3197$	−1447	−1380		+370
$E_8^{2+}(g) \rightarrow E_2^{+}(g) + 0.5[E_5^{+}(g) + E_7^{+}(g)]$					
(42a) E = S	$\Delta_f H = 2151$	1031	939	951	−175
(42b) E = Se	$\Delta_f H = 2071$	1004	982	962	−95
$E_8(AsF_6)_2$ (c) $\rightarrow E_2(AsF_6)$ (c) + 0.5[$E_5(AsF_6)$ (c) + $E_7(AsF_6)$ (c)]					
(42c) E = S	$\Delta_f H = -3122$	−1433	−1471	−1437	+235
(42d) E = Se	$\Delta_f H = -3197$	−1447	−1402	−1402	+348
$E_8^{2+}(g) \rightarrow 0.5E_4^{2+}(g) + E_6^{+}(g)$					
(43a) E = S	$\Delta_f H = 2151$	2318	971		−21
(43b) E = Se	$\Delta_f H = 2071$	2207	996		+29
$E_8(AsF_6)_2$ (c) $\rightarrow 0.5E_4(AsF_6)_2$ (c) + $E_6(AsF_6)$ (c)					
(43c) E = S	$\Delta_f H = -3122$	−3104	−1427		+143
(43d) E = Se	$\Delta_f H = -3197$	−3182	−1380		+226
$E_8^{2+}(g) \rightarrow 0.5[E_4^{2+}(g) + E_5^{+}(g) + E_7^{+}(g)]$					
(44a) E = S	$\Delta_f H = 2151$	2318	939	951	−47
(44b) E = Se	$\Delta_f H = 2071$	2207	982	962	+5
$E_8(AsF_6)_2$ (c) $\rightarrow 0.5[E_4(AsF_6)_2$ (c) + $E_5(AsF_6)$ (c) + $E_7(AsF_6)$ (c)]					
(44c) E = S	$\Delta_f H = -3122$	−3104	−1471	−1437	+116
(44d) E = Se	$\Delta_f H = -3197$	−3182	−1402	−1402	+204

[a] See text.

solutions of S_8^{2+}, none have been reported for Se_8^{2+}. The most favoured dissociation (apart from that in Eqs. (39a,b)) is given in Eq. (42a,b) and implies the presence of the dichalcogen radical cation E_2^+. However, as shown above, two equivalents of the solid $E_2(AsF_6)$ (E = S, Se) salt are not stable towards dimerisation to give $S_4(AsF_6)_2$ [$Se_4(AsF_6)_2$] by 239 (291) kJ mol^{-1}. Consequently, dissociation reactions by formation of the resulting diamagnetic E_4^{2+} dication are also included in Table 11 (Eqs. (43a,b)–(44a,b)). These dissociations are favoured for E = S by 21–47 kJ mol^{-1} but not for selenium (by 5–29 kJ mol^{-1}). A dissociation of E_8^{2+} (g) by formation of two E_4^+ (g) cations is the most exothermic reaction (S, 207; Se, 151 kJ mol^{-1}). This dissociation route was proposed in the first experimental reports [60a,b] on $S_8(AsF_6)_2$ to give an explanation for the paramagnetic nature of solutions of this salt, but later dismissed in the light of the experimental detection of S_5^+(solv.) and the erroneously assigned value of $\Delta_fH(S_4^+$ (g)). In the solid state (Eqs. (40c,d)–(45c,d)), $S_8(AsF_6)_2$ [$Se_8(AsF_6)_2$] is always favoured by at least 116 (204) kJ mol^{-1} (Eq. (40b)). Since the formation of Se_4^{2+} is unfavourable in the gas phase, only dissociation reactions of $Se_8(AsF_6)_2$ by formation of the respective monocations should be taken into account (Eqs. (39d)–(42d)). $Se_8(AsF_6)_2$ is then favoured by at least 303 kJ mol^{-1}. Thus the $E_8(AsF_6)_2$ salts are further examples of compounds where the parent dication is not stable in the gas phase and the solid state structures are lattice enforced because the lattice energy of the 2:1 salt is ca. three times that of the respective 1:1 salt [178].

The oxidation of $E_8(AsF_6)_2$ (E = S, Se) using arsenic pentafluoride (Eq. (45)) was assessed using $\Delta_fH(AsF_5$ (g)) = −1234 kJ mol^{-1}, $\Delta_fH(AsF_3$ (l)) = −858 kJ mol^{-1} [198,200] and the enthalpies of formation of $S_4(AsF_6)_2$ (c) (−3104 kJ mol^{-1}), $S_8(AsF_6)_2$ (c) (−3122 kJ mol^{-1}), $Se_4(AsF_6)_2$ (c) (−3182 kJ mol^{-1}), $S_8(AsF_6)_2$ (c) (−3197 kJ mol^{-1}) from Ref. [16].

	$E_8(AsF_6)_2$(c) +	$3AsF_5$ (g) →	$2E_4(AsF_6)_2$(c) +	AsF_3 (l)	
Δ_fH(S) =	−3122	−1234	−3104	−858	Δ_rH = −242 kJ mol^{-1}
Δ_fH(Se) =	−3197	−1234	−3182	−858	Δ_rH = −323 kJ mol^{-1}

(45)

Eq. (45), an often employed preparation for $E_4(AsF_6)_2$, is exothermic by 242 (S) or 323 (Se) kJ mol^{-1}, in good agreement with experiment, although for E = S the reaction only proceeds in the presence of a trace of halogen X_2 (X = Cl, Br, I) [179].

5.2.6. The stability of $[E_8^{2+}][AlCl_4^-]_2$ (E = S, Se)

The X-ray crystal structure of $[Se_8^{2+}][AlCl_4^-]_2$ is known [89], however various attempts to prepare the S_8^{2+} homologue always met with failure. The formation of $[S_8^{2+}][AlCl_4^-]_2$ from S_2Cl_2 (l), 6/8 S_8 (c) + 2$AlCl_3$ (c) was considered (Eq. (46)).

$$S_2Cl_2\ (l) + 6/8S_8\ (c) + 2AlCl_3\ (c) \rightarrow [S_8^{2+}][AlCl_4^-]_2\ (c)\ \Delta_rH = -165\ kJ\ mol^{-1} \quad (46)$$

This reaction [see ΔH(46) in Appendix] is found to be exothermic by 165 kJ mol^{-1}, implying that $[S_8^{2+}][AlCl_4^-]_2$ should be accessible using this route of preparation. However, entropy favours the decomposition.

Another possible synthetic route was examined in Eq. (47) for both $[S_8^{2+}][AlCl_4^-]_2$ and $[Se_8^{2+}][AlCl_4^-]_2$ [see $\Delta H(47)$ in Appendix]:

$$8E\ (ss) + 2AlCl_3\ (c) + Cl_2\ (g) \rightarrow [E_8^{2+}][AlCl_4^-]_2\ (c)\ E = S,\ Se \quad (47)$$

Both reaction enthalpies and free energies of Eq. (47) were estimated to be favourable for the formation of $[E_8^{2+}][AlCl_4^-]_2$ [E = S (Se): ΔH (Eq. (47)) = -220 (-278) kJ mol^{-1}; ΔG (Eq. (47)) = -204 (-268) kJ mol^{-1}]. The formation of the selenium homologue is more favoured by about 70 kJ mol^{-1} than that of $[S_8^{2+}][AlCl_4^-]_2$. Considering the experimental failure to prepare the latter salt, it seems likely to assume that a yet unassessed decomposition pathway is more favourable. It is likely that the S_8^{2+} cation in $[S_8^{2+}][AlCl_4^-]_2$ abstracts a chloride ion to form S_8Cl^+, which rearranges to give S_7Cl^+ (cf. S_7Br^+ [180], and evidence for S_7Cl^+ [181] has been presented). However, the differences in ΔG (Eq. (47)) between E = S and E = Se of only 74 kJ mol^{-1} indicates that the stability of $[Se_8^{2+}][AlCl_4^-]_2$ is only marginal. This is in agreement with the observation that $[Se_8^{2+}][AlCl_4^-]_2$ disproportionates upon washing with large amounts of SO_2 to give $[Se_{10}^{2+}][AlCl_4^-]_2$, Se_2Cl_2 and $AlCl_3$ [80a]. However, no thermodynamic data of the Se_{10}^{2+} dication is available which prevents the assessment of the underlying thermodynamics of this decomposition reaction.

6. Kinetics and reaction pathways in the formation of the homopolyatomic cations of Groups 16 and 17

Thermodynamics clearly play a very critical role in the synthesis, stability and structure of the homopolyatomic cations of these chalcogens and halogens. However kinetic factors can play a role. For example elemental sulphur reacts with a large excess of AsF_5 in SO_2, AsF_3, or HF to give only blue $[S_8^{2+}][AsF_6^-]_2$, even under pressure with increased temperature and for several weeks. However the addition of minute amounts of halogen facilitates the increase in effective oxidising power of the pentafluoride and white $[S_4^{2+}][AsF_6^-]_2$ is formed in 5 min [43]. The analogous reaction with selenium to give $[Se_4^{2+}][AsF_6^-]_2$ proceeds without addition of halogen but requires heating to 60°C for several days. With traces of halogen the reaction proceeds within minutes at r.t. Reaction pathways with (Fig. 58) and without halogen (Fig. 59) have been proposed (J. Passmore) [43]. Halo-polychalcogen cations are suggested as key intermediates, some of which have been independently identified [182,183]. The analogous reactions of the chalcogens and the peroxide $S_2O_6F_2$, which is a pseudo halogen as the oxidising agent, proceed readily [11]. We propose that fluorosulphate–polychalcogen cations are key intermediates.

Selenium and tellurium react with mixtures of the elemental halide and aluminium halide on heating to give salts of the corresponding homopolyatomic cation, e.g. Eq. (48):

$$TeCl_4 + 7Te + 4AlCl_3 \rightarrow 2[Te_4^{2+}][AlCl_4^-]_2 \quad (48)$$

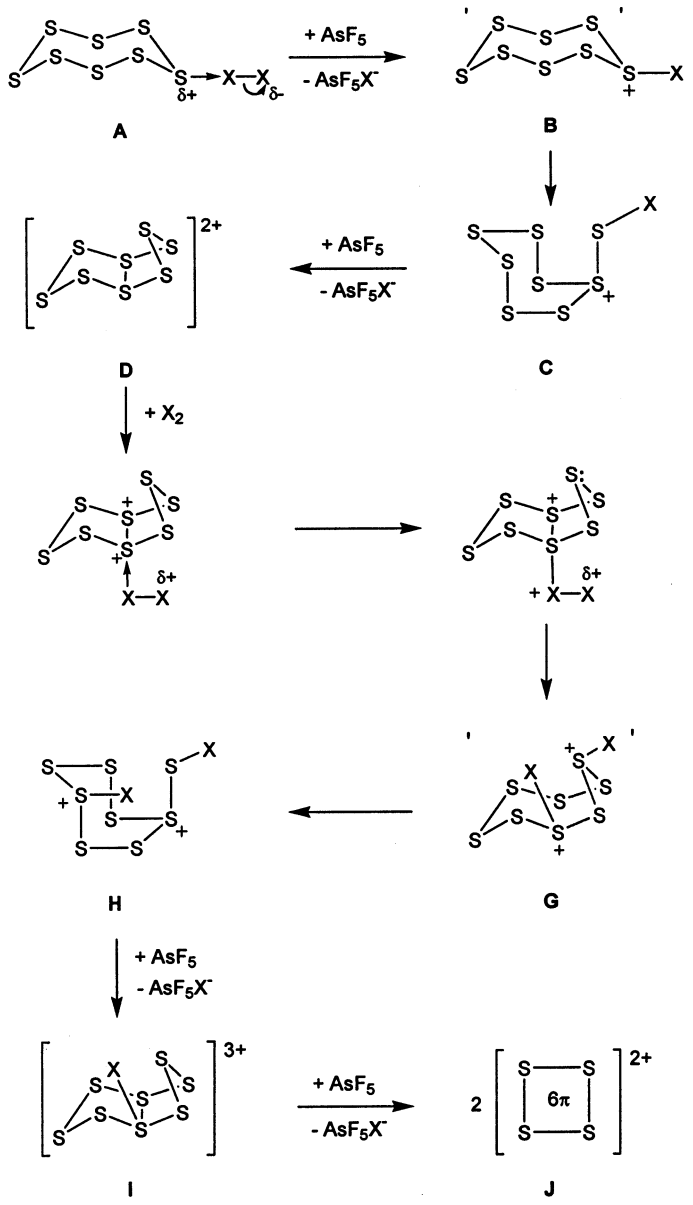

Fig. 58. Proposed formation of S_4^{2+} with halogen.

It is likely that halo-polychalcogen cations are also intermediates in these reactions. Reaction of O_2^+ salts, and those with oxidising hexahalides or high valent oxyhalides (e.g. Eqs. (2) and (3)), proceed by one electron oxidation transfer reactions.

The reaction of tellurium and arsenic pentafluoride is very dependent on the purity and source of the elemental tellurium. With very high purity Te (99.999%) the reaction goes no further than $[Te_4^{2+}][AsF_6^-]_2$, but with less pure and some sources of apparently very pure element the reaction proceeds further to give $[TeF_3^+][AsF_6^-]$ and a mixture of what appears to be elemental tellurium and an hexafluoride salt of a lower tellurium homopolyatomic cation [36,37,184]. With halogen facilitator the reaction proceeds in liquid sulphur dioxide to $[Te_6^{4+}][AsF_6^-]_4$, TeF_4 or $[TeF_3^+][AsF_6^-]$ as shown in Eqs. (49)–(51).

$$6Te + 6AsF_5 \rightarrow [Te_6^{4+}][AsF_6^-]_4 + 2AsF_3 \quad (49)$$

$$E + 2AsF_5 \rightarrow EF_4 + 2AsF_3 \ (E = S, Se, Te) \quad (50)$$

$$Te + 3AsF_5 \rightarrow [TeF_3^+][AsF_6^-] + 2AsF_3 \quad (51)$$

The analogous reactions do not proceed for selenium and sulphur. This is partly thermodynamics as the reactions (Eq. (50)) are most favoured for E = Te ($\Delta H = -180$ kJ mol^{-1}), only slightly exothermic for Se ($\Delta H = -25$ kJ mol^{-1}), and endothermic for S ($\Delta H = +69$ kJ mol^{-1}) [51,185].

7. Conclusions and outlook

New salts of homopolyatomic cations of Groups 16 and 17 continue to be prepared and characterised, especially those of tellurium and, very recently, also chlorine. We have made considerable advances in the understanding of the energetics of at least the salts of the simpler homopolyatomic cations and we can answer most of the questions posed in the beginning of the review, e.g. why is $[S_4^{2+}][AsF_6^-]_2$ formed and not $[S_2^+][AsF_6^-]$ (cf. $[O_2^+][AsF_6^-]$, see Section 5.2.2)? Why does S_4Cl_2

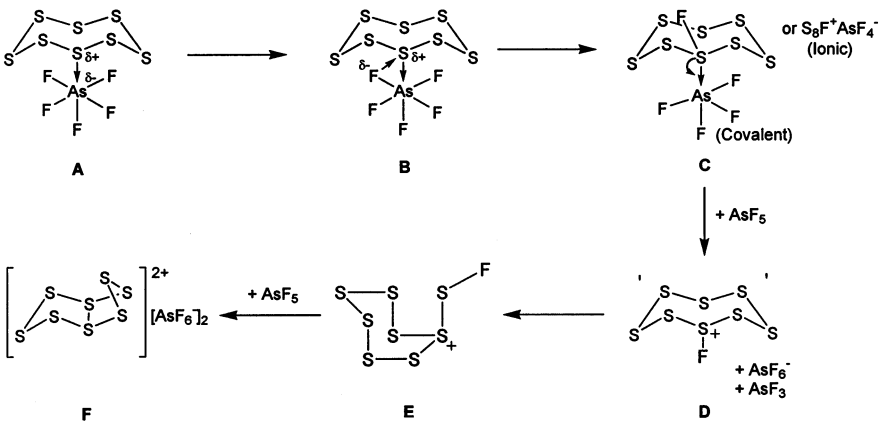

Fig. 59. Proposed formation of S_8^{2+} without halogen.

adopt a chain like, molecular geometry and not the salt like structure of the square planar 6π aromatic S_4^{2+} dication found in a variety of $[S_4^{2+}][A^-]_2$ salts (A = fluoroanion, see Section 5.2.4)? The question as to why Te_6^{4+} is formed but not S_6^{4+} is still under investigation and will be answered at a later occasion. This represents a significant step forward in the maturation of the field from the butterfly collecting stage towards the point where systematic investigations are possible. We are moving to the point when the planning of syntheses of yet unknown homopolyatomic cations of these and other elements can be based on well established thermodynamic values. These include lattice potential enthalpies, which depend on anion size and basicity. We anticipate that advances will be made in understanding and predicting the behaviour of these salts in solutions of various dielectric constants, and of the molten salts. We are presently investigating, by theoretical methods, the solution behaviour of S_8^{2+} and conclude that the species largely responsible for the blue colour of S_8^{2+} in its various salts and in solution may not be S_5^+ as thought previously [186].

The chemistry of these homopolyatomic cations has not been referred to here, as it warrants a review on its own. We anticipate that the investigation of the chemistry of the homopolyatomic cations of Groups 16 and 17 will continue to yield new discoveries.

High level calculations of E_8^{2+} (E = S, Se, Te) now correctly reproduce their geometries for the first time [16]. An analysis of the bonding in these cations established the nature of the long cross ring interactions and their overall bonding. The earlier thesis that unusual non classical structures and related homopolyatomic cations result from positive charge delocalisation leading to the formation of np_π–np_π ($n \geq 3$) and intracationic π*–π* bonds, bond lengths alternation and cluster like geometry is supported. The bond lengths alternation is shown to be attributable to $np^2 \rightarrow n\sigma^*$ and np_π–np_π ($n \geq 3$) bond formation which is one of the ways in which the positive charge is delocalised. The cluster like geometries are shown to be due to intracationic four centre and six centre two electron π*–π* (π* with respect to the atoms on each side of the ring, p_σ across the ring), $np^2 \rightarrow n\sigma^*$ and weak np^2–np^2 interactions, leading to positive charge delocalisation and lowering of the energy. The structures of all of the observed homopolyatomic cations of Groups 16 and 17 can be understood in terms of this simple model, including the recently prepared polymeric tellurium homopolyatomic cations. Alternatively the geometries of the more cluster like chalcogen homopolyatomic cations can be understood by the Wade–Mingos rules, consistent with the positively charged atoms adopting positions on a sphere, i.e. minimising repulsion between positive charges.

The non classical geometries of many of these cations were shown [16,33] to be quantitatively lower in energy than their classically σ bonded isomers, e.g. in the M_4^{2+} case (see Fig. 60). The rectangular I_4^{2+} was calculated [191] to be marginally more stable than the isomer with a Te_2I_2 structure (Fig. 61). The observed np_π–np_π bonded S_8^{2+} with long transannular interactions [S3–S7 = 2.859 (3) Å, calculated

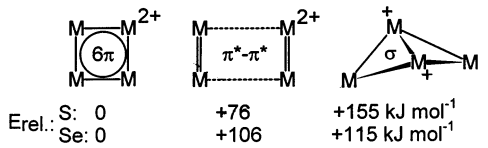

Fig. 60. Relative energies of different M_4^{2+} isomers [33].

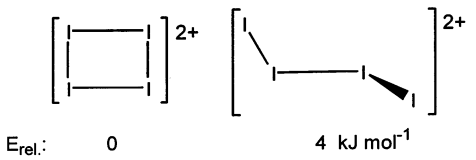

Fig. 61. Relative energies of two forms of I_4^{2+} [191].

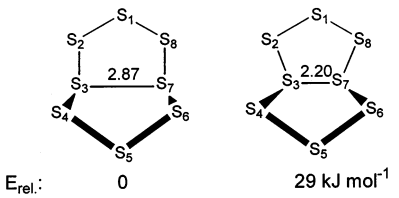

Fig. 62. Relative energies of np_π–np_π bonded and classically bonded forms of S_8^{2+} [16]. Distances are given in Å.

2.87 Å] is more stable, by 29 kJ mol^{-1}, than a classically bonded structure with localised positive charges and a transannular S–S bond length of 2.20 Å (Fig. 62) [16].

However, the classically bonded isomers also delocalise positive charge, by $np^2 \rightarrow n\sigma^*$ interactions, leading to lowering of energy.

The np_π–np_π ($n \geq 3$) homoatomic bonds formed between the heavier chalcogen and halogen atoms in these cations is reminiscent of those observed in the sterically hindered compounds of the main Groups 13, 14 and 15 e.g. $R_2Si{=}SiR_2$ (R = bulky organo-ligand) [187b,188]. The stability of these compounds is not just kinetic, but thermodynamic as well, they are more stable than the σ bonded oligomers which are destabilised by steric hindrance of the bulky groups [189]. The presence of np_π–np_π ($n \geq 3$) bonds is more widespread than sometimes generally appreciated. The short S–S bond lengths in both isomers of S_2F_2 (1.86 and 1.89 Å [190]), and S_7 (1.99 Å [138]), have been known for some time. The halo-polychalcogen cations show related geometries and similar π bonding [183]. The most highly π bonded compound of the main group elements, excluding second row elements, is the cluster-like $S_2I_4^{2+}$ with an S–S bond of 1.818 Å indicative of bond order 2.33 [187a], confirmed by our recent computations [191]. Intra and intermolecular π*–π* bonding in related compounds has been reviewed [11]. Delocalisation of the unfavourable localised charges leads to intra and intermolecular $np^2 \rightarrow n\sigma^*$ bonding

and is well documented in such diverse compounds as ONF_3 [192], OCF_3^- [193], S_7 [138]. The structures of the polyhalogen anions and the chalcogen-rich chalcogenides [194] presumably can also be interpreted based on this model. It is responsible for cation?anion interactions in salts of the type $[MX_3^+][AsF_6^-]$ (M = chalcogen, X = halogen [195]) and for intermolecular interactions between molecules of the halogen and chalcogen elements in the solid state, increasing in importance as the group is descended. Therefore it is apparent that the structures of the homopolyatomic cations of Groups 16 and 17 are now largely understood, and are driven by positive charge delocalisation by well established bonding modes, and integrated into the main stream of inorganic chemistry.

Acknowledgements

We thank George Zhor and Hongbin Du for help preparing the manuscript, and Professor Johannes Beck for supplying us with published and unpublished crystallographic data files, the Alexander von Humboldt Foundation (Germany) and NSERC (Canada) for financial support (I. Krossing, J. Passmore). J. Passmore thanks Jesus College, Oxford for a Senior Visiting Research Fellowship for 1996/1997 during which time the foundation for this review was laid. H.D.B. Jenkins thanks the EPSRC (UK) and the University of Warwick for financial support.

Appendix A

A.1. Equations

Lattice enthalpy, ΔH_L, and its relation to the lattice potential energy, U_{POT} [208]

$$\Delta H_L = U_{POT} + \left[p\left(\frac{n_M}{2} - 2\right) + q\left(\frac{n_x}{2} - 2\right)\right]RT \quad \text{(A1)}$$

where p and q are the number of cations and anions, respectively in the salt of molecular formula M_pX_q, n_M, n_x are equal to 3 for monoatomic ions, 5 for linear polyatomic ions and 6 for non-linear polyatomic ions, R is the gas constant and T is the absolute temperature.

A.2. Entropy [196]

$$\text{diatomic gas} = 53.8 + 0.043M - 240M^{-1}$$

$$\text{polyatomic gas} = 39.0 + 0.34M - 6.2 \times 10^{-4}M^2$$

where M is the molecular mass. Entropies of salts were estimated using Latimer's rules [197]: $[S°([Cl_3^+][AsF_6^-]\ (c)) = 61\ \text{kJ mol}^{-1}]$.

For thermochemical data used in the review, see Tables 12–15.

Table 12
Standard enthalpy of formation and ionic volumes

Species	$\Delta_f H°$ (kJ mol^{-1})	Reference	Ion volumes (nm^3)	Reference/estimated
$AlCl_3$ (c)	−704	[15c]	–	–
$AlCl_4^-$ (g)	−1196	[15c]	0.156	[15b]
AsF_3 (l)	−821	[198]	–	–
AsF_5 (g)	−1237	[199]	–	–
AsF_6^- (g)	−1919	[15c]	0.110	[15b]
Br (g)	112	[198]	–	–
Br^+ (g)	1252	[200]	0.029	$Br_2^+/2$
Br_2^+ (g)	1046	[200]	0.057	[15b]
BrF (g)	−59	[198]	–	–
$[BrF_2^+][SbF_6^-]$ (c)	−1773	[201]	0.040 (ca.)	[15b]
$[BrF_2^+][TaF_6^-]$ (c)	−2251	[201]	0.040 (ca.)	[15b]
BrF_5 (l)	−459	[198]	–	–
Cl (g)	122	[198]	–	–
Cl^+ (g)	1372	[200]	0.015	$Cl_2^+/2$
Cl_2^+ (g)	1108	[200]	0.030	$O_2^+ < Cl_2^+ < S_2^+$
$[Cl_2F^+][AsF_6^-]$ (c)	−1487	[202]	0.035	[15b]
ClF (g)	−55	[198]	–	–
ClF_5 (g)	−238	[198]	–	–
F (g)	79	[198]	–	–
F^+ (g)	1760	[200]	0.004	$F_2^+/2$
F^- (g)	−249	[200]	–	–
F_2^+ (g)	1515	[200]	0.007	Hal_2^+ versus $Chal_2^+$
I (g)	107	[198]	–	–
I^+ (g)	1115	[200]	0.036	$I_2^+/2$
I_2^+ (g)	969	[200]	0.072	[15b]
IF (g)	−95	[198]	–	–
IF_2^+ (g)	652	[203]	0.061	[15b]
IF_5 (l)	−883	[198]	–	–
O^+ (g)	1563	[200]	0.008	$O_2^+/2$
O_2^+ (g)	1165	[200]	0.015	[15b]
S^+ (g)	1284	[200]	0.023	$S_2^+/2$
S_2^+ (g)	1031	[200]	0.045	[15b]
S_8^{2+} (g)	2151	[16]	0.180	[15b]
S_2Cl_2 (l)	−59	[15c]	–	–
SF_4 (g)	−763	[51,185]	–	–
SO_2 (g)	−296.8	[198]	–	–
SbF_3 (g)	−916	[198]	–	–
SbF_5 (l)	−1328	[204]	–	–
SbF_6^- (g)	−2100	[15c]	0.121	[15b]
$Sb_2F_{11}^-$ (g)	< −3482	[15c]	0.227	[15b]
Se^+ (g)	1168	[200]	0.030	$Se_2^+/2$
Se_2^+ (g)	985	[200]	0.060	[15b]
Se_8^{2+} (g)	2071	[16]	0.214	[15b]
SeF_4 (l)	−857	[51,185]	–	–
TaF_6^- (g)	−2593	[205]	–	–
Te^+ (g)	1066	[200]	0.043	$Te_2^+/2$
Te_2^+ (g)	933	[200]	0.086	[15b]
Te_4^{2+} (g)	2077	[206]	0.115	[15b]
TeF_3^+ (g)	213	[207]	0.074	[15b]
TeF_4 (ss)	−1012	[51,185]	–	–

Table 13
Ionisation potentials (I_P)

Species	I_P (kJ mol^{-1})	Reference
Br (g)	1140	[200]
Cl (g)	1251	[200]
I (g)	1008	[200]
O_2 (g)	1165	[200]
F^- (g)	328	[200]

Table 14
Fluoride ion affinities (FIA)

Species	FIA (kJ mol^{-1})	Reference
AsF_5 (g)	433	[15c]
$AsF_5{\cdot}SO_2$ (c)	402	[15c]
SbF_5 (g)	526 (502)	[15c,163]
$2SbF_5$ (l)	>582	[15c]

Table 15
Entropies

Species	Absolute entropy (JK^{-1} mol^{-1})	Reference/estimated
AsF_5 (g)	330	Estimated
Cl_2 (g)	223	[208]
$[Cl_3^+][AsF_6^-]$ (c)	61.25	Estimated
ClF (g)	218	[208]

A.3. Born–Fajans–Haber cycles employed

N.B.: ΔH_L = lattice enthalpy.

A.3.1. For Section 5.1.1, Eq. (10)

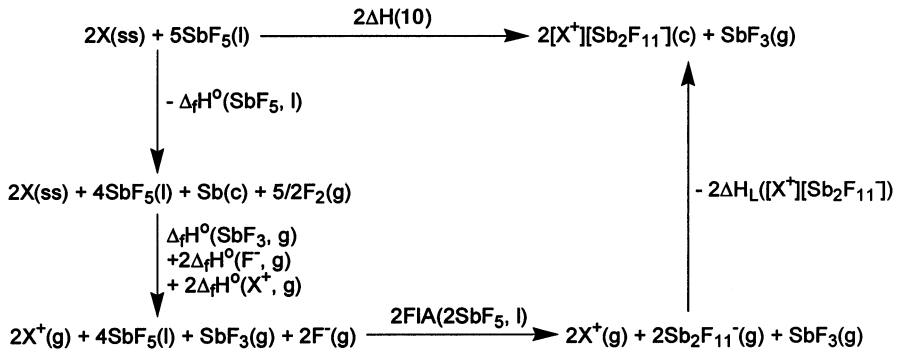

A.3.2. For Section 5.1.1, Eq. (11)

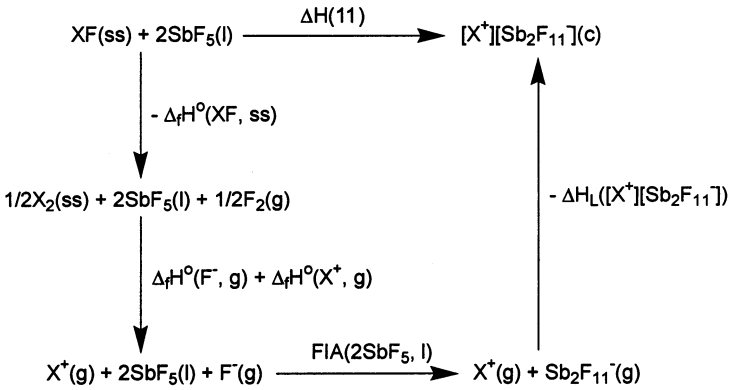

A.3.3. For Section 5.1.1, Eq. (12)

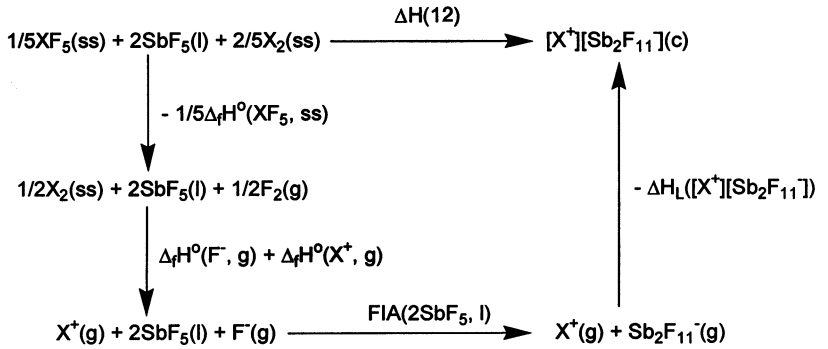

A.3.4. For Section 5.1.1, Eq. (13)

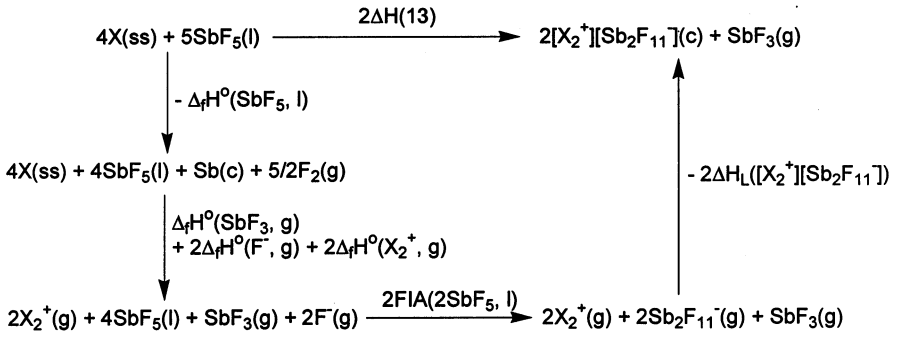

A.3.5. For Section 5.1.1, Eq. (14)

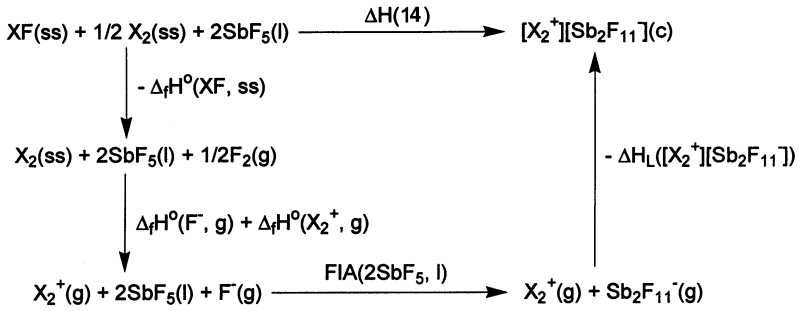

A.3.6. For Section 5.1.1, Eq. (15)

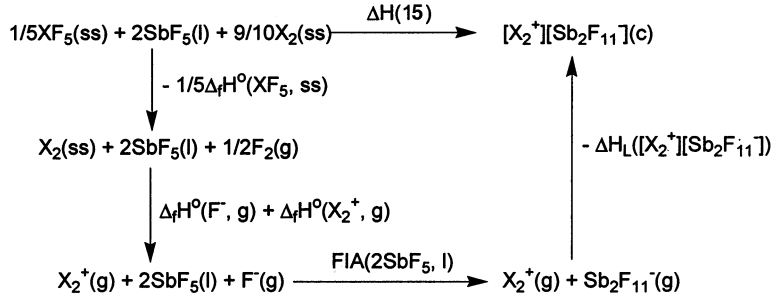

A.3.7. For Section 5.1.1, Eq. (16)

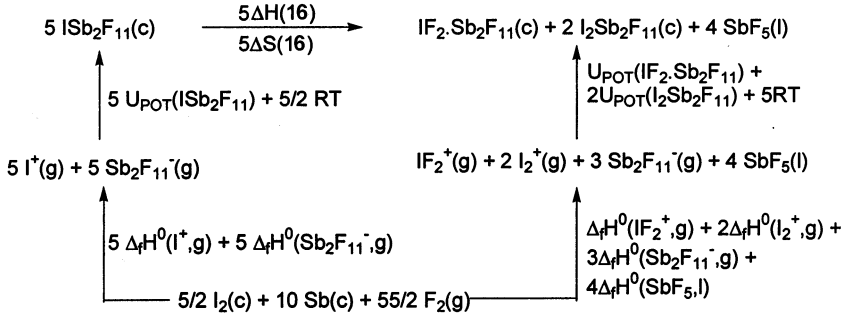

$$5\Delta H_{16} = 5U_{\mathrm{POT}}(\mathrm{ISb_2F_{11}}) - 5\Delta_{\mathrm{f}}H°(\mathrm{I^+},\ \mathrm{g}) - 2\Delta_{\mathrm{f}}H°(\mathrm{Sb_2F_{11}^-},\ \mathrm{g}) + \Delta_{\mathrm{f}}H°(\mathrm{IF_2^+},\ \mathrm{g}) + 2\Delta_{\mathrm{f}}H°(\mathrm{I_2^+},\ \mathrm{g}) + 4\Delta_{\mathrm{f}}H°(\mathrm{SbF_5},\ \mathrm{l}) - U_{\mathrm{POT}}(\mathrm{IF_2Sb_2F_{11}}) - 2U_{\mathrm{POT}}(\mathrm{I_2Sb_2F_{11}}) - 5/2RT$$

$\Delta_f H°(IF_2^+, g) = 652$ kJ mol^{-1} was calculated (MPW1PW91/3-21G*), which is in agreement with: $\Delta_f H°(IF^+, g) = 927.6$ kJ mol^{-1} and $\Delta_f H°(IF_5^+, g) = 432.6$ kJ mol^{-1} [203].

$\Delta H_{15} = 383$ kJ mol^{-1}. Since $\Delta S_{15} > 0$, $T\Delta S_{15} > 0$, ΔG_{15} will be negative by at least -382.6 kJ mol^{-1}

A.3.8. For Section 5.1.2, Eq. (18)

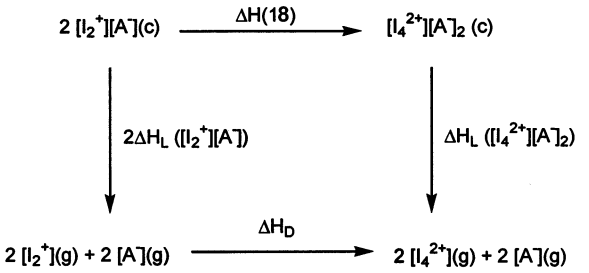

ΔH_D has been determined to be 429 ± 28 kJ mol^{-1} [15c]. Using the data from Ref. [15], the lattice energies have been determined:

ΔH_L $[I_2^+][AsF_6^-] = 521$ kJ mol^{-1} ΔH_L $[I_4^{2+}][AsF_6^-]_2 = 1500$ kJ mol^{-1}

ΔH_L $[I_2^+][Sb_2F_{11}^-] = 455$ kJ mol^{-1} ΔH_L $[I_4^{2+}][Sb_2F_{11}^-]_2 = 1310$ kJ mol^{-1}

ΔH_L $[I_2^+][AlCl_4^-] = 488$ kJ mol^{-1} ΔH_L $[I_4^{2+}][AlCl_4^-]_2 = 1578$ kJ mol^{-1}

A.3.9. For Section 5.1.3, Eq. (20)

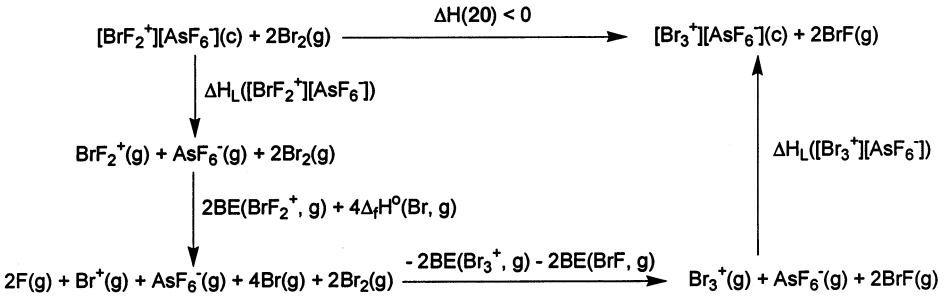

BE(BrF_2^+ (g)) is estimated to be 263 kJ mol^{-1} by employing:

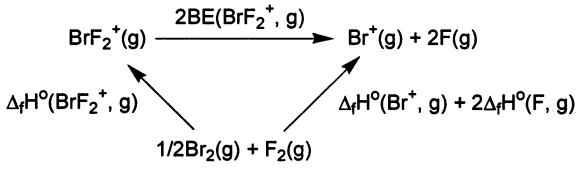

$\Delta_f H°(BrF_2^+$ (g)) is estimated to be 885 kJ mol^{-1} by employing:

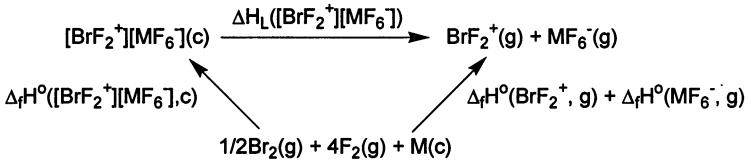

BE(BrF (g)) = 250 kJ mol^{-1} is obtained using:

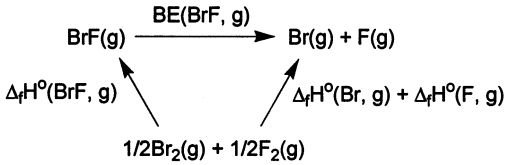

A.3.10. For Section 5.1.3, Eqs. (21) and (25)

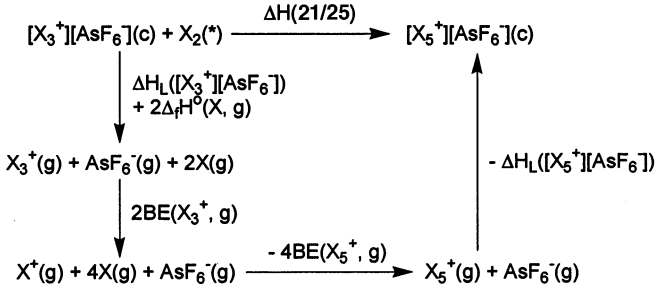

*for X = Br, I are in standard state: ΔH(20) < 0
X = Cl in non-standard state, 195 K: ΔH(24) > 0

Error associated with X = Br due to BE(Br_3^+ (g)) > 259 kJ mol^{-1} whilst $\Delta H(20) < 0$ kJ mol^{-1} as approximation BE(Br_5^+ (g)) ~ 192 kJ mol^{-1}.

A.3.11. For Section 5.1.3, Eq. (22)

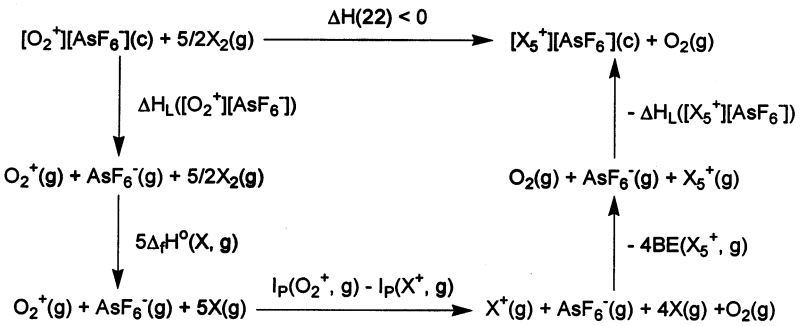

A.3.12. For Section 5.1.3, Eq. (23)

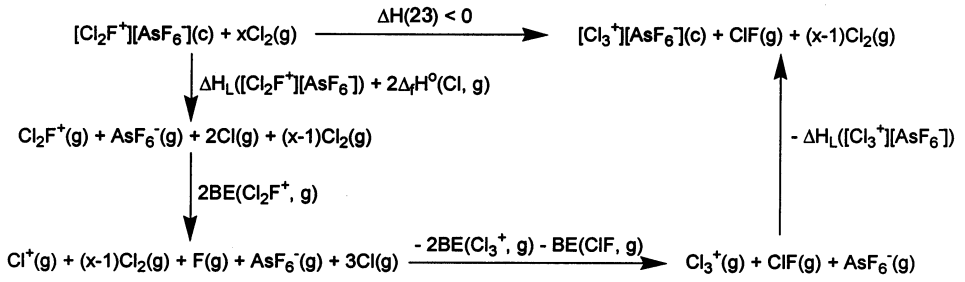

$BE(Cl_2F^+$ (g)) is calculated to be 290 kJ mol^{-1} by employing:

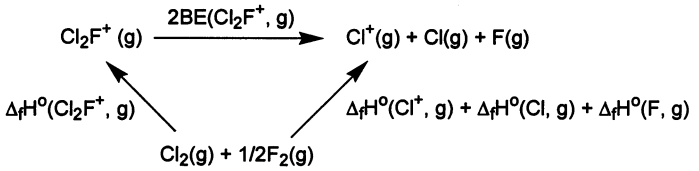

$\Delta_f H°(Cl_2F^+$ (g)) is estimated to be 994 kJ mol^{-1} using $\Delta_f H°([Cl_2F^+][AsF_6^-]$ (g)):

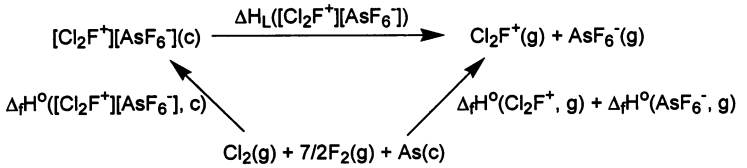

and BE(ClF (g)) is calculated to be 256 kJ mol^{-1} by employing:

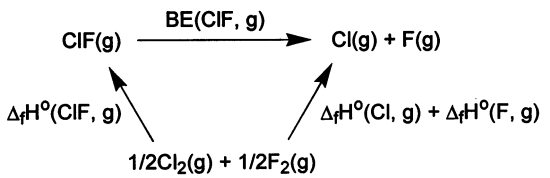

A.3.13. For Section 5.1.3, Eq. (24)

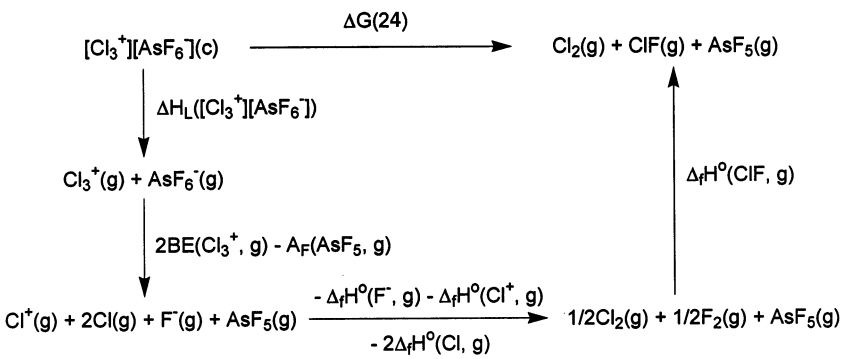

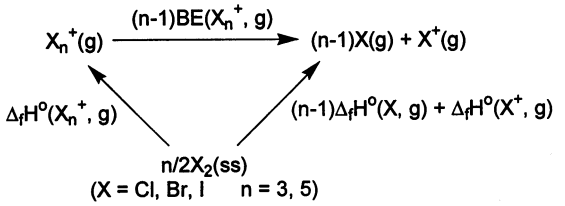

A.3.14. For Section 5.1.3, Eq. (26)

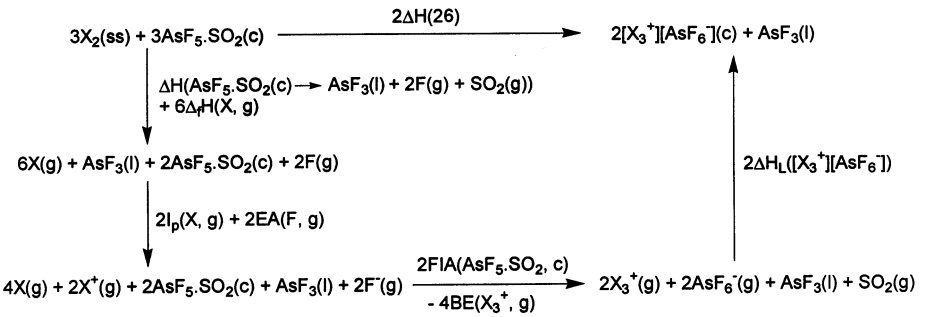

A.3.15. For Section 5.1.3, Eq. (27)

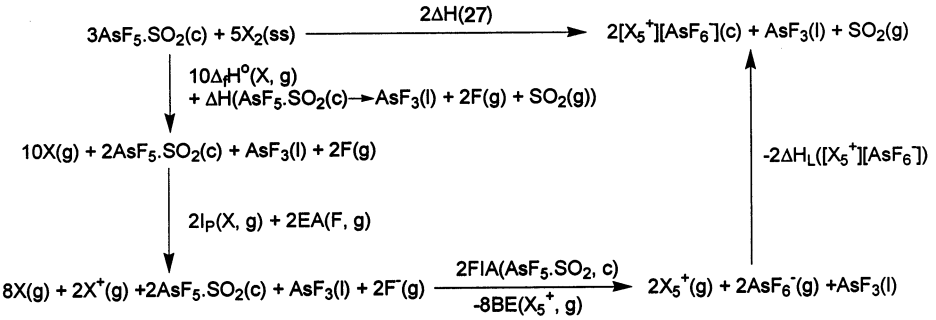

where $\Delta H(\mathrm{AsF_5{\cdot}SO_2\ (c) \rightarrow AsF_3\ (l) + 2F\ (g) + SO_2\ (g)}) = 605\ \mathrm{kJ\ mol^{-1}}$ by employing:

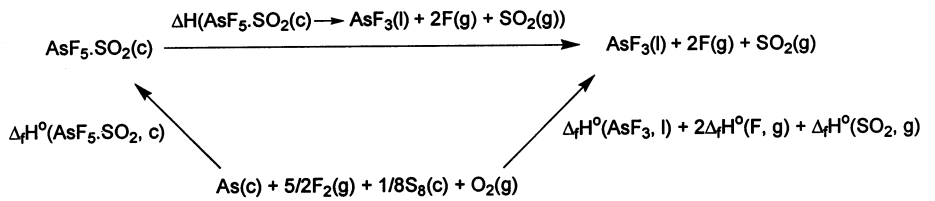

and $\Delta_f H°(AsF_5{\cdot}SO_2\ (c))$ is found to be -1565 kJ mol^{-1} using:

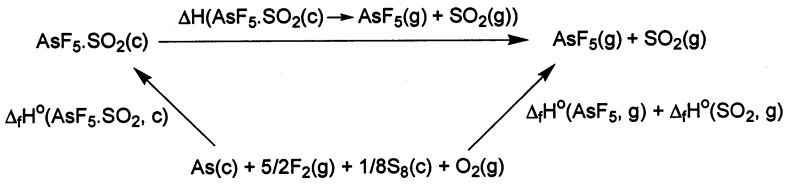

where $\Delta H(AsF_5{\cdot}SO_2\ (c) \rightarrow AsF_5\ (g) + SO_2\ (g)) = 31$ kJ mol^{-1} [209].

A.3.16. For Section 5.1.3, Eq. (28)

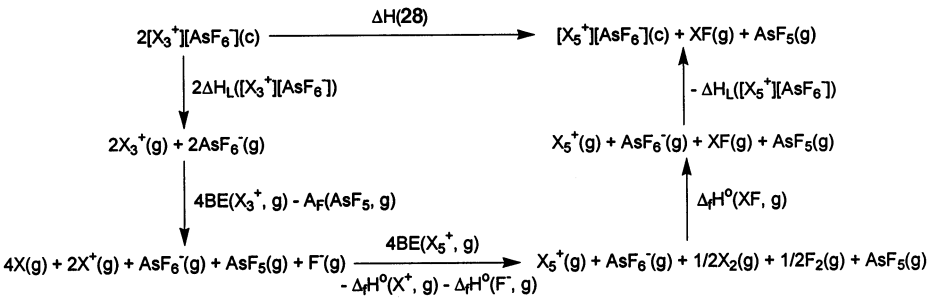

A.3.17. For Section 5.2.1, Eq. (31)

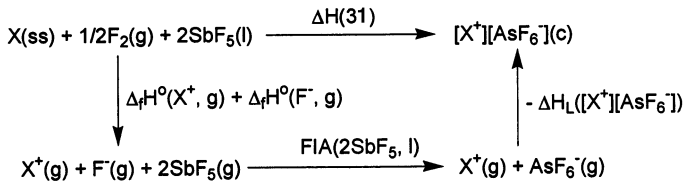

A.3.18. For Section 5.2.1, Eq. (32)

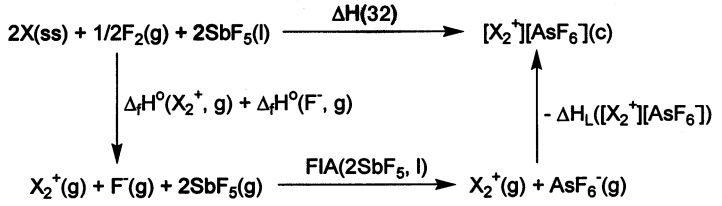

A.3.19. Decomposition of $[Te][Sb_2F_{11}]$

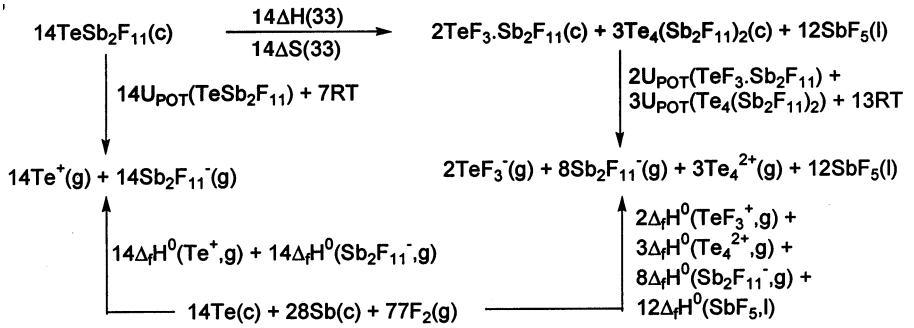

$$\Delta H_{33} = 14U_{POT}(TeSb_2F_{11}) - 14\Delta_f H°(Te^+, g) - 6\Delta_f H°(Sb_2F_{11}^-, g)$$
$$+ 2\Delta_f H°(TeF_3^+, g)\ 3\Delta_f H°(Te_4^{2+}, g) + 12\Delta_f H°(SbF_5, l)$$
$$- 2U_{POT}(TeF_3{\cdot}Sb_2F_{11}) - 3U_{POT}(Te_4(Sb_2F_{11})_2) - 6RT$$

$\Delta_f H°(TeF_3^+$ (g)): B3PW91/3-21G* calculation of ΔH for

$$TeF_{6(g)} + Te_{(g)}^{2+} \overset{\Delta H}{\rightarrow} 2TeF_{3(g)}^{+}$$
$$\Delta H = -1130 \text{ kJ mol}^{-1}$$

$$\Delta H = 2\Delta_f H°(TeF_3^+, g) - \Delta_f H°(Te^{2+}, g) - \Delta_f H°(TeF_6, g) = -1130 \text{ kJ mol}^{-1}$$
$$\Delta_f H°(Te^{2+}, g) = 2874 \text{ kJ mol}^{-1};\ \Delta_f H°(TeF_6, g) = -1318 \text{ kJ mol}^{-1},$$
$$\Rightarrow \Delta_f H°(TeF_3^+, g) = 1/2(-1130 + 2874 - 1318) = 213 \text{ kJ mol}^{-1}$$

A.3.20. Preparation of $E_8(AlCl_4)_2$ ($E = S$, Se)

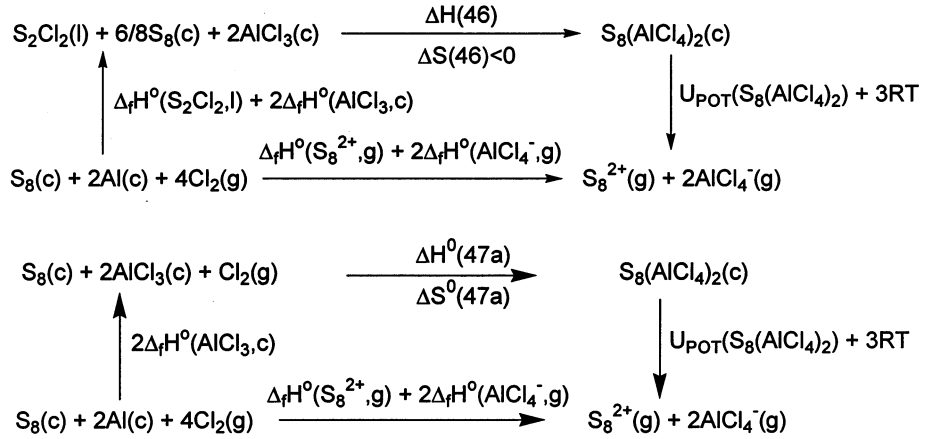

$$\Delta S°(47a) = S°(S_8(AlCl_4)_2) - S°(S,\ \text{rhombic, c}) - 2S°(AlCl_3\ (c)) - S°(Cl_2\ (g))$$

$$= (646) - 8(31.80) - 2(110.67) - (223.1)$$

$$= -52.8\ \text{JK}^{-1}\ \text{mol}^{-1} < 0$$

$$T\Delta S°(47a) = -15.7\ \text{kJ mol}^{-1}$$

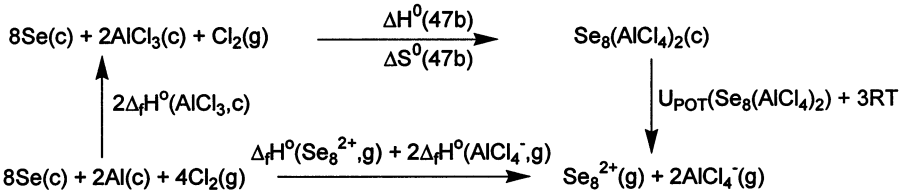

$$S°(Se_8(AlCl_4)_2) = 8S°(Se) + 2S°(Al) + 8S°(Cl)$$

$$= 8(48.5) + 2(33.47) + (36.82) = 749.8\ \text{JK}^{-1}\ \text{mol}^{-1}$$

$$\Delta S°(47b) = S°(Se_8(AlCl_4)_2) - S°(Cl_2\ (g)) - 2S°(AlCl_3\ (c) - 8S°(Se\ (c))$$

$$= (749.8) - (223.1) - 2(110.67) - 8(42.442) = -34.2\ \text{JK}^{-1}\ \text{mol}^{-1}$$

$$T\Delta S°(47b) = -10.2\ \text{kJ mol}^{-1}$$

$$\Delta G°(47b) = \Delta H°(47b) - T\Delta S°(47b) < 0$$

References

[1] (a) C.F. Bucholz, Gehlen's Neues J. Chem. 3 (1804) 7. (b) G. Magnus, Ann. Phys. Leipzig 10 (1827) 491; ibid. 14 (1828) 328. (c) J.W. Meller, Comprehensive Treaties on Inorganic and Theoretical Chemistry, vol. 10, Longmans, Green, New York, 1930, p. 922. (d) M.H. Klaproth, Phil. Mag. 1 (1798) 78. (e) J. Arotsky, M.C.R. Symons, Q. Rev. Chem. Soc. 16 (1962) 282 and references therein.
[2] (a) R. Weber, J. Prakt. Chem. 133 (1882) 218. (b) I. Masson, C. Argument, J. Chem. Soc. (1938) 1705.
[3] R.A. Garrett, R.J. Gillespie, J.B. Senior, Inorg. Chem. 4 (1965) 563.
[4] (a) N. Bartlett, D.H. Lohmann, J. Chem. Soc. (1962) 5253. (b) N. Bartlett, D.H. Lohmann, Proc. Chem. Soc. Lond. (1962) 115.
[5] N. Bartlett, Proc. Chem. Soc. (1962) 218.
[6] (a) R.J. Gillespie, J. Passmore, Acc. Chem. Res. 4 (1971) 413. (b) R.J. Gillespie, M.J. Morton, J. Chem. Soc. Q. Rev. (1971) 553. (c) R.J. Gillespie, J. Passmore, Chem. Ber. 8 (1972) 475. (d) R.J. Gillespie, M.J. Morton, Inorg. Chem. Series 1, MPT International Review of Science, vol. 3, Butterworth, Baltimore, 1972, p. 199. (e) R.J. Gillespie, J. Passmore, Adv. Inorg. Chem. Radiochem. 17 (1975) 49. (f) R.J. Gillespie, J. Chem. Soc. Rev. 8 (1979) 315.
[7] J.D. Corbett, Prog. Inorg. Chem. 21 (1976) 129.
[8] J. Shamir, Struct. Bonding 37 (1979) 141.
[9] R. Steudel, E.-M. Strauss, Adv. Inorg. Chem. Radiochem. 28 (1984) 135.

[10] (a) T.A. O'Donnell, Chem. Soc. Rev. 16 (1987) 1. (b) T.A. O'Donnell, Superacids and Acidic Melts as Inorganic Chemical Reaction Media, VCH, New York, 1993.
[11] N. Burford, J. Passmore, J.C.P. Sanders, in: J.F. Liebman, A. Greenberg (eds.), From Atoms to Polymers, Isoelectronic Analogies, 1989, p. 53 and references therein.
[12] I.C. Tornieporth-Oetting, T.M. Klapötke, Heteroatom. Chem. 4 (1993) 543.
[13] (a) J. Beck, Angew. Chem. Int. Ed. Engl. 33 (1994) 163. (b) J. Beck, Coord. Chem. Rev. 163 (1997) 55.
[14] J. Passmore, The chemistry of inorganic ring systems in: R. Steudel (ed.), Studies in Inorganic Chemistry, vol. 14, 1992, pp. 373–406, Chapter 19.
[15] (a) H.K. Roobottom, H.D.B. Jenkins, J. Passmore, L. Glasser, J. Chem. Ed. 76 (1999) 1570. (b) H.D.B. Jenkins, H.K. Roobottom, J. Passmore, L. Glasser, Inorg. Chem. 38 (1999) 3609. (c) H.D.B. Jenkins, H.K. Roobottom, J. Passmore, Acc. Chem. Res., to be submitted.
[16] T.S. Cameron, R.J. Deeth, I. Dionne, H.D.B. Jenkins, I. Krossing, J. Passmore, H.K. Roobottom, Inorg. Chem. 2000 (in press).
[17] I. Dionne, J. Passmore, H.D.B. Jenkins, H.K. Roobottom, Inorg. Chem. 2000 (in press).
[18] C.J. Marsden, G.E. Quelch, H.F. Schaefer, J. Am. Chem. Soc. 114 (1992) 6802.
[19] K. Tanaka, T. Yamabe, H. Terama, K. Fukui, Inorg. Chem. 18 (1979) 3591.
[20] (a) L.J. Saethre, O. Gropen, Can. J. Chem. 70 (1992) 348. (b) O. Gropen, L.J. Saethre, E. Wilsoff-Nielssen, in: Carbo (ed.), Studies in Physical and Theoretical Chemistry, Elsevier, Amsterdam, 1982, p. 427.
[21] J. Kao, J. Mol. Struct. 63 (1980) 293.
[22] T.H. Tang, R.F.W. Bader, P.J. McDougall, Inorg. Chem. 24 (1985) 2047.
[23] F.L. Skrezenek, R.D. Harcourt, Theor. Chim. Acta 67 (1985) 271.
[24] G.V. Landwijk, R.A.J. Janssen, H.M. Buck, J. Am. Chem. Soc. 112 (1990) 4155.
[25] M. Sannigrahi, F. Grein, Can. J. Chem. 72 (1994) 298.
[26] N.C. Baird, J. Comp. Chem. 5 (1984) 35.
[27] T.H. Tang, R.F.W. Bader, P.J. MacDougall, Inorg. Chem. 24 (1985) 2047.
[28] J. Cioslowski, X. Gao, Int. J. Quant. Chem. 65 (1997) 609.
[29] M. Bühl, W. Thiel, U. Fleischer, W. Kutzelnigg, J. Phys. Chem. 99 (1995) 4000.
[30] V.G. Zakrzewski, W. von Niessen, Theor. Chim. Acta 88 (1994) 75.
[31] P.D. Lyne, D.M.P. Mingos, T. Ziegler, J. Chem. Soc. Dalton Trans. (1992) 2743.
[32] H.D.B. Jenkins, L.C. Jitariu, I. Krossing, J. Passmore, R. Suontamo, J. Comp. Chem. 21 (2000) 218.
[33] I. Krossing, J. Passmore, Inorg. Chem. 38 (1999) 5203.
[34] J. Thomasi, M. Persico, Chem. Rev. 94 (1994) 2027.
[35] I. Krossing, J. Passmore, D. Wood, (in preparation).
[36] I. Tomaszkiewicz, J. Passmore, G. Schatte, P.A.G. O'Hare, J. Chem. Therm. 28 (1996) 1019.
[37] I. Tomaszkiewicz, J. Passmore, G. Schatte, G.W. Sutherland, P.A.G. O'Hare, J. Chem. Therm. 26 (1994) 299.
[38] R.H. Huang, S.Z. Huang, J.L. Dye, J. Coord. Chem. 46 (1998) 13 and references therein.
[39] K. Wade, Adv. Inorg. Chem. Radiochem. 18 (1976) 1.
[40] D.M.P. Mingos, Acc. Chem. Res. 17 (1984) 311.
[41] W. Rudolph, Acc. Chem. Res. 9 (1976) 446.
[42] E.g. reactions with multiple bonds such as in C_2F_4, R–C≡C–R, R–C≡N, where R is a variety of fluorinated and nonfluorinated organic ligands, reactions with the halogens etc.
[43] (a) M.P. Murchie, J. Passmore, G.W. Sutherland, R. Kapoor, J. Chem. Soc. Dalton Trans. (1992) 503. (b) J. Passmore, G.W. Sutherland, P.S. White, J. Chem. Soc. Chem. Commun. (1980) 330.
[44] J.F. Liebman, H.L. Paige, J. Passmore, Struct. Chem. 9 (1998) 315.
[45] (a) R. Lindh, L.A. Barnes, J. Chem. Phys. 100 (1994) 224, and reference therein. (b) L.A. Barnes, R. Lindh, Chem. Phys. Lett. 223 (1994) 207.
[46] G.v. Zandwijk, R.A.J. Jansen, H.M. Buck, J. Am. Chem. Soc. 112 (1990) 4155.
[47] (a) R.D.W. Kemmitt, M. Murray, V.M. McRae, R.D. Peacock, M.C.R. Symons, T.A. O'Donnell, J. Chem. Soc. A (1968) 862. (b) R.J. Gillespie, M.J. Morton, J. Mol. Spectrosc. 30 (1969) 178. (c) C.G. Davies, R.J. Gillespie, P.R. Ireland, J.M. Sowa, Can. J. Chem. 52 (1974) 2048. (d) W.W. Wilson, R.C. Thompson, F. Aubke, Inorg. Chem. 19 (1980) 1489.

[48] (a) J. Passmore, G. Sutherland, P.S. White, Inorg. Chem. 20 (1981) 2169. (b) J. Passmore, P. Taylor, J. Chem. Soc. Dalton Trans. (1976) 804.
[49] (a) R.J. Gillespie, R. Kapoor, R. Faggiani, C.J.L. Lock, M.P. Murchie, J. Passmore, J. Chem. Soc. Chem. Commun. (1983) 8. (b) R. Faggiani, R.J. Gillespie, R. Kapoor, C.J.L. Lock, J.E. Vekris, Inorg. Chem. 27 (1988) 4350.
[50] R.J. Gillespie, M.J. Morton, J.B. Milne, Inorg. Chem. 7 (1968) 2221.
[51] M. Murchie, University of New Brunswick, PhD thesis, Canada, 1986.
[52] A. Apblett, F. Grein, J.P. Johnson, J. Passmore, P.S. White, Inorg. Chem. 25 (1986) 422.
[53] J. Passmore, P. Taylor, T.K. Whidden, P.S. White, Can. J. Chem. 57 (1979) 968.
[54] A. Smalc, Institute Jozef Stefan, IIS Rep. R-612, vol. 1, 1972, [chemical abstract: 79:13032t, 1973].
[55] A.J. Edwards, G.R. Jones, J. Chem. Soc. A (1971) 2318.
[56] D.K. Padma, R.D. Peacock, J. Fluor. Chem. 17 (1981) 539.
[57] (a) O. Glemser, A. Smalc, Angew. Chem. Int. Ed. Engl. 8 (1969) 517. (b) K.O. Christe, R. Bau, D. Zhao, Z. Anorg. Allg. Chem. 593 (1991) 46. (c) K. Lee, F. Aubke, Inorg. Chem. 19 (1980) 119.
[58] K.C. Lee, F. Aubke, Inorg. Chem. 23 (1984) 2124.
[59] H. Hartl, J. Nowicki, R. Minkwitz, Angew. Chem. Int. Ed. Engl. 30 (1991) 328.
[60] K.O. Christe, D.A. Dixon, R. Minkwitz, Z. Anorg. Allg. Chem. 612 (1992) 51.
[61] T. Drews, W. Koch, K. Seppelt, J. Am. Chem. Soc. 121 (1999) 4379.
[62] R.J. Gillespie, M.J. Morton, Inorg. Chem. 9 (1970) 811.
[63] R.J. Gillespie, M.J. Morton, J.M. Sowa, Adv. Raman Spectrosc. 1 (1972) 539.
[64] R. Minkwitz, J. Nowicki, H. Hartl, W. Sawodny, Spectrochim. Acta 47A (1991) 1673.
[65] M.J. Collins, G. Dénès, R.J. Gillesipe, J. Chem. Soc. Chem. Commun. (1984) 1296.
[66] C. Chung, G.H. Cady, Inorg. Chem. 11 (1972) 2528.
[67] (a) D.J. Merryman, P.A. Edwards, J.D. Corbett, R.E. McCarley, J. Chem. Soc. Chem. Commun. (1972) 779. (b) D.J. Merryman, P.A. Edwards, J.D. Corbett, Inorg. Chem. 14 (1975) 428.
[68] (a) J. Passmore, G. Sutherland, P.S. White, J. Chem. Soc. Chem. Commun. (1980) 330. (b) K. Seppelt, Preliminary X-ray crystal structure presented at the RSC-GDCh Conference on Inorganic Chemistry, Brighton, UK, July 1999. (c) M.P. Murchie, J. Passmore, G.W. Sutherland, R. Kapoor, J. Chem. Soc. Dalton Trans. (1992) 503.
[69] J. Passmore, G.W. Sutherland, P.S. White, Inorg. Chem. 21 (1982) 2717.
[70] R. Faggiani, R.J. Gillespie, J.F. Sawyer, J.E. Vekris, Acta Crystallogr. Sect. C 45 (1989) 1847.
[71] (a) R. Minkwitz, J. Nowicki, W. Sawdony, K. Haertner, Spectrochim. Acta A 47 (1991) 151. (b) L.-H. Chen, E.M. Nour, J. Laane, J. Raman Specrosc. 14 (1983) 232.
[72] (a) J. Barr, R.J. Gillespie, P.K. Ummat, J. Chem. Soc. Chem. Commun. (1970) 264. (b) R.J. Gillespie, J. Passmore, P.K. Ummat, O.D. Vaidya, Inorg. Chem. 10 (1971) 1327.
[73] (a) C.G. Davies, R.J. Gillespie, J.J. Park, J. Passmore, Inorg. Chem. 10 (1971) 2781. (b) R.J. Gillespie, J. Passmore, J. Chem. Soc. Chem. Commun. (1969) 1333.
[74] R.C. Burns, R.J. Gillespie, J.F. Sawyer, Inorg. Chem. 19 (1980) 1423.
[75] J. Beck, Z. Anorg. Allg. Chem. 621 (1995) 131.
[76] R. Minkwitz, H. Borrmann, J. Nowicki, Z. Naturforsch. B 46 (1991) 629.
[77] G. Cardinal, R.J. Gillespie, J.F. Sawyer, J.E. Vekris, J. Chem. Soc. Dalton Trans. (1982) 765.
[78] (a) I.D. Brown, D.B. Crump, R.J. Gillespie, D.P. Santry, Chem. Commun. (1968) 853. (b) I.D. Brown, D.B. Crump, R.J. Gillespie, Inorg. Chem. 10 (1971) 2319.
[79] J. Barr, D.B. Crump, R.J. Gillespie, R. Kapoor, P.K. Ummat, Can. J. Chem. 46 (1968) 3607.
[80] (a) R.K. McMullen, D.J. Prince, J.D. Corbett, J. Chem. Soc. Chem. Commun. (1969) 1438. (b) R.K. McMullen, D.J. Prince, J.D. Corbett, Inorg. Chem. 10 (1971) 1749.
[81] (a) R.C. Burns, M.J. Collins, R.J. Gillespie, G.J. Schrobilgen, Inorg. Chem. 25 (1986) 4465. (b) R.J. Gillespie, P.K. Ummat, Can. J. Chem. 48 (1970) 1239.
[82] (a) R.C. Burns, W.-L. Chan, R.J. Gillespie, W.-C. Luk, J.F. Sawyer, D.R. Slim, Inorg. Chem. 19 (1980) 1432. (b) M.J. Collins, R.J. Gillespie, J.F. Sawyer, G.J. Schrobilgen, Acta Crystallogr. Sect. C 42 (1986) 13.
[83] J. Beck, A. Fischer, Z. Anorg. Allg. Chem. 623 (1997) 780.
[84] J. Beck, J. Wetterau, Inorg. Chem. 34 (1995) 6202.
[85] J. Beck, Z. Naturforsch. B 45 (1990) 1610.

[86] M.J. Collins, R.J. Gillespie, J.W. Kolis, J.F. Sawyer, Acta Crystallogr. Sect. C 43 (1987) 2033.
[87] J. Beck, Z. Naturforsch. B 45 (1990) 413.
[88] J. Beck, Z. Naturforsch. B 49 (1994) 1159.
[89] (a) D.J. Prince, J.D. Corbett, B. Garbisch, Inorg. Chem. 9 (1970) 2731. (b) N.J. Bjerrum, Inorg. Chem. 11 (1972) 2648. (c) T. Couch, D.A. Lokken, J.D. Corbett, Inorg. Chem. 11 (1972) 357. (d) R.C. Burns, R.J. Gillespie, Inorg. Chem. 21 (1982) 3877.
[90] J. Beck, G. Bock, Z. Naturforsch. B 51 (1996) 119.
[91] J. Beck, K.J. Schlitt, Chem. Ber. 128 (1995) 763.
[92] J. Beck, M. Kasper, A. Stankowski, Chem. Ber. 130 (1997) 1189.
[93] J. Beck, Chem. Ber. 124 (1991) 677.
[94] J. Barr, R.J. Gillespie, G.P. Pez, P.K. Ummat, O.C. Vaidya, Inorg. Chem. 10 (1971) 362.
[95] (a) R.J. Gillespie, J. Barr, R. Kapoor, G. Pez, J. Am. Chem. Soc. 90 (1968) 6855. (b) R.J.H. Clarke, T.J. Dines, L.T.H. Ferris, J. Chem. Soc. Dalton Trans. (1982) 2237.
[96] P.A.W. Dean, R.J. Gillespie, P.K. Ummat, Inorg. Synth. 15 (1974) 213.
[97] J. Beck, G. Bock, Z. Anorg. Allg. Chem. 622 (1996) 823.
[98] J. Beck, Chem. Ber. 128 (1995) 23.
[99] R.C. Burns, R.J. Gillespie, W.-C. Luk, D.R. Slim, Inorg. Chem. 18 (1979) 3086.
[100] G.W. Drake, G.L. Schimek, J.W. Kolis, Inorg. Chem. 35 (1996) 1740.
[101] J. Beck, G. Bock, Z. Anorg. Allg. Chem. 620 (1994) 1971.
[102] J. Beck, Z. Anorg. Allg. Chem. 619 (1993) 237.
[103] J. Beck, Angew. Chem. Int. Ed. Engl. 30 (1991) 1128.
[104] J. Beck, K. Muller-Buschbaum, Z. Anorg. Allg. Chem. 623 (1997) 409.
[105] J. Beck, Angew. Chem. Int. Ed. Engl. 29 (1990) 293.
[106] J. Beck, G. Bock, Angew. Chem. Int. Ed. Engl. 34 (1995) 2559.
[107] M.J. Collins, R.J. Gillespie, J.F. Sawyer, Acta Crystallogr. Sect. C 44 (1989) 405.
[108] R.J. Gillespie, M.J. Morton, J. Mol. Spectrosc. 30 (1969) 178.
[109] K. Tanemoto, G. Mamantov, R. Marassi, J. Inorg. Nucl. Chem. 43 (1981) 1779.
[110] R.J. Gillespie, J.B. Milne, Chem. Commun. (1966) 158.
[111] (a) R.J. Gillespie, K.C. Malhotra, Inorg. Chem. 8 (1969) 1751. (b) S. Brownridge, J. Passmore, G. Schatte, Phosphorous, Sulfur and Selenium and related elements 93 (1994) 483. (c) J. Arotsky, H.C. Mishra, M.C.R. Symons, J. Chem. Soc. (1961) 12. (d) W. Gottardi, Monatsh. Chem. 106 (1975) 1203. (e) A. Bali, K.C. Malhotra, J. Inorg. Nucl. Chem. 38 (1976) 411.
[112] R.J. Gillespie, J.B. Milne, Inorg. Chem. 5 (1966) 1577.
[113] J. Besida, T.A. O'Donnell, Inorg. Chem. 28 (1989) 1669.
[114] (a) J. Arotsky, H.C. Mishra, M.C.R. Symons, J. Chem. Soc. (1962) 2582. (b) F. Aubke, G.H. Cady, Inorg. Chem. 4 (1965) 269.
[115] R.J. Gillespie, M.J. Morton, Inorg. Chem. 11 (1972) 586.
[116] R.J. Gillespie, M.J. Morton, Chem. Commun. (1968) 1565.
[117] W.W. Wilson, J.M. Winfield, F. Aubke, J. Fluor. Chem. 7 (1976) 245.
[118] R.S. Eachus, M.C.R. Symons, J. Chem. Soc. Dalton Trans. (1976) 431.
[119] R.C. Paul, J.K. Puri, K.C. Malhotra, J. Chem. Soc. Chem. Commun. (1970) 776.
[120] N.J. Bjerrum, Inorg. Chem. 9 (1970) 1965.
[121] G.J. Schrobilgen, R.C. Burns, P. Granger, J. Chem. Soc. Chem. Commun. (1978) 957.
[122] C.R. Lassigne, E.J. Wells, J. Chem. Soc. Chem. Commun. (1978) 956.
[123] J. Barr, R.J. Gillespie, R. Kapoor, K.C. Malhotra, Can. J. Chem. 46 (1968) 149.
[124] (a) R.J. Gillespie, P.K. Ummat, Inorg. Chem. 11 (1972) 1674. (b) P.J. Stephens, J. Chem. Soc. Chem. Commun. (1969) 1496.
[125] H.S. Low, R.A. Beaudet, J. Am. Chem. Soc. 98 (1976) 3849.
[126] A. Bali, K.C. Malhotra, Aust. J. Chem. 28 (1975) 983.
[127] W.F. Giggenbach, Chem. Commun. (1970) 852.
[128] R. Fehrmann, N.J. Bjerrum, F.W. Poulsen, Inorg. Chem. 17 (1978) 1195.
[129] R. Fehrmann, N.J. Bjerrum, Inorg. Chem. 16 (1977) 2089.
[130] R. Fehrmann, N.J. Bjerrum, H.A. Andersen, Inorg. Chem. 15 (1976) 2187.
[131] R. Faggiani, R.J. Gillespie, J.W. Kolis, K.C. Malhotra, J. Chem. Soc. Chem. Comm. (1987) 591.

[132] (a) I. Krossing, J. Passmore, presented at the 12th European Symposium on Fluorine Chemistry, Berlin, Germany, August (September, 1998, Abstract C22). (b) T.S. Cameron, A. Decken, I. Krossing, J. Passmore, Dalton Trans. (submitted).
[133] (a) F. Klaibo, W. Petter, F. Hulliger, J. Solid State Chem. 46 (1983) 112. (b) M. Julien-Poazol, S. Jaulmes, F. Alapini, Acta Crystallogr. Sect. B 33 (1977) 2270.
[134] (a) However, Se_6I^+ has two valence electrons more than Te_7^{2+} (40 vs. 42 VE) and therefore the bridge connecting the six-membered rings is not linear (as in Se_6I^+) but bent (one lone pair orbital pair less). (b) J. Passmore, P.S. White, C.-M. Wong, J.C.S. Chem. Commun. (1985) 1178.
[135] J.H.J. Collins, R.J. Gillespie, J.F. Sawyer, Inorg. Chem. 26 (1987) 1476.
[136] L. Graham, Ph.D. thesis, October 1978, LBL-8088, pp. 54–61 (experimental) and 63–76 (discussion) under supervision of N. Bartlett.
[137] (a) R. Steudel, R. Reinhard, F. Schuster, Angew. Chem. Int. Ed. 16 (1977) 715. (b) R. Steudel, F. Schuster, J. Mol. Struct. (1978) 143. (c) R. Steudel, J. Steidel, J. Pickard, F. Schuster, R. Reinhard, Z. Naturforsch. B 35 (1980) 1378.
[138] R. Steudel, Top. Curr. Chem. 102 (1982) 149.
[139] At the QCISD(T)/TZ(2p) level of theory.
[140] I. Krossing, J. Passmore, unpublished results.
[141] P.D. Lyne, D.M.P. Mingos, in: Z.B. Maksic, M. Eckert-Maksic (eds.), An Econium to Linus Pauling-Molecules in Natural Science and Medicine, Ellis Horwood, Chichester, 1992.
[142] I. Krossing, J. Passmore, unpublished results at the B3PW91/3-21G* level of theory.
[143] MP3/DZP//HF/DZP; $r_1 = 2.037$ Å; $r_2 = 2.775$ Å. The long distance is presumably considerably overestimated leading to a lower dissociation energy, see Ref. [18].
[144] P. Cassoux, J.-F. Labarre, O. Glemser, J. Mol. Struct. 13 (1972) 405.
[145] R. Steudel, Angew. Chem. Int. Ed. Engl. 10 (1975) 655.
[146] (a) J. Passmore, G. Sutherland, T. Whidden, P.S. White, C.-M. Wong, J. Chem. Soc. Chem. Comm. (1982) 1098. (b) W.A.S. Nandana, J. Passmore, P.S. White, C.-M. Wong, Inorg. Chem. 29 (1990) 3529.
[147] K. Tanaka, T. Yamabe, H. Teramae, K. Fukui, Nouv. J. Chim. 3 (1979) 379.
[148] N. Burford, J. Passmore, unpublished results.
[149] I.D. Brown, in: M. O'Keefe, A. Navrotsky (eds.), Structure and Bonding in Crystals, vol. 2, Academic, London, 1981, p. 1.
[150] For the thorough definition of a bond and ring critical point see: R.F.W. Bader, Acc. Chem. Res. 18 (1985) 9.
[151] F. Iwasaki, N. Toyoda, R. Akaishi, H. Fujihara, N. Furukawa, Bull. Chem. Soc. Jpn. 61 (1988) 2563.
[152] W.A.S. Nandana, J. Passmore, P.S. White, C.-M. Wong, Inorg. Chem. 28 (1989) 3320.
[153] A.J. Banister, Nat. Phys. Sci. 239 (1972) 69.
[154] It is recognised that this polyhedron is not a deltahedron but possesses one rectangular face (all other faces are triangular). However, it is assumed that there is nearly approximately no energetic difference between this 14 cornered polyhedron and a pure triangularly faced 14 cornered deltahedron.
[155] C.G. Davies, R.J. Gillespie, P.R. Ireland, J.M. Sowa, Can. J. Chem. 52 (1974) 2048.
[156] J. Passmore, G. Sutherland, T. Whidden, P.S. White, J. Chem. Soc. Chem. Commun. (1982) 289.
[157] M.P. Murchie, J.P. Johnson, J. Passmore, G.W. Sutherland, M. Tajik, T.K. Whidden, P.S. White, F. Grein, Inorg. Chem. 31 (1992) 273.
[158] Y. Li, X. Wang, F. Jensen, K.N. Houk, G.A. Olah, J. Am. Chem. Soc. 112 (1990) 3922.
[159] J. Li, S. Irle, W.H.E. Schwarz, Inorg. Chem. 35 (1996) 100.
[160] Z. Lin, M.B. Hall, Polyhedron 12 (1993) 1499.
[161] A.F. Kapustinskii, Q. Rev. 10 (1956) 283.
[162] T.E. Mallouk, G.L. Rosenthal, R. Muller, R. Brusasco, N. Bartlett, Inorg. Chem. 23 (1984) 3167.
[163] K.O. Christe, D.A. Dixon, D. McLemore, W.W. Wilson, J.A. Sheehy, J.A. Boatz, J. Fluorine Chem. 101 (2000) 151.
[164] J.A. Ibers, W.C. Hamilton, J. Chem. Phys. 44 (1966) 1748.
[165] The larger anion $Sb_3F_{16}^-$ is weaker Lewis base than $Sb_2F_{11}^-$.

[166] (a) T. Birchall, P.A.W. Dean, B. Della Valle, R.J. Gillespie, Can. J. Chem. 51 (1973) 667. (b) W.A.S. Nandana, J. Passmore, D.C.N. Swindells, P. Taylor, P.S. White, J.E. Vekris, J. Chem Soc. Dalton Trans. (1983) 619. (c) W.A.S. Nandana, J. Passmore, P. White, J. Chem Soc. Dalton Trans. (1985) 1623. (d) W.A.S. Nandana, J. Passmore, P.S. White, C.-M. Wong, J. Chem. Soc. Dalton Trans. (1987) 1989.
[167] J.E. Huheey, E.A. Keiter, R.L. Keiter, Inorganic Chemistry: Principles of Structure and Reactivity, fourth ed., Harper Collins, New York, 1993.
[168] J. Passmore, W.A.S. Nandana, E.K. Richardson, P. Taylor, J. Fluor. Chem. 15 (1980) 435.
[169] M.W. Schmidt, P.N. Truon, M.S. Gordon, J. Am. Chem. Soc. 109 (1987) 5217.
[170] I. Krossing, J. Passmore, unpublished results. O_4^{2+} (D_{4h}) and O_2^+ were optimised at the B3PW91/6-311 + G(3df) level of theory and energies obtained at the B3PW91/6-311 + G(3d2f) level utilising this geometries. d(O–O) in O_2^+, 1.101 Å; in O_4^{2+}, 1.342 Å.
[171] J. Passmore, G.W. Sutherland, P. Taylor, T.K. Whidden, P.S. White, Inorg. Chem. 20 (1981) 2839.
[172] J. Berkowitz, C. Lifshitz, J. Chem. Phys. 48 (1968) 4346.
[173] J. Berkowitz, W.A. Chupka, J. Chem. Phys. 45 (1966) 4289.
[174] Se_4^+ (D_{4h} symmetry) was fully optimised at the MPW1PW91/3-21G* level of theory and is a true minimum, d(Se–Se) = 2.319 Å. Energies given [MPW1PW91/6-311G(2df)//MPW1PW91/3-21G*] include the zero point energy and are corrected to 298 K.
[175] The geometries of Se_3 and Se_3^+ (C_{2v}, employing the minima found previously for S_3 and S_3^+) [30] were fully optimised at the MPW1PW91/3-21G* level of theory and are true minima, Se_3: d(Se–Se) = 2.188 Å, Se–Se–Se = 115.5, Se_3^+: d(Se–Se) = 2.195 Å, Se–Se–Se = 95.2. Energies given were computed at the MPW1PW91/6-311G(2df)//MPW1PW91/3-21G* level and include the zero point energy and are corrected to 298 K. Thus the ionisation potential of Se_3 is calculated (938 kJ mol^{-1}). The enthalpy of formation of gaseous Se_3 is calculated from the experimental enthalpy of formation of gaseous Se_8 (170 kJ mol^{-1}) and the subsequent calculated enthalpy of reaction of 3/8 Se_8 (g) = Se_3 (g) (145 kJ mol^{-1}). Thus we conclude to a gaseous enthalpy of formation of Se_3^+ of 1083 kJ mol^{-1}.
[176] Volumes employed in our generalised equation of Ref. [15b] (respective lattice enthalpies of the AsF_6^- salts in kJ mol^{-1}): 110 $Å^3$ for AsF_6^-, S_8^{2+} 180 $Å^3$ (based on X-ray, 1462), S_4^{2+} 84 $Å^3$ (1584), S_2^+ 45 $Å^3$ (545), S_3^+ 79 $Å^3$ (518), S_4^+ 90 $Å^3$ (510), S_5^+ 122 $Å^3$ (479), S_6^+ 146 $Å^3$ (479), S_7^+ 166 $Å^3$ (469). [Ion volumes estimated assuming: $Br_2^+ > S_2^+ > SN^+$; $Br_3^+ > S_3^+ > Cl_3^+$; $S_3N^{2+} > S_4^+ > S_4^{2+}$; $Br_5^+ > S_5^+ > S_3N^{2+}$; $S_3Br_3^+ > S_6^+ > S_5^+$, $S_7I^+ > S_7^+ > S_4N_3^+$].
[177] Volumes employed in our generalised equation of Ref. [15b] (respective lattice enthalpies of the AsF_6^- salts in kJ/mol): 110 $Å^3$ for AsF_6^-, Se_8^{2+} 214 $Å^3$ (1430), Se_4^{2+} 94 $Å^3$ (1551), Se_2^+ 59 $Å^3$ (532), Se_3^+ 114 $Å^3$ (495), Se_4^+ 127 $Å^3$ (488), Se_5^+ 175 $Å^3$ (465), Se_6^+ 196 $Å^3$ (457), Se_7^+ 230 $Å^3$ (445). [Ion volumes estimated assuming: $I_2^+ > Se_2^+ > S_2^+$; $I_3^+ > Se_3^+ > Br_3^+$; $SeI_3^+ > Se_4^+ > Se_4^{2+}$; $I_5^+ > Se_5^+ > Se_3N_2^{2+}$; $Se_6I^+ > Se_6^+ > Se_3Br_3^+$. Se_7^+ ion volume found from extrapolation of Se_n^+.]
[178] Compare with the Kapustinskii treatment of the lattice potential energy.
[179] J. Passmore, G.W. Sutherland, P.S. White, J. Chem. Soc. Chem. Commun. (1980) 330.
[180] J. Passmore, G.W. Sutherland, T.K. Whidden, P.S. White, C.-M. Wong, Can. J. Chem. 63 (1985) 1209.
[181] M.P. Murchie, J. Passmore, G.W. Sutherland, R. Kapoor, J.C.S. Dalton Trans. (1992) 503 and references therein.
[182] S. Brownridge, T.S. Cameron, J. Passmore, G. Schatte, T. Way, J. Chem. Soc. Dalton Trans. (1996) 2553 and references therein.
[183] T. Klapötke, J. Passmore, Acc. Chem. Res. 22 (1989) 234 references therein.
[184] J. Passmore, G. Schatte, personal communication.
[185] T.S. Cameron, I. Dionne, H.D.B. Jenkins, S. Parson, J. Passmore, H.K. Roobottom, Inorg. Chem. (1999) submitted.
[186] I. Krossing, J. Passmore, D. Wood, manuscript in preparation.
[187] (a) M.P. Murchie, J.P. Johnson, J. Passmore, G.W. Sutherland, M. Tajik, T.K. Whidden, P.S. White, F. Grein, Inorg. Chem. 31 (1992) 273. (b) R. West, F.G.A. Stone (eds.), Multiply Bonded Main Group Metals and Metalloids, Academic, New York, 1996, and references therein.

[188] (a) J. Su, X.-W. Li, R.C. Crittendon, G.H. Robinson, J. Am. Chem. Soc. 119 (1997) 5471. (b) Y. Xie, R.S. Grev, J. Gu, H.F. Schaefer, P.v.R. Schleyer, J. Su, X.-W. Li, G.H. Robinson, J. Am. Chem. Soc. 120 (1998) 3773. (c) P.P. Power, J. Chem. Soc. Dalton Trans. (1998) 2939.
[189] N. Burford, J.A.C. Clyburne, M.S.W. Chan, Inorg. Chem. 36 (1997) 3204.
[190] R.L. Kuczkowski, J. Am. Chem. Soc. 86 (1964) 3617.
[191] S. Brownridge, J. Passmore, unpublished results.
[192] (a) A.E. Reed, P.v.R. Schleyer, J. Am. Chem. Soc. 112 (1990) 1424. (b) R.P. Messmer, J. Am. Chem. Soc. 113 (1991) 433.
[193] (a) R.J. Gillespie, E.A. Robinson, G.L. Heard, Inorg. Chem. 37 (1998) 6884. (b) X. Zhang, K. Seppelt, Inorg. Chem. 36 (1997) 5689.
[194] P. Böttcher, T. Doert, Phosphorus Sulfur Silicon 136–138 (1998) 255.
[195] (a) J.P. Johnson, M. Murchie, J. Passmore, M. Tajik, P.S. White, C.-M. Wong, Can. J. Chem. 65 (1987) 2744. (b) B.H. Christian, M.J. Collins, R.J. Gillespie, J.F. Sawyer, Inorg. Chem 25 (1986) 777.
[196] W.E. Dasent, Nonexistent Compounds, Compounds of Low Stability, Marcel Dekker, New York, 1965.
[197] W.E. Latimer, Oxidation Potentials, second ed., Prentice Hall, Engelwood Cliffs, NJ, 1952, p. 359.
[198] D.D. Wagman, W.H. Evans, V.B. Parker, R.H. Schumm, I. Halow, S.M. Bailey, K.L. Churney, R.L. Nuttal, J. Phys. Chem. Ref. Data 11 (1982).
[199] P.A.G. O'Hare, W.N. Hubbard, J. Phys. Chem. 69 (1965) 4358.
[200] S.G. Lias, J.E. Bartmess, J.F. Liebman, J.L. Holmes, R.D, Levin, W.G. Mallard, J. Phys. Chem. Ref Data 17 (1988).
[201] N. Bartlett, K. Leary, Rev. Chim. Miner. 13 (1976) 82.
[202] K.O. Christe, W. Sawodny, Inorg. Chem. 8 (1969) 212.
[203] S. Brownridge, H.D.B. Jenkins, unpublished results at the MPW1PW91/3-21G* level of theory.
[204] M.T. Nguyen, R. Flammang, N. Goldberg, H. Schwarz, Chem. Phys. Lett. 236 (1995) 201.
[205] H.K. Roobottom, H.D.B. Jenkins, unpublished work.
[206] I. Krossing, J. Passmore, presented at the 12th European Symposium on Fluorine Chemistry, Berlin 1998, abstract C22.
[207] I. Krossing, H.D.B. Jenkins, unpublished results at the B3PW91/3-21G* level of theory.
[208] H.D.B. Jenkins, Lattice energies in: D.R. Lide (ed.), Handbook of Chemistry and Physics, 79th ed., vol. 9, CRC, Times Mirror Books, Boca Raton, Ann Arbor, London, Tokyo, 1998, p. 1222.
[209] I.C. Tornieporth-Oetting, T.M. Klapötke, T.S. Cameron, J. Valkonen, P. Rademacher, K. Kowski, J. Chem. Soc. Dalton Trans. (1992) 537.